INVESTIGATION OF THE USABILITY OF RADIOCHROMIC FILMS FOR DETERMINATION OF DOSE UNIFORMITY OF FOOD SURFACE IN UV-C TREATMENT

A Thesis Submitted to
the Graduate School of Engineering and Sciences of
İzmir Institute of Technology
in Partial Fulfillment of the Requirements for the Degree of

MASTER OF SCIENCE

in Food Engineering

by
Yadigar SEYFİ

July 2022
İZMİR

ACKNOWLEDGMENTS

There are several people who directly or indirectly contributed to the creation of this thesis and to whom I would like to express my gratitude.

Firstly, I would like to express my intimate appreciation to my supervisor Prof. Dr. Sevcan ÜNLÜTÜRK for her guidance, support, and endless patient. I am really a lucky person for having a working opportunity with her. Her vision and support gave me a lot of knowledge in the academic field.

I would like to express my thankfulness to defense committee members Prof. Dr. Figen KOREL from İzmir Institute of Technology at Department of Food Engineering and Prof. Dr. Gülten TİRYAKİ GÜNDÜZ from Ege University at Department of Food Engineering for their valuable contributions and spending their time.

I have never work with a lab-mate, but I learned lots of things from my colleagues. So, I would like to thank to my colleague Research Assist. Kevser SABANCI for her positive perspective, friendship, and support and my colleague Research Assist. Çağrı ÇAVDAROĞLU for helping me without thinking whenever I need a guidance. I also thank to my IZTECH colleagues for their enjoyable contributions during working hours.

Lastly, I would like to express my thankfulness to my dear precious family. I would like to express my gratitude to my mother Fatma SEYFİ and father Arif SEYFİ for their patience and for running next to me whenever I needed them. Making them proud as their eldest child is one of my goals in life and I hope I have given them the pride they deserve.

ABSTRACT

INVESTIGATION OF THE USABILITY OF RADIOCHROMIC FILMS FOR DETERMINATION OF DOSE UNIFORMITY OF FOOD SURFACE IN UV-C TREATMENT

The microbial inactivation efficiency of UV light is dependent on product shape and surface morphology on non-planar food surfaces. Since every point of the product is not exposed to the same level of UV light, the efficiency decreases. In addition, during UV light illumination, blind spots may occur, and sufficient inactivation cannot be achieved. So, it is essential to determine UV fluence (dose) applied to surfaces. Actinometry, biodosimetry and mathematical techniques are used to evaluate UV fluence on solid surfaces and in liquid foods. In this study, use of radiochromic films (RCFs) integrated with a computer vision system (CVS) based on image analysis is proposed as an alternative method to evaluate UV fluence on food surfaces. For this purpose, the color change of RCFs on non-planar surfaces exposed to different UV intensity and exposure time was correlated with UV fluence. The results were compared with actinometric and radiometric measurement techniques. Experimental results have been tested and verified on real food surfaces such as apples.

It was revealed that there is a linear correlation between the color change of RCF and UV fluence. The maximum UV fluence that could be determined using RCF at 254 nm was approximately 60 mJ/cm^2. It was found that films were stable up to 15 days at room and refrigerated conditions. The shape of the apples resulted in different UV fluence distribution profiles on the surface. As a result, it has been demonstrated that RCFs can be successfully used to determine UV fluence on sample surfaces.

.

ÖZET

RADYOKROMİK FİLMLERİN UV-C İŞLEMİNDE GIDA YÜZEYLERİNİN DOZ HOMOJENLİĞİNİN BELİRLENMESİ İÇİN KULLANABİLİRLİĞİNİN ARAŞTIRILMASI

UV ışığının mikrobiyal inaktivasyon verimliliği, düzlemsel olmayan gıda yüzeylerinde ürün şekline ve yüzey morfolojisine bağlıdır. Ürünün her noktası aynı seviyede UV ışığına maruz kalmadığından verim düşmektedir. Ayrıca UV ışık aydınlatması sırasında kör noktalar oluşabilir ve yeterli inaktivasyon sağlanamaz. Bu nedenle yüzeylere uygulanan UV akımının (dozunun) belirlenmesi önemlidir. Katı yüzeylerde ve sıvı gıdalarda UV akışını değerlendirmek için aktinometri, biyodozimetri ve matematiksel teknikler kullanılır. Bu çalışmada, gıda yüzeylerindeki UV akışını değerlendirmek için alternatif bir yöntem olarak görüntü analizine dayalı bilgisayarlı görme sistemi (CVS) ile entegre radyokromik filmlerin (RCF) kullanımı önerilmiştir. Bu amaçla, farklı UV yoğunluğuna ve maruz kalma süresine maruz kalan düzlemsel olmayan yüzeylerdeki RCF'lerin renk değişimi UV akısı ile ilişkilendirilmiştir. Sonuçlar aktinometrik ve radyometrik ölçüm teknikleri ile karşılaştırılmıştır. Deneysel sonuçlar elma gibi gerçek gıda yüzeylerinde test edilmiş ve doğrulanmıştır.

RCF'nin renk değişimi ile UV akısı arasında doğrusal bir ilişki olduğu ortaya çıkmıştır. 254 nm'de RCF kullanılarak belirlenebilen maksimum UV akısı yaklaşık 60 mJ/cm^2'dir. Filmlerin oda ve soğutma koşullarında 15 güne kadar stabil olduğu belirtilmiştir. Elmaların şekli, yüzeyde farklı UV akısı dağılım profilleri oluşturmaktadır. Sonuç olarak, RCF'lerin gıda yüzeylerinde UV akısını belirlemek için başarılı bir şekilde kullanılabileceği gösterilmiştir.

This Master thesis is dedicated to my dear parents,

Fatma SEYFİ and Arif SEYFİ,

and my little brother,

Semih SEYFİ

TABLE OF CONTENTS

LIST OF FIGURES

Figures **Pages**

Figures **Pages**

LIST OF TABLES

CHAPTER 1

INTRODUCTION

Food safety and food security are two crucial phenomena in the food industry to regularly supply food products to customers. According to Food and Agriculture Organization (FAO), Food security "exists when all people, at all times, have physical, social and economic access to sufficient, safe and nutritious food which meets their dietary needs and food preferences for an active and healthy life."(FAO, n.d.) Food safety is described as methods that prevent food products from foodborne pathogens in food products' handling, processing, and storage stages. Approximately 600 million people get sick from contaminated food each year around the world, and 420 million have died (WHO 2022). Therefore, food safety is an important issue that needs to be considered. Some principles and protection methods are used to ensure food safety. Cleaning, separation of process lines of different product groups to prevent cross-contamination, and preservation methods such as cooking, and chilling can be counted under the food safety concept. Food preservation methods can be separated into thermal and non-thermal methods (Skåra and Rosnes 2016).

Radiation treatment is one of the non-thermal methods and classified as ionizing and nonionizing radiation. Ionizing radiation such as Gamma-rays, X-rays, beta-rays, alpha-rays, and protons leads to ionizing atoms and molecules. In contrast, nonionizing radiation includes Ultraviolet (UV) light, less energetic types, and causes excitation of electrons of atoms and molecules (Koutchma, Forney, and Moraru 2009).

UV treatment has been widely used for disinfection of airborne microorganisms, sterilization of liquids, and disinfection of surfaces of solid foods and food contact materials (Bintsis, Litopoulou-Tzanetaki, and Robinson 2000). The main advantage of UV treatment overheat treatment is that, in addition to microbial inactivation, it provides better food quality properties such as flavor, color, texture, and nutritional value. Besides, UV treatment also has disadvantages such as lack of penetration and being an unsuitable process for non-uniformly shaped food products. Furthermore, the determination of applied UV fluence on products or surfaces is challenging. Some techniques such as radiometry, actinometry and biodosimetry can be used to determine the irradiance (I).

Then UV fluence is calculated from I and the exposure time (t) (Guerrero-Beltrán and Barbosa-Cánovas 2004). All of these techniques have their own strengths and weaknesses. However, it is difficult to determine the UV fluence applied to the surfaces. In this study, the usability of radiochromic films (RCFs) used in food radiation applications and other radiology fields as an alternative tool for UV fluence determination will be determined (Fan, Huang, and Chen 2017).

Radiochromic films are generally transparent and colorless, and gradually turn into colored forms when exposed to UV light. Different color intensities can be obtained depending on the applied UV fluences (Devic, Tomic, and Lewis 2016). Color densitometers, scanners, and spectrophotometers generally analyze these color intensities. Computer vision system (CVS) based on image analysis and use of radiochromic films (RCFs) can be an alternative tool to determine the UV irradiance on the surface and ultimately calculating the UV fluence depending on the color change in the films. The aim of this thesis is to examine the color change of RCFs in response to UV intensity (irradiance), exposure time, temperature, and storage time by means of image analysis, to compare the accuracy of the UV intensity (irradiance) measurement with the radiometer and actinometer methods, and to determine the usability of RCFs for UV fluence measurement on surfaces of solid food products.

CHAPTER 2

LITERATURE REVIEW

2.1. Ultraviolet Light (UV)

Ultraviolet Light (UV) corresponds to the wavelength range of 100-400 nm and covers the electromagnetic spectrum between X-rays and visible light. In general, the UV light region is divided into four parts:

- UV vacuum region (100-200 nm)
- UV-C region (200-280 nm)
- UV-B region (280-315 nm)
- UV-A region (315-400 nm)(Guerrero-Beltrán and Barbosa-Cánovas 2004).

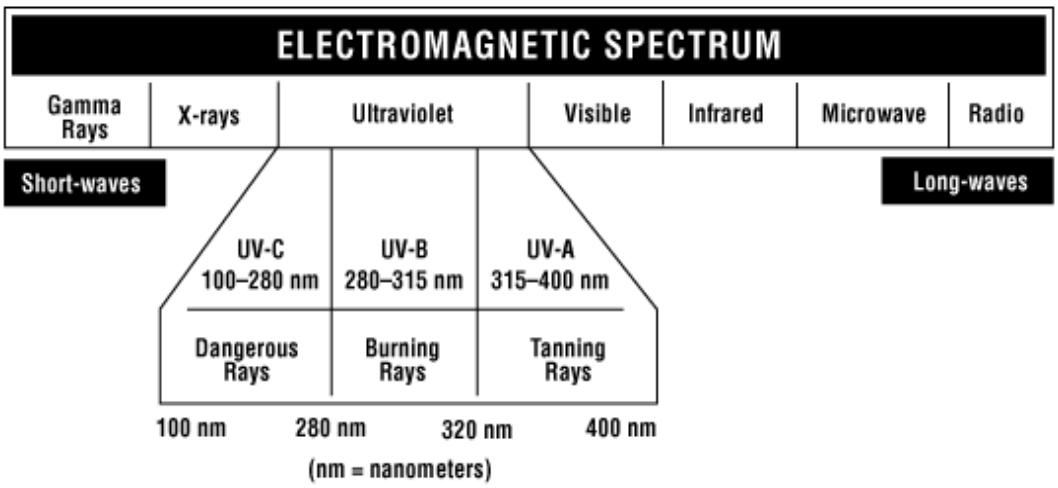

Figure 2. 1. Electromagnetic spectrum for UV region (Source:URL1)

UV lights in the vacuum region can be transferred due to absorption by all substances (Koutchma, Orlowska, and Zhu 2012). UV-C region is known as short-wavelength, germicidal wavelength, or germicidal light. It is because of its lethal effect on microorganisms (bacteria, viruses, protozoa, mold, yeast, and algae)(Guerrero-Beltrán and Barbosa-Cánovas 2004). Its highest inactivation effect of UVC light is found at about 260-265 nm wavelength. It corresponds to UV absorption of bacterial DNA (Kowalski 2009). UV-B region is the medium-wavelength region and causes skin cancer. Lastly,

the UV-A region is also called a long wavelength and is responsible for human skin tanning (Koutchma, Orlowska, and Zhu 2012).

2.1.1. History

UV light was discovered by Johann Wilhelm Ritter -father of modern electrochemistry- in 1801 (Barth 1987). In 1877, the inactivation of microorganisms by sunlight was discovered by Downes and Blunt. In 1930, the most effective antimicrobial peak on DNA of microorganisms was determined and published as 260-265 nm by Gates. This peak was very close to the wavelength of low-pressure mercury lamps (254 nm) (Reed 2010). From 1930 to 2000, there were many studies applying UV light treatment. UV light treatment was first used to inhibit airborne microorganisms in the 1930s. Between 1940 and 2000, some improvements in the system, methodology, and other factors were made by scientists on UV light treatment (Reed 2010). UV light treatment was also used in the food industry. In 2002, the US FDA approved UV-C light treatment as a disinfectant for food and food contact surfaces (FDA 2000). UV-C light treatment is actively applied in water treatment, liquid food pasteurization, and decontamination of food and food contact surfaces in the food industry (Bintsis, Litopoulou-Tzanetaki, and Robinson 2000). Canada Food Inspection Agency (CFIA) or Health Canada proposed the UV treatment on mango, poultry, shrimp, and ground beef in 2002. Currently, irradiated foods, such as potatoes, onions, wheat, whole wheat flour, and whole or ground spices, are permitted for sale in Canada (CFIA, n.d.). In addition to Health Canada, the Food Safety and Standard Authority of India (FSSAI) accepted as a safe process of UV treatment on milk (Koutchma 2018). In 2016, the European Food Safety Authority (EFSA) approved the UV treatment on milk as safe (EFSA 2016). Lastly, the Israeli food regulations agency declared that UV treatment could reduce milk's microbial load in 2017 (Koutchma 2018).

2.1.2. UV Light Sources

UV light can be produced in two ways: solar irradiation and artificial sources. Solar irradiation is obtained by the Sun. Sun emits the radiation, and different atmosphere layers absorb this radiation with different portions. Generally, UV-B and UV-A lights reach the earth’s surface. This situation corresponds to 290-400 nm wavelength. At the

sea level, the intensity flux of UV-A radiation is reported as approximately 35-50 W/m^2 (Bintsis, Litopoulou-Tzanetaki, and Robinson 2000). Also, there are artificial sources to produce UV radiation. Current technology makes it possible to use two types of UV light systems. The first UV light system uses continuous shortwave UV light (UV-C). Shortwave UV is produced by low pressure mercury arcs, with a wavelength of 254 nm. The second one uses high intensity pulsed light. Pulsed light is supplied with a capacitor, and pulses are obtained through flashing a source lamp (Bouslimi et al. 2012). The light produced by pulsed UV lamps consists of a continuous broadband spectrum from deep UV to infrared, spanning several hundred microseconds and rich in the UV range below 400 nm (Keklik and Demirci 2009).

According to (Koutchma, Forney, and Moraru 2009), artificial UV lamps used in food applications can be classified as mercury lamps, excimer lamps, broadband-pulsed lamps, light-emitting diodes (LED), and microwave-powered UV lamps (MPUVL).

Mercury lamps are usually used in the food industry. They are also known as vapor discharge lamps. Mercury lamps generally consist of an envelope, an electrode, a seal, and a ballast (Koutchma, Forney, and Moraru 2009). The envelope made from silica glass sealed with both ends contains a small amount of mercury and inert gas, which can be argon, neon, xenon, or helium, but mostly argon preferred (Bouslimi et al. 2012; LightTech 2013). Mercury is chosen due to its volatile property, which provides enough activation energy in the gas phase, and this phase can be obtained at temperatures compatible with the lamp structure. The role of argon is to support the start-up of the lamp, assist the start-up activation - ionization of mercury, extend the electrode life and reduce thermal losses. It is not responsible for the spectral output of the lamp (Bouslimi et al. 2012; Koutchma, Forney, and Moraru 2009). An electrode is placed at the ends of the envelope, and the envelope is connected to the outside through a seal. There is also a ballast which is current limiting device and provides required operating voltages (Bouslimi et al. 2012). When the sufficient voltage applied to the lamp, the free electrons inside the mercury atom are accelerated, and collisions occur between the electrons and argon. Therefore, ionization of mercury atoms take place and emission of light is observed (Koutchma, Forney, and Moraru 2009).

Mercury lamps are divided into three subparts: low-pressure mercury lamps (LPM), low-pressure high output mercury lamps (LPMHO), and medium pressure

mercury lamps (MPM). LPM lamps contain elementary mercury and produce monochromatic emission, where the lamp gives a limited number of well-defined peaks at a certain wavelength. Conversely, MPM lamps also contain elementary mercury but perform polychromatic emission which means a series of emissions done by the lamp at a wavelength spectrum. While LPM is broadly used for disinfection of liquids, surfaces, and air, MPM lamps are preferred in the printing industry to dry inks and in wastewater treatment to diminish total organic compounds(Bouslimi et al. 2012). The lifetime of LPM lamps (2,000 hours) is longer than MPM lamps (400 hours). Other properties of LPM and MPM lamps are summarized in Table 2.1 (Koutchma, Forney, and Moraru 2009).

LPMHO lamps contain mercury amalgam. They are generally preferred in disinfection applications (Koutchma, Orlowska, and Zhu 2012). Due their superiorities such as efficiency, operating life, and operating cost, they are designed as an alternative to MPM lamps (Koutchma, Forney, and Moraru 2009).

Excimer lamps are produced from rare gas or halogen excimers or rare-gas halide exciplexes. These lamps have a semi-monochromatic spectrum range with a wavelength of 120-380 nm. They are useful for the sterilization of packaging carton surfaces.

Pulsed lamps form a pulse of intense light emission within about 100 ms. The superiority of pulsed lamps over mercury lamps is high intensity, broad-spectrum, instant start, and mercury-free. They can penetrate opaque liquids better than mercury lamps due to their high-intensity values. For pulse lamps, studies in liquid product treatments are not sufficient right now. But pulsed lamp treatment is applied on food surfaces such as corn, fresh produces, meat and fish. High-intensity pulsed UV light up to 12 J/cm^2 has been approved by the FDA as a tool to control surface microorganisms on food products (Palmieri and Cacae 2005).

Light-emitting diodes or LEDs are semiconductor UV light sources. LEDs consist of p-n junction. In this system, n-type is electron rich side and p-type is electron poor side. Thus, the photon energy is obtained by the excitation of electrons when the current is passed through the diode (Koutchma, Popović, and Green 2019). Mostly used semiconductor materials are aluminum nitride (AlN), aluminum gallium nitride (AlGaN),

Table 2. 1. Comparison of LPM and MPM lamps

	LPM	**MPM**
Material	Elementary mercury	Elementary mercury
Emission type	Monochromatic	Polychromatic
Spectrum	254 nm	250-600 nm
Working temperature	40 ^{o}C	600-800 ^{o}C (minimum 400 ^{o}C)
Potential gradient	0.4-0.6 W/cm	5-30 W/cm
Electrical efficiency	50%	15-30%
UV efficiency	38%	12%

and gallium nitride (GaN) (Song, Mohseni, and Taghipour 2016). UV (100-400 nm), visible (400-800 nm), and infrared (800-1000 nm) LEDs are available on the market. UV-LEDs can be used for disinfection of beverages, food and food contact surfaces, material surfaces and packaging (Koutchma, Popović, and Green 2019). Low-cost requirement, long service life (10,000 hours), easy emission control, energy efficient structure and no mercury residue are the reasons for preference.

Microwave-powered UV lamps (MPUVL) are also new technology products. The electrode requirement for exciting the gas inside the lamp glass is unnecessary. Microwave energy produced by a magnetron is used instead of the electrode. In this lamp, microwaves directly energize the mercury vapor and produce ultraviolet light. UV light at 185 and 254 nm can be obtained with the MPUVL (Florian and Knapp 2001). Compared to mercury lamps, microwave-powered UV lamps require less warm-up time, provide more lamp lifetime (approximately three times greater than mercury lamps), and corrosion and electrical connection issues are minimized (Koutchma, Forney, and Moraru 2009). The general properties of UV sources are summarized in Table 2.2.

Table 2. 2. Properties of UV lamps

UV Source	Emission wavelength	Application area
Mercury lamps	254 nm for LPM 250-600 nm for MPM	LPM for disinfection of water, liquids, and air MPM for wastewater treatment
Excimer lamps	120-380 nm	Sterilization of packaging carton surfaces
Pulsed lamps	200-1100 nm	Disinfection of liquids and food surfaces
Light emitting diodes	100-1000 nm	Disinfection of beverages, food and food contact surfaces, material surfaces and packaging
Microwave powered UV lamps	185 and 254 nm	Wastewater, surface water treatment

2.1.3. Applications of UV Light in the Food Industry

UV light technology is used widely in different industries. For example, UV-A light is applied for curing UV adhesives and plastics and fluorescent inspection. UV-B light, which is in conjunction with UV-A can be used for artificial accelerated aging of materials. Besides them, UV-C light is applied to provide rapid dry inks and lacquers and sterilize surfaces, air, and water (Bouslimi et al. 2012).

In the food industry, UV-C light is mostly preferred and generally used for the inactivation of microorganisms. With UV-C irradiation, pasteurization of liquid products, water purification, air and food disinfection and decontamination of food contact surfaces can be performed (Bintsis, Litopoulou-Tzanetaki, and Robinson 2000). Some applications of UV-C treatment in the food industry in recent years are summarized in the Table 2.3.

Table 2. 3. Application area of UVC treatment in food industry

	Product	Purpose of the study	Reference
Liquid foods	Apple juice	Investigation the effect of single and combined UV-C and ultra-high-pressure homogenisation (UHPH) treatments on inactivation of *Alicyclobacillus acidoterrestris* spores	(Sauceda-Gálvez et al. 2020)
	Apple and grape juices	Determination of inactivation capacity of laboratory scale UV-C reactor	(Antonio-Gutiérrez et al. 2019)
	Buffer solutions	Investigation the effect of the buffer solution types (phosphate-bufferred saline and peptone water) on UV inactivation of some foodborne pathogens	(Jeon and Ha 2018)
	Carrot juice	Investigation the effect of UV-C and thermal treatments on the shelf life of carrot juice	(Riganakos et al. 2017)
	Carrot-orange juice blend	Investigation the effect of UV-C assisted by mild heat treatment on the inactivation of E. coli, S. cerevisiae, Pseudomonas fluorescens	(García Carrillo, Ferrario, and Guerrero 2017)
	Clear and turbid fruit juices	Investigation the inactivation of Saccharomyces cerevisiae KE162, E. coli ATCC 25922, and Lactobacillus plantarum ATCC 8014 in clear pear juice, turbid orange-tangerine juice and orange-banana-mango-kiwi-strawberry juices	(Fenoglio et al. 2020)
	Grape juice	Determination the effect of different reactor arrangements with recirculation on inactivation of Saccharomyces cerevisia	(Antonio-Gutiérrez et al. 2019)
	Grape must and wine	Investigation of effect of UV-C treatment of grape must on the sensory characteristics	(Golombek et al. 2021)
	Orange juice	Investigation the individual and combined efficacies of mild heating and UV-C treatment on inactivation of E. coli O157:H7	(Pagal and Gabriel 2020)
	Orange-tangerine juice blend	Investigation the response of single Saccharomyces cerevisiae KE162 or composited with three cocktails	(Fenoglio et al. 2019)

Cont. on the next pages

Table 2.3. (cont)

Liquid foods	Liquid egg white	Comparison the UV-C resistance of foodborne microorganisms E. coli O157:H7, Listeria monocytogenes, Pseudomonas aeruginosa, and Salmonella enterica	(Gabriel et al. 2017)
	Simulated fruit juice	Investigation the effect of UV-C on inactivation of Cryptococcus albidus, and physicochemical properties	(Feliciano and Gabriel 2019)
	Soymilk	Investigation the effect of temperature on the inactivation kinetics of Salmonella enteriditis by UV-C treatment	(Possas et al. 2018)
	Water	Investigation the effect of 222 nm krypton-chlorine lamp on bacteria	(Ha, Lee, and Kang 2017)
Solid foods	Apple peel and juice	Investigation the effect of UV-C treatment on the inactivation of E. coli, Salmonella enterica and Listeria monocytogens in two steps of the process (before and after juice processing)	(Nicolau-Lapeña et al. 2022)
	Apple	Comparison the efficacy of UVC-LEDs and UV-C lamp to inactivate Penicillium expansum spores on apple surface	(Rios de Souza et al. 2020)
	Broccoli and radish sprouts	Investigation the effect of single and combined UV lighting (UV-B and UV-C) treatments on quality preservation and nutraceutical compounds	(Martínez-Zamora, Castillejo, and Artés-Hernández 2021)
	Brown, black, and red rice	Determination the formation of fungal colonies, mycotoxins, phenolic compounds, cooking quality and color properties	(Ferreira et al. 2021)
	Chicken breast fillets	Investigation the effect of UV-LED treatment on the reduction of microbial load and quality parameters	(Soro et al. 2021)
	Coconut flakes	Investigation the effect of UV-C treatment on Salmonella enterica serovars	(Gabriel et al. 2018)
	Cold-smoked and raw salmon fillets	Investigation the ability of UV-C treatment to reduce Listeria monocytogenes strains on salmon.	(Holck et al. 2018)
	Dried bay leaves	Determination the efficacy of UV-C irradiation for food safety and quality	(Gabriel, Melo, and Michelena 2020)

Table 2.3. (cont)

	Dried persimmon	Investigation the effect of the UV-C treatment on molds and determination of the inactivation kinetics	(Gündüz and Korkmaz 2019)
	Egg	Investigation of the effect of pulsed light on the inactivation of bacteria during storage	(B. Wang et al. 2021)
	Fresh and frozen berries	Investigation chemical safety of UV-C irradiated berries, sensory quality, and inactivation of bacterial and viral pathogens	(Butot et al. 2018)
	Fresh-cut lotus root	Investigation the effect of UV-C treatment on the quality of lotus roots	(D. Wang et al. 2019)
	Grape tomato and spinach	Determination the optimum process parameters of UV-C treatment to reduce microbial load	(Yao and Chen 2021)
	Leafy vegetables	Investigation of effect of postharvest UV-C treatments on primary (protein, dietary fiber) and antioxidative compounds (carotenoids, chlorophylls) and microbial population	(Gogo et al. 2017)
	Maize and peanut	Investigation the effect of UV-C treatment on Aspergillus flavus and Aflotoxin B1	(Udovicki et al. 2022)
	Oyster mushroom	Investigation the effect of UV-C treatment on quality parameters and senescence of oyster mushroom	(Q. Wang, Chu, and Kou 2017)
	Peanuts	Investigation the effect of three type of UV (UV-A, UV-B and UV-C) treatments on aflatoxin reduction and oil quality of peanuts	(Shen and Singh 2022)
	Sliced cheese surfaces	Investigation the basic properties of a 222 nm krypton-chlorine lamp and inactivation efficacy against foodborne pathogens	(Ha, Lee, and Kang 2017)
	Spinach	Investigation the effect of UV-C treatment on sensorial, microbial and psycochemical properties of spinach during three different maturity stages	(Martínez-Sánchez et al. 2019)
	‘Şalak’ apricot	Investigation the effect of the UV-C treatment on inactivation of the natural flora found on cv. ‘Şalak’ apricot surfaces	(Hakguder Taze and Unluturk 2018)

Table 2.3. (cont)

	Walnut	Evaluation the decontamination efficacy of pulsed UV light on walnut and the effect of quality characteristics	(Izmirlioglu, Ouyang, and Demirci 2020)
	Wheat flour	Investigation the impact of UV-C treatment on solubility behavior and structural analysis of wheat proteins	(Kumar et al. 2021)
Surface decontamination	Plastic, stainless steel (ss), glass	Investigation of the resistance of SARS-CoV-2 on inanimate surfaces during UV-C treatment	(Gidari et al. 2021)
	Polyethylene (PE), stainless steel (SS) and raw salmon	Investigation the effect of two light-based technologies (UV-C and pulsed light) on decontamination of different surfaces (PE and SS) that inoculated with typical microbiota of salmon	(Pedrós-Garrido et al. 2018)
	Stainless steel (SS)	Investigation of effect of UV-C on inactivation of Salmonella spp.	(Gabriel et al. 2018)

2.1.4. Inactivation Mechanism of UV light

UV light has a germicidal effect on different microorganisms, including bacteria, viruses, protozoa, molds, yeasts, and algae (Bintsis, Litopoulou-Tzanetaki, and Robinson 2000). UV light treatment generally inactivate microorganisms by damaging genetic material structure. Nucleic acids, which are responsible for the reproduction of microorganisms, can absorb UV light in the range of 200 and 310 nm wavelength (Koutchma, Forney, and Moraru 2009).

UV-C light has different inactivation mechanisms on microorganisms. The most common one is the formation of pyrimidine dimers (cyclo-butyl type dimers) under the influence of UV light. Both DNA and RNA of microorganism cells consist of purines (adenine and guanine) and pyrimidines (cytosine, thymine, and uracil) (Koutchma, Forney, and Moraru 2009; Bouslimi et al. 2012). When microorganisms are exposed to UVC light, bonds are formed between adjacent pyrimidine dimers on DNA or RNA strand. Due to this dimer formation, the replication mechanism of microorganisms is damaged, the cell cannot reproduce and eventually dies (Koutchma, Forney, and Moraru 2009).

According to Bintsis, Litopoulou-Tzanetaki, and Robinson (2000), purines are about 10-fold more resistant than pyrimidines to photochemical changing. Some purine modifications also occur, and these modifications are biologically insignificant. The actual inactivation mechanism is the formation of pyrimidine dimers. It is reported that the UV resistance of microorganisms can be listed as viruses, bacteria and protozoa, respectively. UV-C dose treatment of 40 mJ/cm^2 is determined as the typical UV fluence for inactivation of microorganisms (except Adenovirus 40) and enough to inactive *Vibrio cholerae, Shigella dysenteriae, E. coli O157:H7, Salmonella typhi, Shigella sonnei, Salmonella enteritidis,* Hepatitis A virus, Poliovirus Type 1, Coxsackievirus B5,

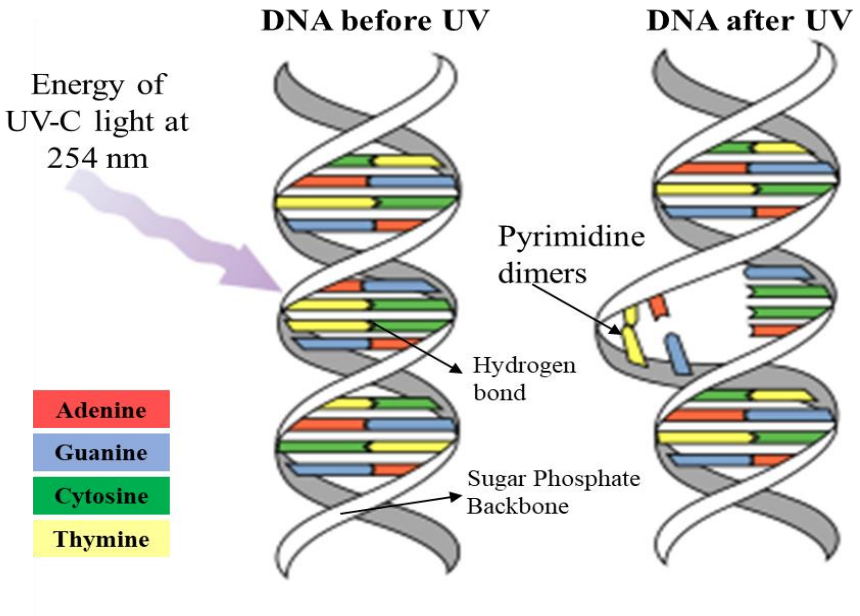

Figure 2. 2. Inactivation Mechanism of UVC Light on Microorganism Genetic Material (Source: Koutchma et al., 2009)

Rotavirus SA11 (Templeton, n.d.). Furthermore, Gram (+) bacteria (e.g., *Staphylococcus aureus, Streptococcus thermophilus, Bacillus cereus, Clostridium botulinum*, and *Listeria monocytogens*) are more resistant to UV-C treatment than Gram (-) bacteria, such as *Pseudomonas flourescens, Campylobacter jejuni, Escherichia coli, Salmonella*, and *Shigella* species (Koutchma, Forney, and Moraru 2009).

In addition to damaging DNA, recent studies reveal the different inactivation mechanisms of UV light on microorganisms. The UV light can inactivate the microorganism via lipid oxidation and protein alteration (Kebbi et al. 2020). UV light can cause a photochemical reaction of protein molecules in the cell apart from DNA or RNA.

Proteins can absorb UV light at 280 nm and below 240 nm wavelength (Kowalski 2009). It has been reported that UVA light led to tRNA photo-damage and slackening in protein synthesis can be observed. Due to the protein damage, amino acid oxidation and other modifications to biochemical processes, such as glycosylation and phosphorylation, can occur, and eventually, cell death is observed (Kebbi et al. 2020).

The final inactivation mechanism of UV light is lipid oxidation. The UVA light is mainly associated with reactive oxygen species (ROS) formation. ROS attacks the cell membrane of the microorganisms due to the lipid content. Fatty acids in the phospholipid bilayer of cell membrane oxides and pore formation occur on the cell membrane. The structural change of the cell membrane leads to cell death (Kebbi et al. 2020).

2.1.5. Advantages and Disadvantages of UV Light Treatment

Choudhary and Bandla (2012) summarizes the advantages of UV-C light for decontamination of food products or food contact surfaces as follows:

- UV-C application is safe.
- Applying UV-C radiation on food surfaces does not leave chemical residue on food surfaces.
- UV-C treatment increases the shelf life of food products and improves the antioxidant capacity of food products.
- There is low investment and operating costs for UV-C installation.
- There are no legal restrictions about UV-C treatment on foods.

Like every technique, UV-C treatment of food has some drawbacks too. First handicap is penetration capacity of UV-C light in the liquid materials. UV-C light has a short penetration depth in absorbent materials (Barut Gök, Gräf, and Stahl 2020). When a material is exposed to the UV light, UV light can be absorbed by the material or transmitted into the material or reflected from the material. The behavior of UV light pattern depends on the material optical and physicochemical properties for liquids. Liquids in terms of optical properties can be transparent, semi-transparent, or opaque (Koutchma 2021). Transparent liquids such as clear juices easily absorb UV light. On the other hand, semi-transparent and opaque liquids such as cloudy juices can not effectively absorb UV light due to the containing suspended solids. Absorbance (A) values these liquids can be listed as follows:

- A < 1 for transparent liquids
- 1 < A < 2 for semi-transparent liquids
- A > 1 for opaque liquids (Koutchma 2021).

Furthermore, physicochemical properties of the liquids such as viscosity, dissolved solids (°Brix), pH and turbidity can affect the delivery of UV light into the liquid (Koutchma 2021). 30% of the UV intensity is lost through 40 cm of distilled water, 10 cm of sea water and 5 cm of 10% sucrose solution. Therefore, lethal action of the UV-C light can be diminished by these properties. In solids, penetration capacity of UV light is limited due to absorption of the UV light from opaque solid materials. Therefore, UV-light is appropriate only for surface decontamination of solid products and food contact surfaces for low penetration capacity (Fan, Huang, and Chen 2017).

Secondly, UV-C treatment is inappropriate for non-uniform (indented) surfaces. The blind spots might occur on the surface of the product. During the UV-C light treatment, the non-uniform-shaped product like apple, apricot, blueberries, etc. is exposed to light from all directions with different angles. Some surface points of the products are fully exposed to UV-C light, but UV-C light cannot reach some parts of the product, such as spacing and blooming close to the stem of the product for the irregular shape of the surface points. Finally, these parts are called blind spots and are not exposed to the same amount of UV light as the fully irradiated part. Hence, formation of blind spot means ineffective pasteurization/sterilization condition (Fan, Huang, and Chen 2017).

2.1.6. UV Light Terminology

UV radiation is a form of electromagnetic radiation; therefore, UV light emits radiant energy to the environment. To clearly understand this phenomenon, (Barut Gök, Gräf, and Stahl 2020), (Gayán, Condón, and Álvarez 2014), (Koutchma 2021), (Falguera et al. 2011) and (Bolton and Linden 2003) have discussed the UV radiation concept in detail.

Radiant power (Φ) is a radiant energy in W or mW unit that is emitted from all directions by a radiation source (Gayán, Condón, and Álvarez 2014). The output radiant power supplied by LPM and MPM lamps are about 30% and 10% of the total radiant power of the lamps, respectively (Koutchma 2021).

Irradiance (E) is defined by Gayán, Condón, and Álvarez (2014) as "the radiant power per surface area reaching an infinitesimal surface element d*S* from all directions." Unit of irradiance is W/m^2 or mW/cm^2, or $\mu W/cm^2$.

Fluence rate (E´) and **incident UV intensity (I_0)** terms are analogues of irradiance term, and their unit is W/m^2 or mW/cm^2, or $\mu W/cm^2$, but there is a nuance between them. Fluence rate means that the radiant power passing from all directions through an infinitesimally small sphere of cross-sectional area d*A*, divided by d*A*. Therefore, fluence rate term is suitable for UV disinfection, since microorganisms are affected from any direction during the UV treatment, whereas irradiance or UV intensity terms are suitable for surface irradiation applications (Gayán, Condón, and Álvarez 2014; Bolton and Linden 2003). In summary, fluence rate term can be used in the UV treatment of the liquid products such as fruit juices and water, while irradiance and UV intensity terms are used in the UV treatment of food surfaces or food contact material surfaces (stainless steel, plastics, etc.) in the food industry.

UV dose (D) or **incident fluence (H_o)** term that is widely used in UV disinfection literature can be expressed as the total amount of radiant energy from all direction incident on an infinitesimally small sphere of cross-sectional area *d*A divide by *d*A. The unit of these terms is J/m^2 or mJ/cm^2 (Koutchma, Forney, and Moraru 2009; Koutchma 2021). The difference between UV dose and the incident fluence terms is that fluence is appropriate to define incident UV energy, but UV dose is generally used to determine absorbed UV energy by the microorganisms since nearly all incident UV light impinge on the microorganisms, but a few portions of the incident light is absorbed by the microorganisms (Bolton and Linden 2003). Determination of UV dose is generally made with "Bench scale" or "Collimated beam" apparatus.

The relation between the incident fluence (H_0) and incident UV intensity (I_0) can be expressed as incident fluence is calculated by the multiplication of the incident UV intensity with exposure time (in seconds).

$$H_0\ (mJ/cm^2) = I_0\ (mW/cm^2) \times t_{exposure}\ (s)$$

Incident irradiance of the UV lamps is generally stated by the manufacturer, but it should be also measured with radiometers time by time. Thus, incident irradiance taken by the radiometer is multiplied the exposure time and the incident fluence is obtained.

In the liquids, **average UV dose or fluence (H_{avg})** is calculated with the multiplication of known absorbed UV irradiance (I_{avg}) with the exposure time.

$$H_{avg}\ (mJ/cm^2) = I_{avg}\ (mW/cm^2) \times t_{exposure}\ (s)$$

The delivered or **germicidal UV fluence** or **dose (H_{germ})** is another term. It means that the remaining available energy in the product that is virtually delivered to the microorganisms (Koutchma 2021).

The transmitted UV fluence (H_{trans}) is defined as remaining fluence that is not absorbed by the microorganisms and liquid. Transmitted fluence can be calculated by subtracting of absorbed and delivered fluence from the incident fluence (Koutchma 2021).

$$H_{trans} = H_0 - H_{avg} - H_{germ}$$

Decimal reduction dose (D_{UV}) is a dose that is the necessary to reduce 90% of the initial microbial load (Falguera et al. 2011). All concepts that are defined above are illustrated in Figure 2.3.

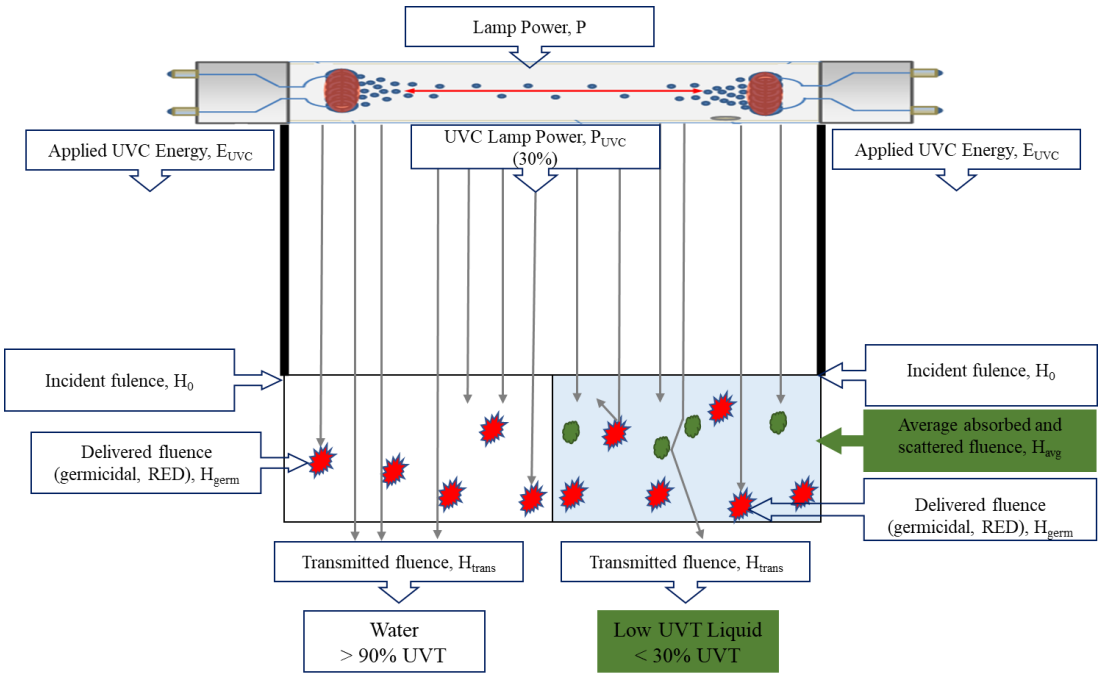

Figure 2. 3. UV terminology scheme (Source: Koutchma, 2019)

In water treatment, reduction equivalent dose, operational dose, and design dose terms for continuous reactors are also used. **Reduction equivalent dose (RED)** is defined as the dose that is appointed to a UV reactor based on the reactor validation testing. It can be also measured with bench-scale UV-C apparatus for inactivation of the target microorganism. **The design UV dose** in the mJ/cm^2 unit is used to size the UV disinfection system. It means that the RED to require a specific logarithmic inactivation of the target microorganism. **Operational UV dose** is a dose obtained from the results of the equipment validation testing. It can be beneficial for determination of the reactor behavior (Koutchma 2021).

2.2. Methods for the Determination of UV Dose

The following terms for characterization of UV light lethal action are often used: total UV energy, applied UVC energy, incident fluence, average absorbed fluence and delivered or germicidal fluence (dose). Determination of the delivered UV dose on the microorganisms is a prominent issue due to indicator of the effectiveness of UV process and providing microbial safety of the products (Koutchma 2021). The concept for specifying the dose delivered to an object is called as dosimetry. Radiation dosimetry is defined as a process of identifying radiant energy absorbed in a specified object from the radiation source (Arshak 2006). Dosimetry is subdivided two groups: absolute dosimetry and relative dosimetry. Absolute dosimetry means obtaining data directly about absorbed dose, and measurements are performed with detectors such as calorimetry, ionometry, and chemical dosimetry. On the other hand, relative dosimetry needs a reference measurement to compare with experimental results (Butson et al. 2003). Biodosimetry, actinometry, computational fluid dynamics (CFD) are among the most common methods used in the determination of UV dose in the food industry. Recently, there are a few examples of the use of radiochromic films for this purpose.

2.2.1. Biodosimetry

Biodosimetry is the most consistent method to determine the delivered UV dose to the product (Guerrero-Beltrán and Barbosa-Cánovas 2004). Biodosimetry in principle measures the rate of inactivation of the target microorganism. In biodosimetry, firstly, the known amount of the target microorganism is inoculated into the product, and then the

product is exposed to the UV treatment at a specified UV irradiance and time. For this purpose, the collimated beam apparatus with LPM lamps (static system) or continuous UV reactors are generally used. After the treatment, the inactivation ratio of the microorganism is calculated by comparing the concentration of the viable microorganisms in the unirradiated (before UV treatment) and the irradiated (after UV treatment) samples. *Escherichia coli* K12 is generally used as target microorganisms for fruit juices, since it is a surrogate of the *E. coli* O157:H7. To calculate delivered UV dose, UV dose-response curve is obtained by plotting UV dose against inactivation rate data taken from the system (Koutchma, Forney, and Moraru 2009). In the plot, x-axis represent inactivation rate of the target microorganism which is the logarithmic ratio of the number of the viable microorganism (N) in irradiated sample to the initial number of the microorganisms (N_0) in unirradiated sample, and the applied UV dose values that are obtained from multiplication of the certain UV irradiance with the exposure times are replaced at the y-axis (Atılgan 2013). Thus, the delivered germicidal UV dose determined by the curve is called as the reduction equivalent dose (RED) and it is between the minimum and the average UV dose values of the system (Koutchma, Forney, and Moraru 2009). Principles of the biodosimetry is summarized in the Figure 2.4.

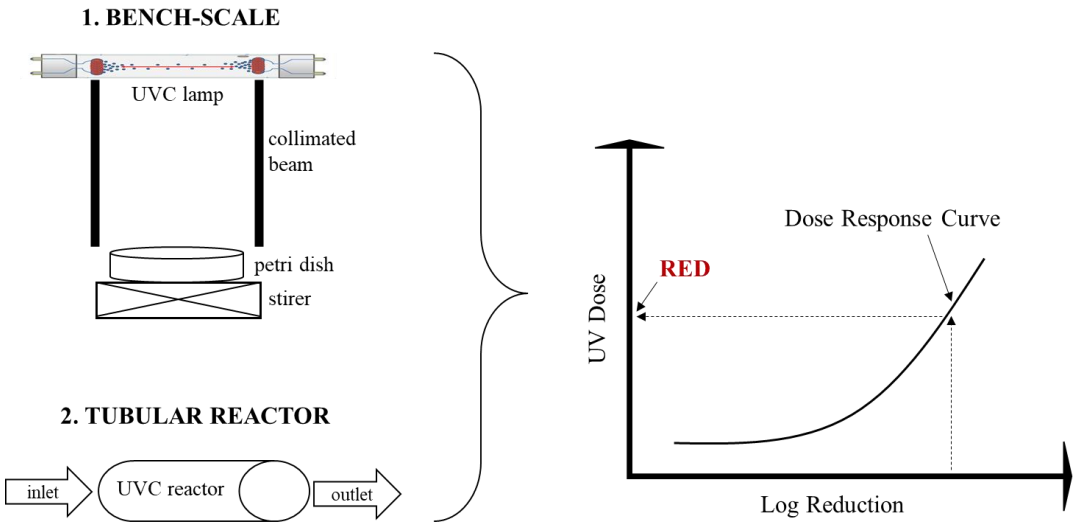

Figure 2. 4. Principles of Biodosimetry (Source: Atılgan, 2013)

The specified UV irradiance at the surface of the product is usually measured with a calibrated radiometer. Radiometer is a portable device in which thermal or photonic UV sensors are used to determine emitted radiant energy by the source (Guerrero-Beltrán and Barbosa-Cánovas 2004). Radiometers measure the incident UV

intensity at the surface of the material (Koutchma 2021). All radiometers basically consist of a diffuser, a filter, a detector, case and printed circuit board (Banerjee et al. 2017). The light came from all directions is collected by the diffuser and it transmits the light uniformly to the filter. The filter portions each wavelength inside the light and convey the proportions to the detector. Detector is silicon-made material. It converts light to the electrical signal. According to chemical composition of the detector, the spectral response of the radiometer is determined. To display the detector output, printed circuit board is installed on the case. The case is outer frame of the radiometer and protects the electronic components. The main difficulty when using a radiometer is calibration of the device. Radiometers should be sent the manufacturer for calibration once a year since the detector of them losses the performance (Qiang et al. 2015). This process is both time-consuming and costly. Also, radiometers measure the UV intensity on the planar surfaces. Furthermore, radiometers fixed at a point can not measure the correct UV intensity of solutions. This means that radiometers can not be used to determine the average intensity in the absorbent solutions in a reactor.

Biodosimetry is an efficient method to determine the germicidal UV dose, but it has also several handicaps (Adhikari, Koutchma, and Beecham-Bowden 2005; Koutchma, Forney, and Moraru 2009). First, biodosimetry is the time-consuming process. Secondly, the germicidal UV dose is based on the confidence interval of microbial enumeration. The error made on the enumeration cause the wrong results. Thirdly, all microorganisms should be exposed to the same UV irradiance to accept the germicidal UV dose value as correct. If there is a dose distribution among the microorganisms, the germicidal UV dose should be given as the volume average germicidal reduction dose which is lower than the arithmetic mean of the UV dose distribution.

2.2.2. Chemical Actinometry

Incident UV intensity (irradiance) emitted in UV-C reactor system can be measured by chemical actinometry method. The advantages of chemical actinometry over radiometers are calibration-free method and suitable for the changing reactor geometry (Qiang et al. 2015). It is simpler and not require cross- validation with other radiometric methods (Noori et al. 2018). Principle of the chemical actinometry is based on determining the amount of products produced in the photochemical reactions (Guerrero-

Beltrán and Barbosa-Cánovas 2004). In other words, a chemical actinometer is exposed to a light-induced reaction with a known quantum yield (Φ).

In the photochemical reactions, there are several reaction mechanisms (Bolton, Mayor-Smith, and Linden 2015). These reaction mechanisms can be expressed with the Jablonski Energy Diagram (Figure 2.5). When the reactant molecules absorb photon energy from the lamp which should be monochromatic since the reaction depends on the excitation wavelength, they are excited from ground state (S_0) to excited state (S_1, S_2, T_1 or T_2) (Bolton, Mayor-Smith, and Linden 2015; Bouslimi et al. 2012). At the excited state, molecules have higher energy level and unstable. They try to get rid of the excessive energy. Thus, to return the ground state, they release the excessive energy as heat, or they can made fluorescence or phosphorescence, and the excited molecule deactivate itself at the end of these processes. For a photochemical reaction, quantum yield, Φ, is a measure to determine the fraction of these deactivated molecules (Falguera et al. 2011). It can be expressed as

$$\Phi = \frac{total\ number\ of\ deactivated\ molecules}{total\ number\ of\ photons\ absorbed} \tag{2.1}$$

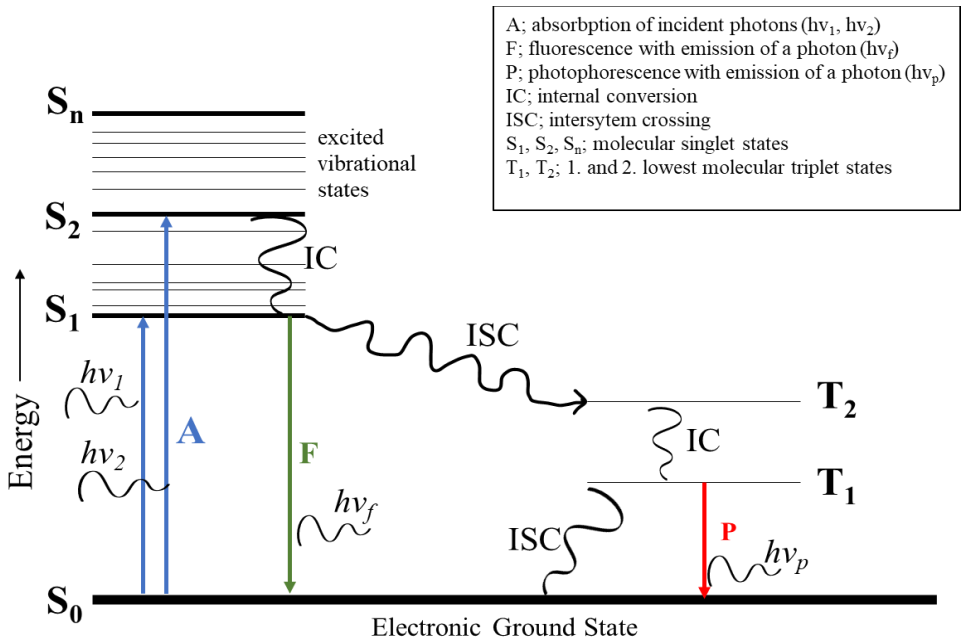

Figure 2. 5. Jablonski Energy Diagram (Source: Bolton et al., 2015)

The well-known chemical actinometers for determining the UV fluence are potassium iodide/iodate and potassium ferrioxalate actinometers (Rabani et al. 2021).

Potassium ferrioxalate actinometry is one of the most preferred methods in chemical actinometry due to some advantages such as easy and fast to use, known quantum yields, not require stirring and quantum yields not depend on extrinsic factors (temperature, light intensity, wavelength etc.) (Murov et al. 1993). It is also recommended by IUPAC (Lehóczki, Józsa, and Ősz 2013). Principle of the method is determination of amount of Fe(II) - 1,10-phenanthroline complex at 510 nm wavelength (Murov et al. 1993). This method is recommended on actinometric applications between 200 and 450 nm (extremely broad range) wavelength (Lehóczki, Józsa, and Ősz 2013). Reaction mechanism is

$$2Fe^{+3} + C_2O_4^{-2} \rightarrow 2Fe^{+2} + 2CO_2 + h\nu \tag{2.2}$$

Potassium iodide (KI)/iodate (KIO_3) actinometry is based on the measurement of the linear formation of triiodide molecules at 352 nm wavelength. This method is suitable for determining the UV intensity emitted from UV lamps at the 254 nm wavelength (Kuhn, Braslavsky, and Schmidt 1989). KI actinometer works at the wavelength below 290 nm and cannot absorb the light above at the 330 nm wavelength (Qiang et al. 2015). Therefore, it is specific for the UV-C region and resistant to room light. Rahn (1997) developed this method as an alternative to potassium ferrioxalate actinometer. The superiorities of the method over the ferrioxalate actinometry can be listed as

- simplified preparation of solutions,
- direct detection of end point,
- elimination of acid solutions, and
- no need to work in the dark (Rahn et al. 2003).

In the presence of suitable solvent that is ultrapure water, a charge transfer occurs in iodine molecules (Equation 2.3). After charge transfer, a caged complex is formed from iodine atom and an electron (Equation 2.4) (Rahn 1997).

$$I^- + H_2O \ + \ \mathrm{h}v \rightarrow I^-H_2O^* \tag{2.3}$$

$$I^-H_2O^* \rightarrow (I, e^-) + H_2O \tag{2.4}$$

This caged complex (I,e^-) undergoes to two different reaction. The first reaction (Equation 2.5) is called as a back reaction which is a reaction between electron and iodine atom to reform iodide.

$$(I, e^-) \rightarrow \ I^- \tag{2.5}$$

The other reaction (Equation 2.6) is breakdown of the caged complex. Thus, the electrons migrate from the caged complex into the solution.

$$(I, e^-) \ \rightleftharpoons \ I \ + \ e^-_{aq} \tag{2.6}$$

If there is no electron scavenger in the solution, the back reaction becomes dominant, and the aqueous electrons recombine with the iodine atoms to form iodide. These iodide atoms in the solution react with an equivalent number of iodine atoms to form triiodide.

$$I + I^- \rightarrow \ I_2^- \tag{2.7}$$

$$2I_2^- \rightarrow I_3^- \ + \ I^- \tag{2.8}$$

Thus, the overall reaction mechanism of the KI actinometry can be expressed by

$$8I^- + IO_3^- + 3H_2O + hv \rightleftharpoons 3I_3^- + 6OH^- \tag{2.9}$$

Triiodide molecules are formed by the reaction of iodide and iodate molecules (Rahn, Xu, and Miller 1999). The role of the iodate molecules is electron scavenger and prevents back reaction of the free electron with the iodine atom following UV excitation of KI (Rahn 1997). The irradiance at a specified distance from the lamp is obtained at the

end of the photochemical reactions. Then, the UV fluence value is calculated by the production of irradiance obtained from the actinometry and the exposure time.

2.2.3. Computational Fluid Dynamics (CFD)

In continuous reactors, computational fluid dynamics (CFD) method can be used to determine UV fluence distribution as well as to simulate the fluid flow throughout a specified reactor geometry (Koutchma, Forney, and Moraru 2009). CFD is a numerical method which is based on fluid dynamic principles to predict the flow behavior of fluid particles in geometrical systems (Atılgan 2013). The flow behavior simulation is obtained using the continuity, momentum, and mass transfer equations (Patras et al. 2020).

CFD method consists of three main steps. The first step is called as **pre-processing of the domain**. The pre-processing step is crucial since it is based on correctly defining the physical problem and the system properties' proper determination, such as boundaries of reactor geometry and construction of grid structure (Atılgan 2013). After the determination of the physical problem and working conditions, the **processing step of the domain** can be performed by a suitable CFD solver (Patras 2020). In the food industry, FLUENT, COMSOL, PHOENICS, and CFX are some of the most preferred CFD solver programs. In this step, the equation of continuity, momentum, and mass transfer equations belonging to the system are converted into algebraic form and solved with direct or iterative methods at grid elements (Atılgan 2013). The UV fluence rate is measured by integrating local UV irradiation and the residence time of particles in the reactor during the determination of the flow pattern of the fluid. The fluence distribution of the reactor is given in the flow volume (Patras et al. 2020). The last step is the **post-processing step**. The results obtained from the program are visualized in numerical and graphical forms (Atılgan 2013).

2.2.4. Radiochromic Film Dosimetry

Radiochromic dosimeters can be thin or thick films, gels, liquid solutions, and liquid-care waveguides for ionizing and nonionizing radiation (Miller, Batsberg, and Karman 1988; Niroomand-Rad et al. 1998). In 1826, the radiochromic reaction of bitumen was discovered and reported by Niepce (Niroomand-Rad et al. 1998; Butson et

al. 2003). Before the discovery of radiochromic reactions, papers and gels containing potassium dichromate were used for direct imaging reactions (Niroomand-Rad et al. 1998). Barium platinocyanide pastille discs were also used to determine absorbed radiation dose at the beginning of the 20th century (Soares 2006).

In recent years, radiochromic films (RCF) have been used for measurement of radiation dose in ionizing and nonionizing radiation applications. RCFs are used for environmental monitoring of radiation levels, medical physics, radiobiology (dose-effect curves), industrial applications (food irradiation, sterilization, cross-linking of materials), radiation hardness (space applications), and beam diagnostics (Butson et al. 2003). Advantages of the using RCF are low cost requirement, minimal processing, high spatial resolution, and high exposure sensitivity (Devic, Tomic, and Lewis 2016). Investigations on radiochromic film dosimetry have been carried out at Risø National Laboratory. These RCFs consisted of polyvinyl butyral (PVB) and pararosaniline due to compatibility with each other (Miller, Batsberg, and Karman 1988). After 1986, Gafchromic™ manufactured the first radiochromic films (Casolaro et al. 2019).

RCFs are transparent or opaque, colorless two-dimensional (2D) films. RCFs provide absolute dose measurement (Devic, Tomic, and Lewis 2016). Densitometers, scanners, and spectrophotometers can be used to read the color values of RCF (Casolaro et al. 2019).

Some characteristics are expected to be satisfied by RCF. These properties can be listed as; sensitivity, image stability, ease of use, tissue equivalence, rate dependence, light dependence, environmental stability, ruggedness, size and construction, and uniformity (Soares 2006).

The main application areas of radiochromic films are medical physics, radiation damage of electronic devices, beam diagnostics, radiation processing of foods, and medical instrumentation (Casolaro et al. 2019). Radiochromic films have been used as a dosimeter in ionizing irradiation of foods and in medical and industrial applications, as well as in monitoring UV rays in terms of occupational safety (Yan et al. 2017). For food irradiation and sterilization applications, the films which can give a response at the range from 10 to 1000 Gy dose is necessary, while response to 0.1-10 Gy dose is enough for medical physics (Butson et al. 2003).

The reaction mechanism of RCF is based on the coloration of the films due to the radiation absorption. Any latent thermal, optical, or chemical reactions are unnecessary for color formation (Butson et al. 2003). RCF gradually turns out the blue color with different color values when exposed to radiation treatment. There are some mechanisms for color formation. One of them is photopolymerization. In photopolymerization, cross-linked carbon chain materials are formed by covalent bonds. Another mechanism is *cis-trans* isomeric dissociations or conversions, and ketonic, anilic, and enolic bonds can be formed at the end of the reactions. When radiation exposes RCFs, relatively slow first-order solid-state polymerization occurs, and then homogenous, planar polyconjugation along the carbon-chain backbone is obtained (Niroomand-Rad et al. 1998).

The known radiochromic film firms are Gafchromic™ films produced by ISP Technologies (Wayne, NJ), Far West Technology, Inc. (Goleta, CA), the GEX Corporations (Centennial, CO), and Gordan Patel at JP Laboratories (Middlesex, NJ) (Soares 2006).

Gafchromic™ films are the first improved and mainly used RCF and generally preferred in medical applications (Butson et al. 2003). These films are suitable for dose mapping, using near interfaces of different materials and product surfaces (Miller, Batsberg, and Karman 1988). They are manufactured as spherical film emulsions (chromophores) based on polydiacetylene, and colorless films turn into colored forms with the irradiation treatment (Soares 2006). Gafchromic™ recently manufactures radiochromic films for radiology and radiotherapy studies. XR series (CT2, M2, QA2, RV3) are produced for fast and precise measurements in modern medical centers, whereas EBT, HD-V2, MD-V3 and RTQA2 series are produced for applications in radiotherapy field at the processor-less environment of modern medical centers (Gafchromic 2022). Gafchromic™ films have transparent yellow color at original and they turn from yellow color to blue color under the radiation treatment. These films are room light resistant, and stable at temperatures at up to 60^{o}C. Films have the same emulsion sensitivity but different emulsion thickness and film constructions (Soares 2006). Structure of these films is shown in Figure 2.6 and other properties are listed in Table 2.4.

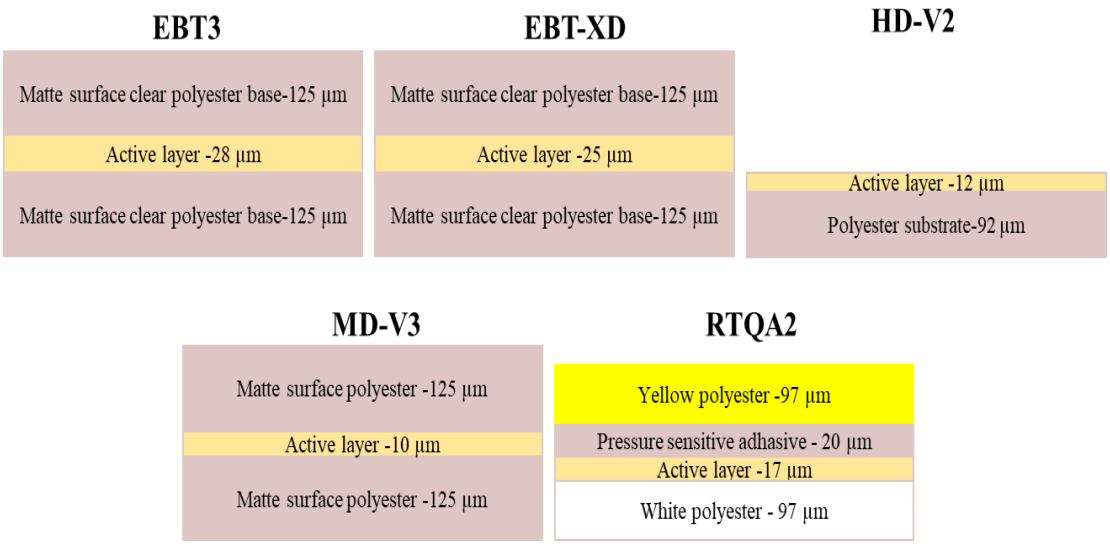

Figure 2. 6. Gafchromic Radiochromic Films Structure Profile

Table 2. 4. Gafchromic Films General Properties

Film Type	Dynamic Dose Range, Gy	Color change wavelength, nm	Application area
EBT3	0.1-20	633	Measurement of absorbed doses of ionizing radiation
EBT-XD	0.1-60	633	Measurement of absorbed doses of ionizing radiation
HD-V2	10-1000	670	Quantitative measurement of absorbed dose of high-energy photons
MD-V3	1-100	635	Quantitative measurement of absorbed dose of high-energy photons
RTQA2	0.02-8	Not specified	Light field alignment Radiation field alignment Precision star shots Position verification for HDR Autoradiography of implantable seeds, plaques and other sources

Far West Technology manufactures FWT films coded as FWT-50, FWT-60, and FWT-70 series (FWT 2022). FWT-50 series known as alanine dosimeters is produced for low- and high-level radiation doses. FWT-60 series is suitable for high dose level radiation and FWT-70 series is designed for low dose level radiation applications. The firm also produces radiochromic readers.

Alanine dosimeters are designed for dose measurement in the diverse radiation fields such as radiotherapy, blood component irradiators and industrial irradiation facilities. They are produced as pellets. Dynamic dose range of the pellets is 2 Gy - 200 kGy. They show sensitivity to temperature and humidity.

FWT-60 series are suitable for high dosage applications such as radiation processing, food irradiation, and sterilization (Soares 2006). The active agent of the films is hexa(hydroxyethyl) aminotriphenylacetonitrile (HHEVC) that is colorless derivatives of the family of the aminotriphenyl-methane (triphenylmethane leucocyanides) dyes. The host material of the film is nylon. Original color of the films is transparent blue and it turns deep blue color depending on the applied UV dose with the lower than 350 nm UV treatment (FWT 2022). The peak color wavelength is 605 nm. Dynamic dose range of the films is 0.5-200 kGy. Films have temperature and humidity dependence. Response of the films decreases <20^{o}C at 50% humidity level and 30 kGy radiation treatment and they are stable at room temperature. Humidity level greater than the 50% cause a decrease in the response at 20^{o}C. They should be stored at dark places due to the sensitivity of the UV fraction came from the daylight.

Finally, FWT-70 series dosimeters are small optical waveguides (3 mm diameter and 5 cm length) and appropriate for low dose level radiation processing. They also consist of HHEVC dye. Dynamic dose range is 0.1-20 kGy.

The GEX Corporation and **Gordhan Patel at JP Laboratories** are the other film manufacturers. Gordhan Patel improved the SIFID detector for radiochromic films. The GEX Corporation puts a series of dosimeters (B3 dosestix, B3 WINdose, B3 FAQ's) and a B3 detector on the market (GEX 2022; Soares 2006). B3 series dosimeters are sterilized and individually numbered dosimeters. GEX dosimeters consist of pararosaniline cyanide dye and polyvinyl butyral (PVB). The color of the dosimeters is pink at unirradiated state and under radiation treatment they turn to purple color. Dose range of the dosimeters are 1-150 kGy. The peak color wavelength is determined as 552 nm. They are resistant to humidity and stored at 15-30^{o}C in darkness. The shelf life of the dosimeters is 5 years (GEX 2022).

The color change that occurs in RCFs is generally measured with densitometers, scanners and spectrophotometers (Casolaro et al. 2019; Cheung, Butson, and Yu 2005). The latest way to determine the color change of the films is using computer vision systems

(CVS). Densitometers and scanners are most widely used devices to evaluate optical properties and color change of the RCF. Densitometers are devices that measure the optical density. Optical density (OD) is a measurement of the reduction of the light (I) passing through the object (Butson et al. 2003). It can be expressed as

$$OD = log\left[\frac{I_o}{I}\right] \tag{2.10}$$

When the RCF is exposed to different doses of UV light, the color of the RCF changes, meaning that each irradiated RCF has a different OD depending on the applied UV dose. OD increases with an increase in UV dose. Hence, OD is a function of the applied UV dose. The relation between the darkness of the film and the UV dose is non-linear (Butson et al. 2003; Casolaro et al. 2019). Scanners are other devices used to evaluate color variation in films. Digitization of the image of irradiated RCFs is provided with the help of the scanners. Then, the pixel values of the films are evaluated with the appropriate software program. The pixels values are the function of the applied UV dose like OD (Casolaro et al. 2019). The information about spectrophotometers and CVS are given in Section 2.3.2.2. and Section 2.3.2.3., respectively.

2.3. Color Analysis of Films

2.3.1. Color and Color Space

Customers have begun to pay attention to the quality of a food product. Quality parameters of a food product for customers can be listed as appearance, color, and taste. It is stated that the color of a food product is the most important quality parameter for the customer to determine the food quality (Pathare, Opara, and Al-Said 2013). Thus, in the food industry, the measurement of the color of a food product is one of the quality parameters. A system is needed to set the color of an object as a standard.

Generally, the color of an object is identified in three-dimensional (3D) color space (Karma 2020). The earliest color space used for color identification and standardization is Munsell color system (Figure 2.7). According to this system, the color of an object is identified by determining hue (H), value (V), and chroma (C) factors. Hue

means the absorbance of reflection of a specific wavelength of light. Value of color is intrinsic luminosity, and chroma means saturation (Ly et al. 2020).

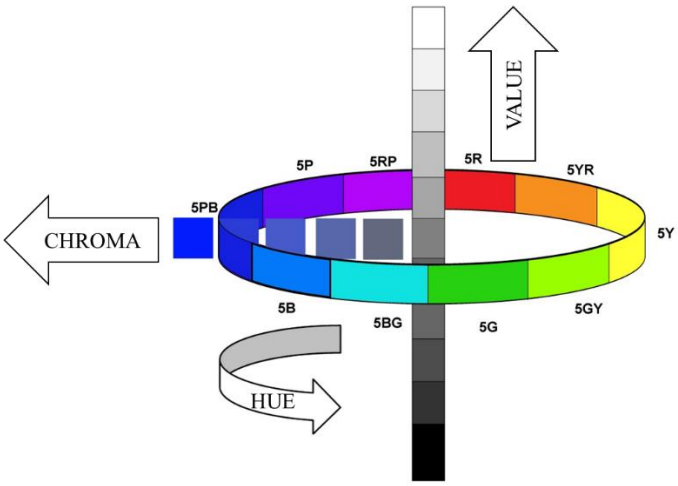

Figure 2. 7. Munsell Color System (Source: URL2)

In 1931, Commission Internationale de l'Eclairage (CIE) published several color identification standards. An object, an observer, and a light source or an illuminant are required to identify the color. According to CIE Standard, the standard illuminant D65 and C lamps can be used as the light source. The standard observer parameters, the mathematical functions, are defined as 2^o and 10^o. While the 2^o observer parameter indicates human vision spectral sensitivity for a small field of view and is usually used for calorimeters, the 10^o observer parameter represents a large field of view and closely correlates with human vision (Ly et al. 2020).

Moreover, RGB (red, green, and blue) and XYZ color systems are introduced by CIE. These systems are called as tristimulus values for color as they are the components of the wavelength of monochromatic red, green, and blue lights (Ly et al. 2020). Each R, G, and B component takes the values between 0 and 255. So, there are 256 x 256 x 256 pieces of different color types, but most of them are indistinguishable from the human eye (Karma 2020).

In 1976, CIE introduced commonly preferred CIEL*a*b* or shortly CIELAB color space. CIELAB system is derived from the Munsell system (Völz 2002). In CIELAB abbreviation, L* symbolizes lightness or luminance and ranges from 0 to 100 whereas, a* and b* values are chromatic components and range between -120 and +120

(Briones and Aguilera 2005). a* indicates the redness-greenness of an object. It takes positive values for reddish colors and negative values for greenish values. On the other hand, b* values indicate the yellowness-blueness of an object. It represents positive values for yellowish colors and negative values for bluish ones (Pathare, Opara, and Al-Said 2013).

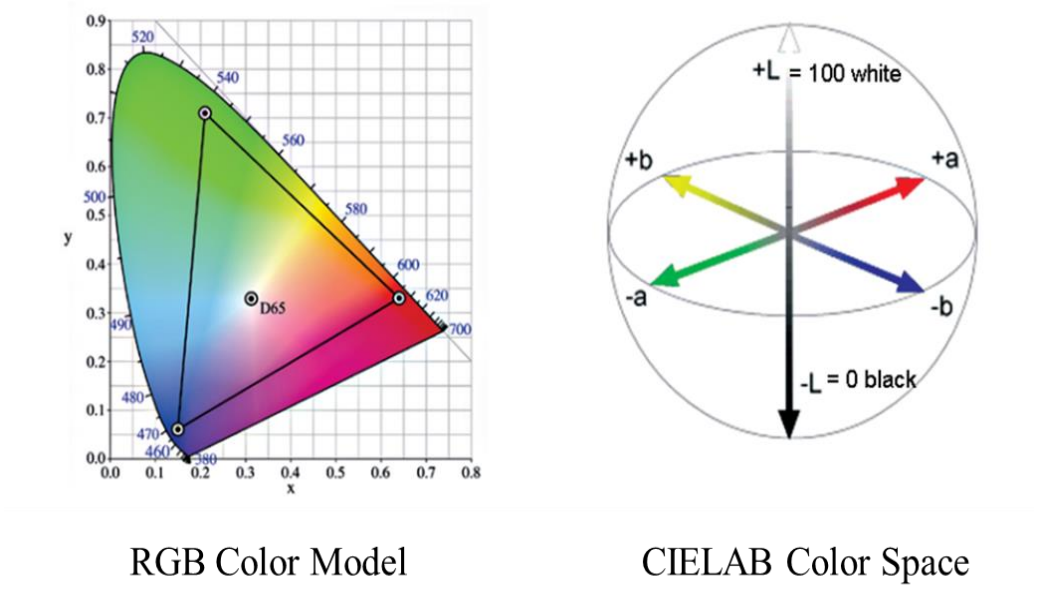

Figure 2. 8. RGB and CIELab Color Spaces (Source: Visscher, 2010)

To obtain meaningful results, L*, a*, b* values of an object can be compared with the control sample. The color difference between a sample and the control is expressed as ΔE. It can be formulated as

$$\Delta E^* = \sqrt{(\Delta L^*)^2 + (\Delta a^*)^2 + (\Delta b^*)^2} \tag{2.11}$$

The greater ΔE* values indicate the more significant color differences between two objects. The Table 2.5 gives the classification of ΔE values for the two objects specified by Karma (2020).

Table 2. 5. ΔE Classification

ΔE values	**Perception**
<1	Not perceptible by human eyes
1-2	Perceptible through close observation
2-10	Perceptible with a glance
11-49	Similar colors
100	Opposite colors

There are some other attributes to describe the colorfulness of an object. Chroma (C*) is a qualitative attribute of colorfulness and indicates the degree of difference of hue in comparison to grey color with the same lightness (Pathare, Opara, and Al-Said 2013). It can be expressed as

$$C^* = \sqrt{(a*)^2 + (b*)^2} \tag{2.12}$$

Another attribute is hue angle (h^o). Hue angle represents a quantitative attribute of colorfulness and specifies the difference of a particular color regarding grey color with the same lightness. It can be calculated as

$$h^\circ = arctan\left(\frac{b*}{a*}\right) \tag{2.13}$$

Hue angle is the degree of color that is generally defined as reddish, bluish, etc. Hue angle degrees are given in the Table 2.6 (Pathare, Opara, and Al-Said 2013).

Table 2. 6. Hue Angle Degrees Correspond to a Color

Angle	**Color Representation**
$0\text{-}360^o$	Red hue
90^o	Yellow hue
180^o	Green hue
270^o	Blue hue

There are also other color space transformations such as CMY, YIQ, HLS, HSB, CIELUV, etc. All of them are listed in Table 2.7. Each of them has different coordinate systems. According to Karma (2020), color space can be divided into two groups:

1.Hardware-oriented color space (RGB, CMY, and YIQ)

2.User-oriented color space (HLS, HCV, HSV, HSB, MTB, CIELAB and CIELUV)

Table 2. 7. Different Color Spaces and Extensions

Color Space	**Expansion of Letters**
CIELAB, CIEL*a*b*	L; lightness, a; redness-greenness, b; yellowness-blueness
CIELUV, CIEL*u*v*	L; luminance, u and v; chromaticity values
CMY	C; cyan, M; magenta, Y; yellow
HCV	H; hue, C; chroma, V; value
HLS	H; hue, L; lightness, S; saturation
HSB	H; hue, S; saturation, B; brightness
HSV	H; hue, S; saturation, V; value
RGB	R; red, G; green, B; blue
YIQ	Y; luminance, I; orange-blue, Q; purple-green

2.3.2. Color Measurement Devices

The color of an object can be determined in several ways. They can be categorized as visual color measurement, instrumental methods for color measurement, and color measurement with a color vision system (Pathare, Opara, and Al-Said 2013).

2.3.2.1. Visual Color Measurement

Visual color measurement is a subjective process in which the color of an object is defined by comparing it to color standards under lighting (Pathare, Opara, and Al-Said 2013). This method is a highly subjective, tedious, and time-consuming process (Udomkun, Innawong, and Jeepetch 2019). So, more objective methods can be preferred to obtain reliable results.

It has been suggested two theories about the perception of color. The first theory is trichromatic color theory. It is mostly accepted theory and explains that the color sensation of an object is actualized by three types of cone cells called as photoreceptors in the human eye (Ly et al. 2020). These photoreceptors are sensitive to blue, green, and red colors. The other one is the rival theory. According to that theory, color perception occurs with the negative effect of certain color pairs (red-green, yellow-blue, and black-white) on each other. It means that color has an inhibitory effect on other pairs of themselves. When the inhibitor signal of color is eliminated, the brain perceives the actual color signal (Ly et al. 2020).

2.3.2.2. Instrumental Methods

Instrumental devices provide objective color measurement. Calorimeters and spectrophotometers are generally used to measure the color of an object (Ly et al. 2020).

Colorimeters are devices based on the principle of measuring the reflected light from a sample by the trichromatic filters inside the device. A calorimeter mainly consists of the illuminant, lens, trichromatic filter, and detector. Light on a specific wavelength is transmitted to the object by the illuminant. The object absorbs the wavelength and reflects the light to the lens. The reflected light is filtered through a trichromatic (red, green, and blue colors) filter, and color data is obtained. The well-known calorimeter brands are Konica Minolta Chromameter CR series, Antera 3D by Miravex Limited, and Colorimeter CL400 by Courage-Khazaka (Ly et al. 2020).

Spectrophotometers are other instrumental devices measuring the transmitted wavelength on the object and reflected light from the object (Pathare, Opara, and Al-Said 2013). Their working principle is similar to colorimeters. Spectrophotometers measure the spectral light between 360 and 700 nm wavelength. They provide high degree accuracy and absolute color detection. Minolta CM508i and CM2002, Check and Mercury of Datacolor, and the Chromasphere can be counted among the most common spectrophotometer brands (Ly et al. 2020).

Colorimeters are used for routine quality control measurements, whereas spectrophotometers are preferred for measurements done by research and development laboratories to provide higher spectral analysis than colorimeters (Pathare, Opara, and Al-Said 2013). Even though colorimeters and spectrophotometers have applicable in a broad

range of areas, they have some drawbacks. Firstly, they need high investment costs. Secondly, they only give average color values of an object, and they provide non-representing color values for the overall appearance of heterogeneous objects. Furthermore, they have a low spatial resolution (Ly et al. 2020; Hutchings, Luo, and Ji 2000).

2.3.2.3. Computer Vision System (CVS)

CVS is non-destructive and one of the most promising technologies for color and size measurements and texture analysis. CVS has several advantages over destructive methods (instrumental methods and human vision). Rapid processing, objective and effective measurement, inexpensive start-up cost, and more versatile evaluation of an object can be specified among the superiorities (Udomkun, Innawong, and Jeepetch 2019; Lukinac et al. 2019).

CVS contains several operations like image capturing, processing, and image analysis. After these operations, the digitization process, which transforms images into numbers, is carried out (Lukinac et al. 2019).

There are some requirements to obtain an image with CVS. Major components of a CVS are the illuminant/s, a digital camera, image acquisition board, computer hardware, and software (Pathare, Opara, and Al-Said 2013).

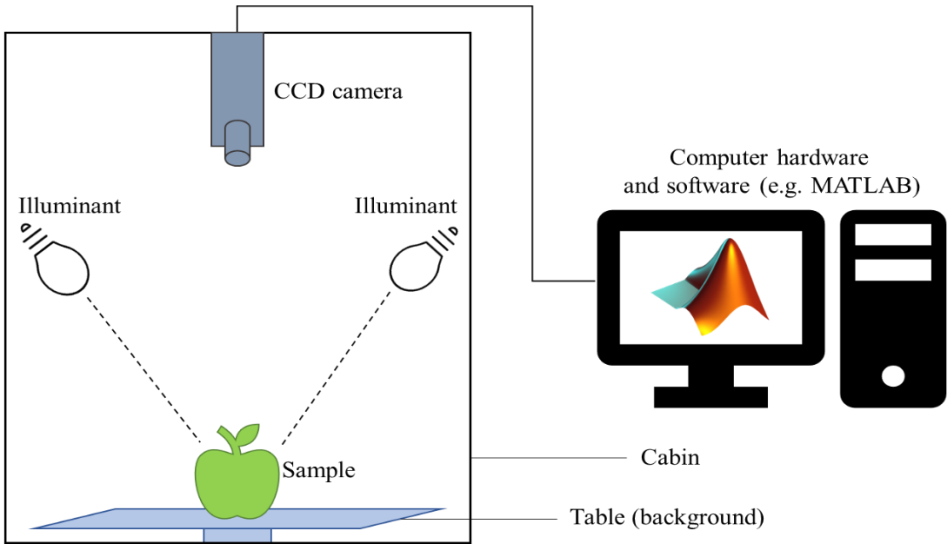

Figure 2. 9. Component of CVS (Source: Zhang et al., 2014)

The illuminant is a light source. The illuminant is responsible for the illumination of an object, reduction of disturbances such as shadows, reflections, noise, and improving image contrast (Lukinac et al. 2019). Selecting the appropriate illuminant is the most crucial issue to obtain high-quality images. Classification of the standard illuminants by CIE are given in Table 2.8 (Pathare, Opara, and Al-Said 2013; Lukinac et al. 2019; Völz 2002).

Table 2. 8. Classification of Illuminants

Illuminant type	**Type of lighting of illuminant**
A lamps	Incandescent light
B lamps	Direct sunlight
C lamps	Artificial daylight
D lamps	Natural daylight at a specified color temperature in K
E lamps	Fluorescent light

The color perception of an object depends on three elements of spectral distribution: the illuminant, object, and observer (Hutchings, Luo, and Ji 2000). Thus, the selection of illuminants is an important parameter. Generally, D series lamps supply more accurate lighting than B and C series lamps. D series lamps are named with two-digit numbers like D65, which represent the first two digits of color temperature in the Kelvin unit of the lamp. D65 lamp is commonly used lamp in lighting applications excluding the requirement of special lighting conditions (Pathare, Opara, and Al-Said 2013).

The surface of the imaged object can be opaque, semi-transparent, glossy, and matt (Lukinac et al. 2019). The surface structure of the object should be considered carefully to obtain high-quality images. To get proper images, selection of the convenient illumination technique is another significant point, as well as selection of the right illuminant. Lukinac et al. (2019) classified the illumination techniques as

- Direct incident lighting (vertical from above, ring or angular type illumination)
- Incident lighting with a diffuser
- Lateral or bilateral lights at angles
- Shallowly
- Backlighting
- Collimated lighting -laser light (Figure 2.10).

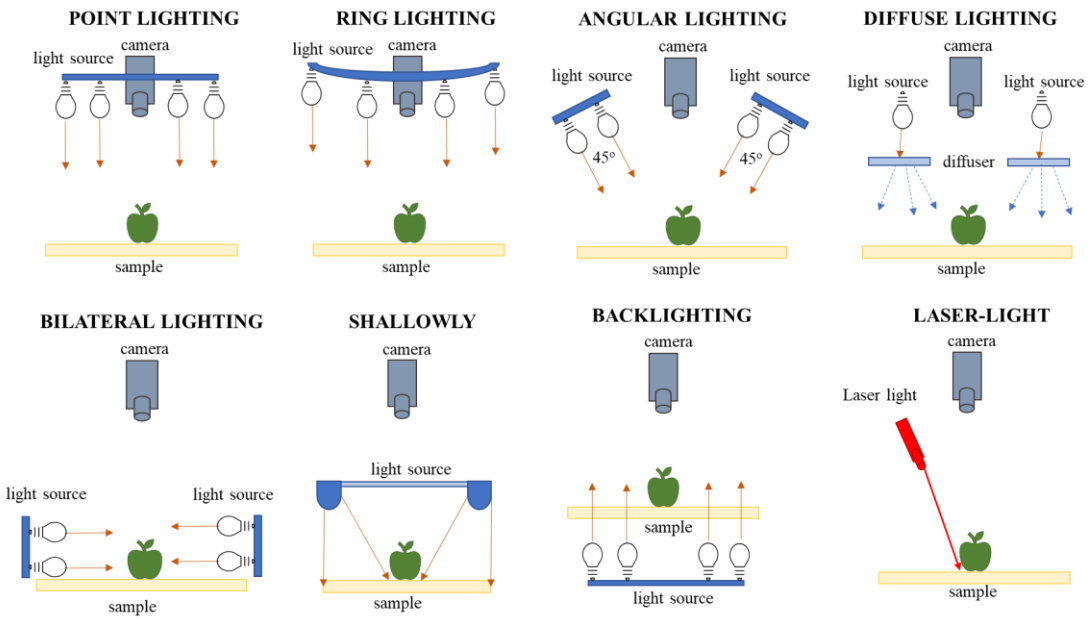

Figure 2. 10. Illumination techniques (Source: Lukinac et al., 2019)

The camera used in food applications of CVS is generally a charge-coupled device (CCD) camera, magnetic resonance imaging (MRI), ultrasound, computed tomography (CT), and electrical tomography (Pathare, Opara, and Al-Said 2013). A CCD camera is enough for general applications, and it is responsible for the transformation of radiation energy to electrical signals. Besides the CCD camera sensor, there is also complementary metal-oxide-semiconductor (CMOS) sensors which are more sensitive than CCD cameras. They provide very quick transferring and a greater dynamic range (Lukinac et al. 2019). After the image is obtained by the camera, feature extraction and quantitative analysis are performed (Briones and Aguilera 2005). Cameras are generally worked with RGB or XYZ color spaces. Joint Photographic Expert Groups (JPEG), Bitmap (BMP), and Graphics Interchange Format (GIF) are commonly preferred image formats (Karma 2020).

CHAPTER 3

MATERIALS AND METHODS

3.1. Materials

The apples (Granny Smith apple) were purchased from a shopping center in İzmir. Apples have an average of 7.67 cm height (minimum 7.3 and maximum 8 cm) and 7.8 cm diameter (minimum 7.4 and maximum 8.3 cm). Thus, all apple samples have different widths and heights. Apples were washed and stored at the refrigerator temperature (~4^{o}C) prior to experimental studies.

3.2. Radiochromic Films

Radiochromic films (FWT-60-00) were purchased from Far West Co. (Goleta, CA, USA). Films have 1cm x 1cm in size and 43.5 μm in thickness. The active agent of films is triphenylmethane leucocyanides dye. The host material is nylon. When the UV light at 254 nm was applied at different fluence levels, the RCF turned from transparent blue color to deep blue color (Figure 3.1).

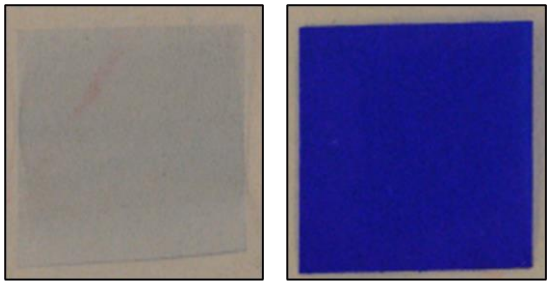

Figure 3. 1. Color Change of RCFs after UVC treatment

3.3. UV-C Apparatus

In this thesis, the Laboratory Scale Bench Top Collimated Beam UV apparatus was used (Figure 3.2). This apparatus contains two parts: cabin and UV source. The cabin part of this apparatus has dimensions 55 cm x 32.5 cm x 81.5 cm and is made of wood. The

inside and outside walls of the cabin are painted black to minimize the scattering of UV-C light from inside the cabin to the environment. The cabin also has a tray system that enables tray placement at 6 cm intervals from the UV source to adjust UV intensity for the surface of films or food materials. The tray is covered with aluminum foil due to its reflecting property.

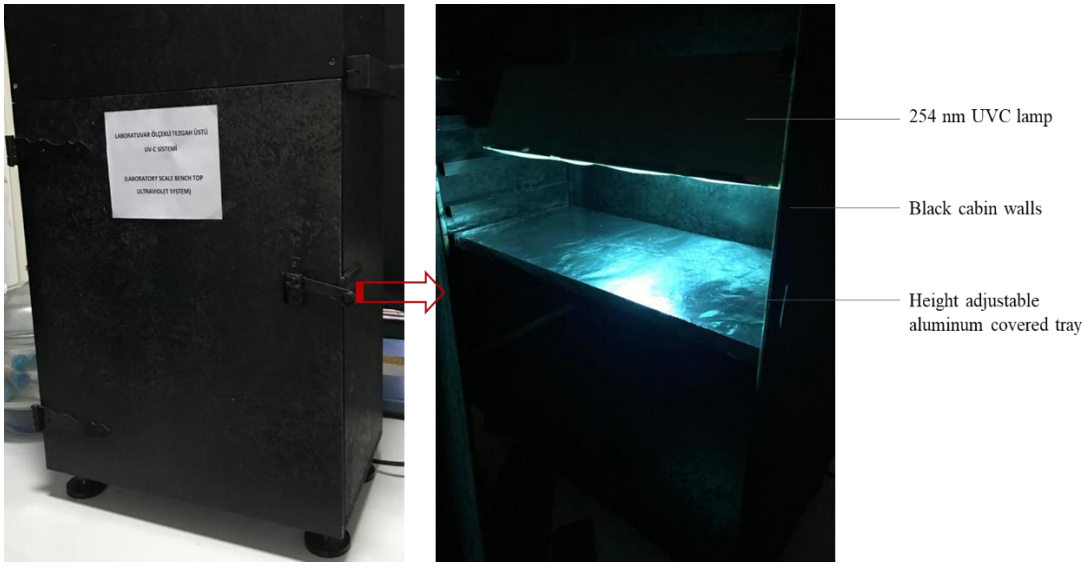

Figure 3. 2. UVC Apparatus Properties

Two identical low-pressure mercury vapor UV lamps at 254 nm wavelength (UVP XX-15, UVP Inc., CA, USA) were used as UV sources. The lamps were placed and fixed in the cabin. The UVC light emitted from the UV lamp in the system ensured that the UVC light was transmitted through a 9 cm wide hole to the 5 cm diameter petri dish. In addition, the light path between the hole through which the light passes and the sample was covered with black background paper to ensure that the light falls on the sample planarly. Thus, the formation of a collimated beam was provided. Prior to experiments, UV lamps were switched on and held for approximately 30 minutes.

3.4. Image Acquisition System

An image acquisition system was designed to obtain photos of irradiated films (Figure 3.3). This system consisted of two identical Mini-Stylo T5 illuminants (Yumpu, Diepoldsau, Switzerland) and a camera (Nikon D90, Tokyo, Japan). The backlighting illumination technique was used to obtain the best result. Illuminants were placed on the

white base side by side. In order to prevent excessive light intensity, illuminants were covered with paper.

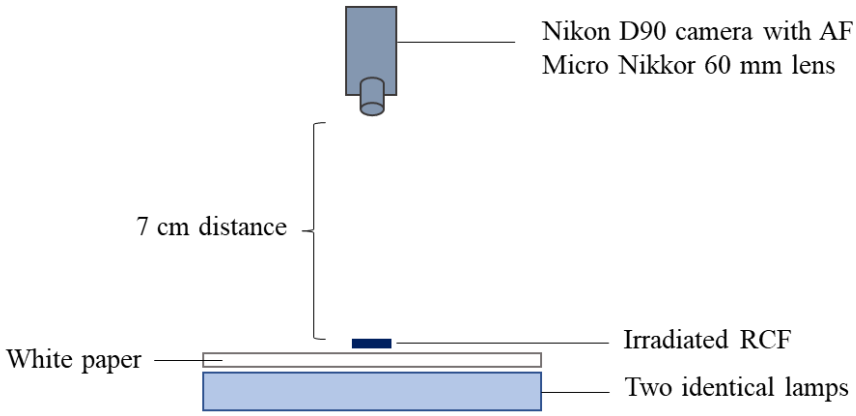

Figure 3. 3. Image Acquisition System

The camera was placed vertically at a distance of 7 cm from the illuminator and the sample. The angle between the camera and the illuminants was fixed. All photo shoots were taken in the dark to eliminate the effect of ambient lighting and use the designated area to avoid baseline differences when performing image analysis. Furthermore, the constant camera settings were used to eliminate image differentiation. The camera features set during the photo shoot are given in Table 3.1.

Table 3. 1. The Camera Features for Image Acquisition

Lens	AF Micro Nikkor; 60 mm – f/2.8D
Mod	Manual
Aperture priority	f4.8
Diagram	1/1000
ISO sensitivity	200
White balance	Flourescent 5
Exposure	0.0
Focusing mode	AF-A
Metering	Matrix
Color space	sRGB
Image quality	JPEG Fine
Image size	Small - 2144 x 1424

3.5. Determination of UV Fluence

The UV fluence applied at different distances from the UV source was calculated by multiplying the exposure time with the UV intensity (irradiance) determined by radiometric and actinometric methods and was also determined by using a radiochromic film dosimeter.

3.5.1. Radiometric Method

A UVX radiometer equipped with a UVX-25 sensor (UVX, UVP Inc. CA, USA) was used to measure the UV intensity in mW/cm^2 at a distance of 2, 4, 6, 8, 10, and 12 cm from the UV-C lamp vertically. After the UV-C lamps were turned on for about 30 minutes, measurements were taken from 5 different points for each level. After obtaining average UV intensity for each level, UV fluence values at these levels were calculated by multiplying UV intensity (mW/cm^2 unit) with exposure times (s).

3.5.2. Potassium Iodide/Iodate Chemical Actinometry Method

The applied UV fluence in the continuous flow UV-C reactor system was measured by using the iodide/iodate actinometrical method with some modifications (Kaya, Yıldız, and Ünlütürk 2015; Rahn 1997; Rahn, Xu, and Miller 1999; Rahn et al. 2003). All chemical substances were purchased from Merck KGaA, Germany. To prepare the solution, 0.6 M (9.96 g) potassium iodide (KI), 0.1 M (2.14 g) potassium iodate (KIO_3) and 0.01 M borax ($Na_2B_4O_7.10H_2O$) were dissolved in 100 mL ultrapure water. The 3 mL unirradiated solution was poured into Petri dishes with a 5 cm diameter (corresponds to 0.153 cm sample depth). The samples were UV treated at 2, 4, 6, 8, 10, and 12 cm distances from the UV-C source. A stirrer was replaced in the bottom of the cabin, and samples were stirred during the exposure to prevent the saturation effect of triiodide photoproducts at the surface of the solution in the petri dish and resulting in an inner filter effect on the absorbing actinometer. The irradiated solution was sampled every 2 minutes for up to 14 minutes. After UV treatment, the irradiated solution was diluted with the unirradiated solution up to 500-fold dilution. The absorbance values of the diluted and irradiated samples were taken within five minutes since the reaction between iodide and iodate molecules still occurs, and the properties of the solution change with time.

Absorbance measurements were taken using 1 cm quartz cuvettes with UV-2450 UV-Visible Spectrophotometer (Shimadzu Corp., Kyoto, Japan). Blank was the unirradiated solution to correct any small changes in absorbance over time due to thermal oxidation. Control measurement was taken with an unirradiated solution against ultrapure water. Control values of undiluted and unirradiated solution were determined as 0.54-0.58 at 300 nm and approximately 0 at 352 nm wavelength.

Initially, the concentration of the triiodide molecules was calculated from Equation 3.1 to find the UV intensity values at different distances (Bolton et al. 2011). Secondly, quantum yield based on temperature and the concentration-dependent formulation was calculated from Equation 3.2 (Rahn 1997).

$$[I_3^-] = \frac{\left[A_{352\ nm,sample} - A_{352\ nm,blank}\right]}{27{,}363}\ (M) \tag{3.1}$$

where $[I_3^-]$ is the concentration of the triiodide, 27,363 $M^{-1}cm^{-1}$ is the molar absorption coefficient of I_3^- at 352 nm, $A_{352\ nm,\ sample}$ and $A_{352\ nm,\ blank}$ is the absorbance values of the sample, and the unirradiated solution.

$$\Phi = 0.75(1 + 0.23[C_{iodide} - 0.577])(1 + 0.02[T - 20.7]) \tag{3.2}$$

where T is the temperature in ^oC and C_{iodide} is the concentration of the iodide molecules in the unirradiated solution. The c_{iodide} value was calculated by Equation 3.3

$$C_{iodide} = \frac{A_{300\ nm}}{\varepsilon \times d} \tag{3.3}$$

In equation 3.3, ε is the molar absorption coefficient of iodide molecules at 300 nm and is equal to 1.061 $M^{-1}cm^{-1}$, and d is the length of the light path (1 cm). If the volume of the actinometer of the solution in the flask disk is V in L, the number of moles of I_3^- is

$$moles\ of\ I_3^-\ generated = [I_3^-] \times V \tag{3.4}$$

In the Einsteins unit, the moles of I_3^- generated can be expressed as

$$Einsteins\ of\ I_3^-\ generated = \frac{moles\ of\ I_3^-}{\Phi} \tag{3.5}$$

Then, photon irradiance was calculated according to Equation 3.6 to obtain the irradiance (E), photon irradiance (E_p) was multiplied by the photon energy at 253.7 nm ($U_{253.7\ nm}$ = 471,420.89 J)

$$E_p = \frac{Einsteins\ of\ I_3^-}{A_{crosssectional} \times t_{exposure}} \tag{3.6}$$

$$E = E_p \times U_{253.7\ nm} \tag{3.7}$$

This irradiance value was adjusted by dividing it to the water surface reflection factor ($R_{water\ surface}$ is 2.5%) (Bolton et al. 2011).

$$E = E \times (1 - R) \tag{3.8}$$

After obtaining irradiance values, the applied UV fluence was calculated using irradiance values (mW/cm^2) and exposure times (s).

3.5.3. Radiochromic Film Dosimeter

3.5.3.1. Determination of Exposure Time Interval for Color Development of Radiochromic Films

RCFs turned from transparent blue color to deep blue color so quickly and irreversibly under the UV-C light and reached a constant color intensity. However, it is difficult to determine the color change in films irradiated for longer periods. The films have close L*, a*, and b* values, and the color difference cannot be detected through a software program and chromameter measurements. Determining the appropriate exposure time is an important part of the experiments to save time and material and to observe clearly the color change. For this purpose, UV lamps were switched on approximately 30 minutes before each experiment. Different UV-C Fluences were

selected by varying exposure times (0 to 60 s with 10 s time intervals) at a specified intensity (3.15 mW/cm^2 measured at a 6 cm distance from the UV lamp). Radiochromic films exposed to UV light were analyzed with the Chroma meter (CM), and the most appropriate time interval was determined according to the ΔE values of the films.

3.5.3.2.Color Development of Radiochromic Films (RCFs) in Response to Different UV-C Fluences and Image Analysis of RCFs

After selecting the time interval, radiochromic films (RCFs) were exposed to different UV-C intensities (6.22 at 2 cm; 3.89 at 4 cm; 3.15 at 6 cm; 2.44 at 8 cm; 1.52 at 10 cm; 1.28 mW/cm^2 at 12 cm) with varying exposure times (2, 4, 6, 8, 10, 15 and 20s). Then, the photos of radiochromic films were taken by the Nikon D90 camera, and values of color space L*, a*, and b* were determined with Konica Minolta CR-400 portable Chroma meter (CM). Nikon D90 digital camera (DC) with Nikkor 60 mm f/2.8D Lens was used under constant shooting conditions to determine the color properties of UV-treated radiochromic films with different UV fluences. The photos were analyzed with a code written using the MATLAB software program. MATLAB (Mathworks, 2017b, Natick, MA, USA) is a programming and numeric computing platform for analyzing data, developing algorithms, and creating models. This program was brought into the science world by the Mathworks firm in 1984. Today, Mathworks has a lot of offices and representatives worldwide. Data analysis, construction of graphics, programming, application building, combining other program languages such as Python, C/C+, Fortran, and Java, connecting to hardware, and parallel computing can be made with MATLAB (Mathworks 2022a). This platform has several toolboxes such as math, statistics and optimization, image processing and color vision, etc.

The images taken by the camera are first loaded into the MATLAB program. Each colored image is 2144x1444 pixels in size. Later, a certain fixed region on each image was selected and cropped. The L*, a*, b* transformation of pixels on each cropped image was done by MATLAB code. Furthermore, the MATLAB code analyzed the cropped images sequentially. The code converted image data to L*, a*, and b* values. Then, L*, a*, and b* values of each cropped image were used to calculate total color change (ΔE) corresponding to different UV fluence values. The total color change was calculated according to Equation 2.11.

Then, a calibration curve representing the relationship between UV fluence and total color change of RCFs (ΔE) was constructed. Validation experiments tested the accuracy of this curve. For this purpose, two different exposure times (7 and 25 seconds) were selected, within and outside the tested exposure time range (0-20 seconds). The RCFs were exposed to UV light at these two exposure times for all distances (2-12 cm). The color values of the irradiated films were determined by code, and the fluence values applied to the films were found from the calibration curve.

3.5.3.3.Color Stability of Radiochromic Films

The color stability of UV-treated films at specified UV intensity (3.15 mW/cm^2) was determined by storing films in light-proof containers at two different temperatures: 4± 2°C and 25 ± 2°C. Then, color readings were done by performing image analysis on the specified days (1^{st}, 7^{th}, and 15^{th} days) with the MATLAB software program.

3.5.3.4.Color Evolution of Radiochromic Films (RCFs) Placed on Apple Surfaces

In this part of the study, RCFs were placed at different points on seven apple samples with different shapes and dimensions (Case 1). The locations of the films on the food samples are shown in Figure 3.4. Six points on the sample were chosen. The locations of these points were the cavity near the blossom (6), the cavity near the stem (5), and the opposing surface points (1, 2, 3, and 4). After placing the films on these points, apple samples were placed in the cabin as stem points (Position 5) facing up and subjected to UV-C treatment. After the treatment, images of the UV-treated films were taken, and color analysis was done. The UV fluence applied to different points of the apple was determined with the help of the calibration curve, details of which are given in section 3.2.3.2.

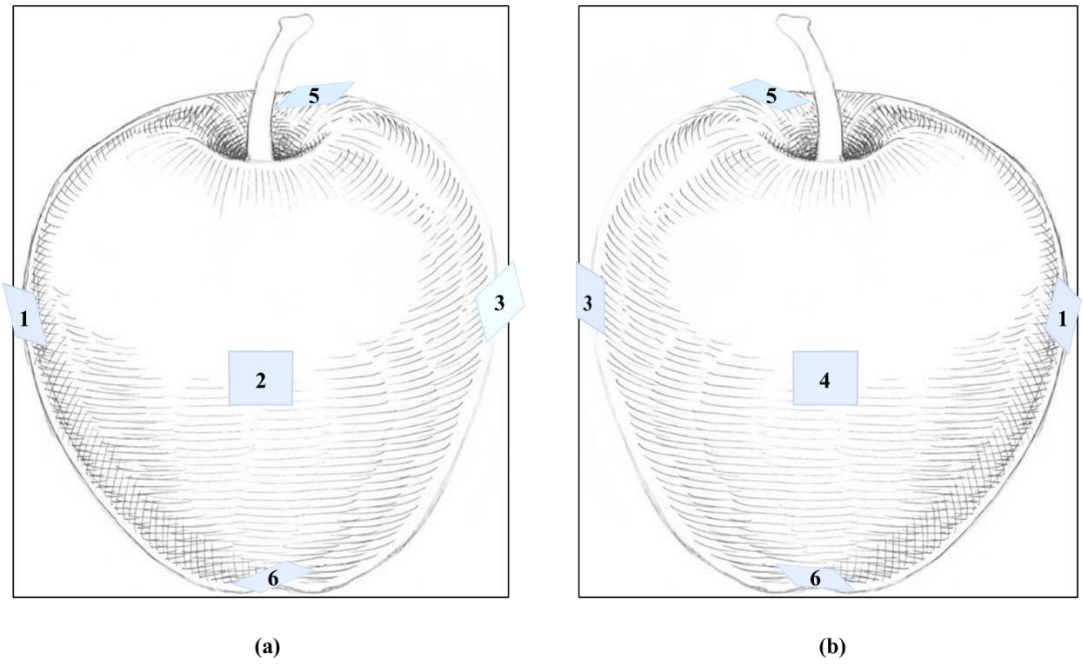

Figure 3. 4. RCFs Settlement on Apple Surface (a) Front View and (b) Back View

For Case 2, RCFs were attached to the nine different points on the hemispherical surface of the selected apple samples used in Case 1. These points are illustrated in Figure 3.5. The apple samples were placed into the cabin as a lateral surface facing up. Then, the same procedures outlined in Case1 were repeated.

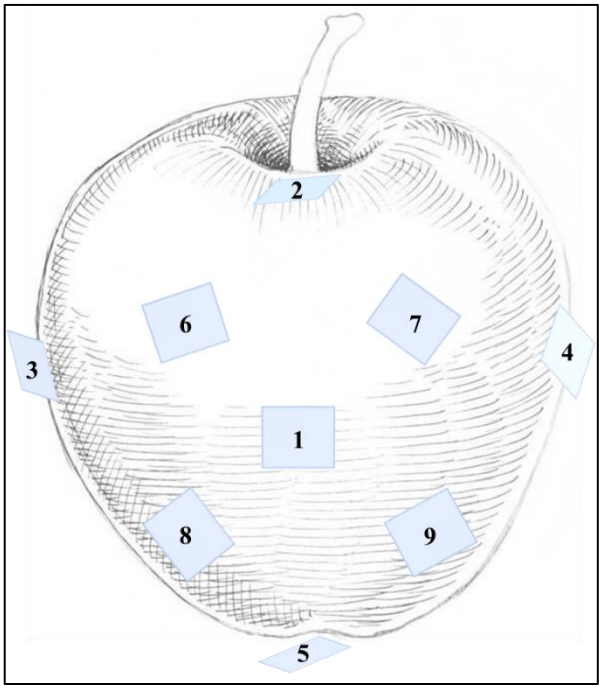

Figure 3. 5. RCFs Settlement on Hemispherical Surface of Apple

3.6. Statistical/Data Analysis

All experiments were repeated three times with two parallels. All data obtained from the experiments were analyzed with Minitab (Minitab® 19, UK). The experimental and calculated data differences were compared with ANOVA at a 95 % confidence interval. Also, the Tukey test was applied to the data to distinguish the differences. Furthermore, response surface methodology (RSM) was applied to the pre-treatment data to determine the optimum condition for the vertical distance and exposure time parameters.

In Section 3.2.3.2, the calibration curve for the UV Fluence-ΔE relationship was constructed. There were two important points for constructing the calibration curve. The first important point was the determination of independent and dependent variables. First, a calibration curve was created with UV fluence values obtained using actinometric UV irradiance values versus ΔE values. UV fluence values for specified irradiance and exposure times were used as the independent variables since UV fluence value was calculated at a specified distance and an exposure time (for example, UV fluence at 2 cm vertical distance to the lamp and t=6 s exposure time is 37.32 mJ/cm^2).

Another essential point in constructing a calibration curve was selecting the appropriate equation representing the data. In order to determine the equation that best represents the data, many types of equations, such as linear, polynomial, exponential, logarithmic, Weibull, Fourier, Gaussian model, etc., were tested using the "Curve Fitting Tool" in the MATLAB program.

In addition, the analysis of residuals from a fitted model, defined as the differences between the observed value of the dependent variable and the value predicted by the estimated regression equation, plays an essential role in validating the regression model. Some points might be the outlier and cause poor model estimation. MATLAB provides two robust fittings: Least Absolute Residuals (LAR) and Bi-square weights, to prevent the equation from the outlier effect.

LAR robust option minimizes the absolute difference of the outliers and can be used for data with fewer outliers, meaning each data point is essential for the model. Conversely, Bi-square weighting minimizes the weighted sum of squares, where the weight given to each point depends on how far the point is from the fitted line. This robust

option can be preferred when the reason for the formation of outliers, such as disturbance, is known since the far data points have nearly zero weight on the model (Mathworks 2022b). LAR can be used for data with fewer outliers/anomalies. Bisquare is used for data with outliers, but the fit is not desired to be affected by these outliers. UV Fluence-ΔE calibration curves were constructed using LAR and Bisquare weight fitting methods.

CHAPTER 4

RESULT AND DISCUSSION

4.1. Determination of UV Fluence by Radiometer

UV irradiance values at different distances from the UVC lamp were measured by a UVP radiometer with a UVX-25 sensor. The radiometer readings were collected from five points for each vertical distance, and the mean irradiance value at a specified distance was calculated. In Figure 4.1, the radiometer readings under the lamp (0 cm distance) for each trial were given in mW/cm^2. The mean irradiance value under the lamp was 4. 15 mW/cm^2. When descending vertically from the UVC lamp, the UV irradiance values were obtained as 1.88 at 2 cm, 1.02 at 4 cm, 0.52 at 6 cm, 0.33 at 8 cm, 0.22 at 10 cm, and 0.16 mW/cm^2 at 12 cm distances from the UV lamp.

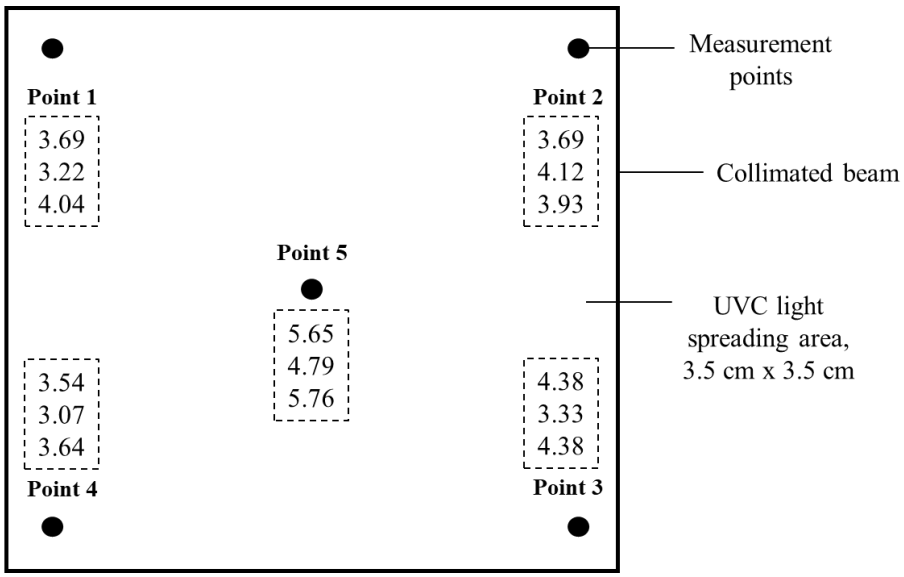

Figure 4. 1. Radiometer readings under the UVC lamp

The variation of irradiance with distance must obey the Beer-Lambert Law. According to Beer-Lambert Law, the intensity loss of the light transmitted through a homogenous medium consisting of an infinitesimally thin layer was proportional to this intensity and thickness of the layer (Mayerhöfer, Pahlow, and Popp 2020). It is expressed mathematically as

$$I\ (d) = I_o . \exp\ (-\alpha d) \quad (4.1)$$

where I(d) is the intensity of the light at a specified distance, I_o is initial light intensity, α is Napierian absorbance coefficient (1/cm), and d (cm) is the distance at which the light intensity is desired to be determined. Therefore, it can be concluded that Beer-Lambert Law explains the absorption behavior of a substance, and UV irradiance decreases exponentially, moving away from the lamp (Koutchma, Orlowska, and Zhu 2012). The relation between irradiance and vertical distance to the lamp was given in Figure 4.2. UV irradiance, measured with a radiometer away from the UVC lamp, decreased exponentially and fitted the Beer-Lambert Law (round marks). Standard deviations of the data were small enough. Therefore, the data obtained from the radiometer were consistent with each other.

Furthermore, the irradiance values at specified distances (0-12 cm) were calculated using Beer-Lambert Law (triangle marks) to confirm the consistency of the data. The initial light intensity (I_o) and Napierian absorbance coefficient of air were taken as 4.15 mW/cm^2 and 0.08 (1/cm), respectively (Bartwal and Kumar 2018). The trend of UV irradiance readings was exponential, meaning the data was well estimated using the Beer-Lambert Law. However, it was determined that there was a difference between the data obtained from the equation and the radiometer readings. The fact that the sensor maintenance has not been done for a long time is seen as a reason for this. Sensor maintenance should be done by sending the sensor to the manufacturer periodically. It is stated that radiometer sensors should be calibrated at 253.7 nm after 12 months, and KI/KIO_3 actinometer can be used to calibrate the radiometer sensor at any time (Bolton et al. 2011). Another reason for the difference found may be related to the absorbance coefficient of the air, and it is known that this value is different in different sources and environments (Bartwal and Kumar 2018).

The variation of the UV fluence depending on the exposure time and the irradiance reading obtained by the radiometer at different vertical distances from the lamp is given in the Figure 4.3. It can be concluded that the UV fluence has a linear relationship with time, and there is an exponential relationship between the UV fluence and the distance from the lamp. Therefore, the highest UV fluence values were obtained at the nearest vertical distances from the lamp (e.g., 2 and 4 cm vertical distance) and most extended exposure times (e.g., t= 20 s).

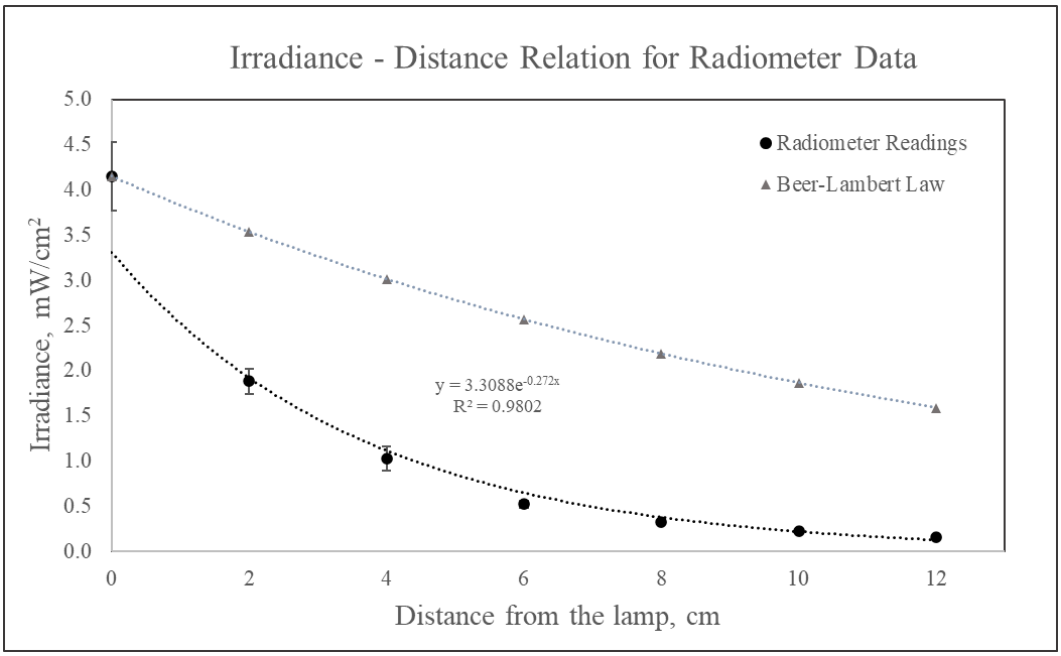

Figure 4. 2. Irradiance Change Depending on the Vertical Distance to the UVC lamp

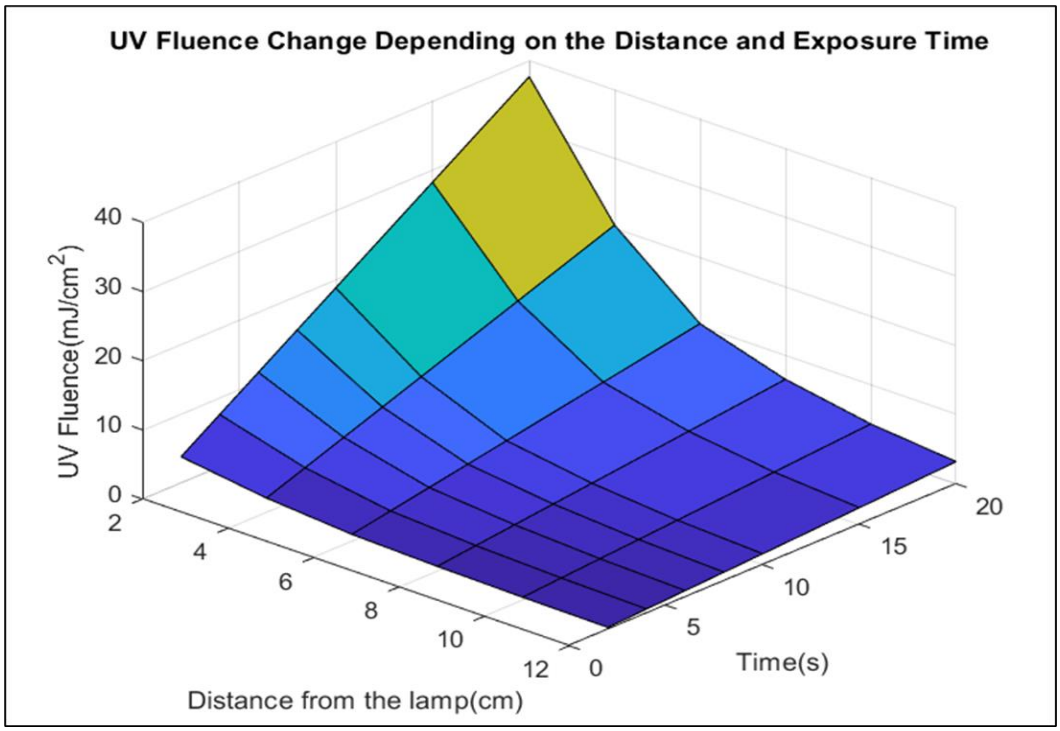

Figure 4. 3. UV Fluence Change Depending on the Exposure Time and Vertical Distance

4.2. Determination of UV Fluence by Potassium Iodate/Iodide Actinometer

4.2.1. Generating Triiodide Formation Curves

Potassium iodate actinometer experiments and calculations were performed according to the method described in Section 3.2.2. Time-dependent triiodide formation curves for each specified distance were obtained. Triiodide formation curve at a distance of 4 cm is given in Figure 4.4, and the other curves are given the Appendix A. In the graph, triiodide formation at the end of the reaction of iodide and iodate molecules showed a linear increase in the beginning. Then it reached saturation (t~10 min) since the reaction had reached the equilibrium point. Although the reaction continued to occur slowly due to the presence of molecules in the medium, the amount of triiodide formed was not statistically different from that obtained in 10 minutes ($p>0.05$).

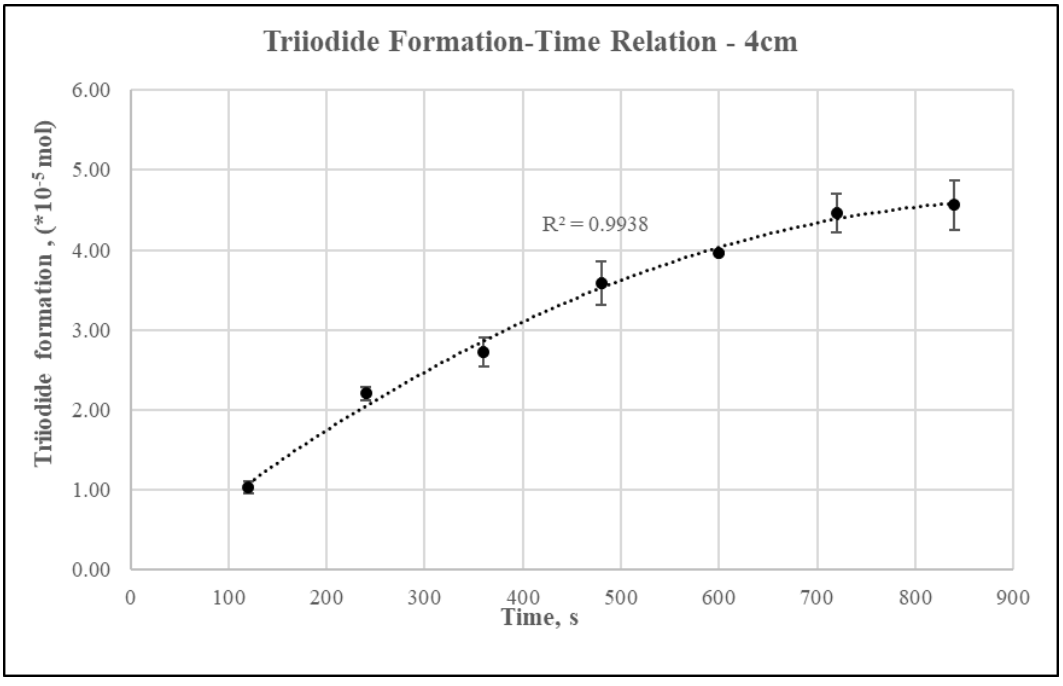

Figure 4. 4. Triiodide Formation at 4 cm Vertical Distance to the UVC Lamp

Triiodide formation curves for 2 and 6 cm distances showed the same trend as the 4 cm distance curve. On the other hand, the triiodide formation curves at 8, 10, and 12 cm from the lamp had an increasing trend, indicating that the reaction is still ongoing. This was expected because the UV irradiation reaching the solution decreases with distance from the lamp, requiring a longer time for the reaction to complete. There is also

the scattering of light from the lamp to the environment. It is known that dust and moisture in the air play an important role in the scattering of light. For this reason, when the distance between the lamp and the solution surface increases, it is expected that the light will scatter and spread over a wider area (Qualls and Johnson 1983).

As a result, at 8, 10, and 12 cm distances from the UV lamp, the chemical reaction was incomplete. However, at 2, 4, and 6 cm distances, the equilibrium point was reached in the formation of triiodide. A longer exposure time was required to reach equilibrium at distances of 8, 10, and 12 cm. However, long-term exposure times caused adverse effects on the chemical reaction occurring at distances of 2, 4, and 6 cm, and there were problems in absorbance values. Therefore, the time required to determine the UV irradiance at a distance is set to be about 600 s.

4.2.2. Determination of UV Irradiance and Calculation of UV Fluence at Different Distances

The UV irradiance at different distances was obtained by applying UV treatment to the actinometer solutions for 600 s. The irradiance values were obtained as 6.22 at 2 cm; 3.89 at 4 cm; 3.15 at 6 cm; 4 at 6 cm; 2,44 at 8 cm, 1.52 at 10 cm and 1.28 mW/cm^2 at 12 cm distances from the lamp. The relation between UV irradiance and distance was shown in Figure 4.5. The relation between the UV irradiance and distance was exponential and fitted the Beer-Lambert Law.

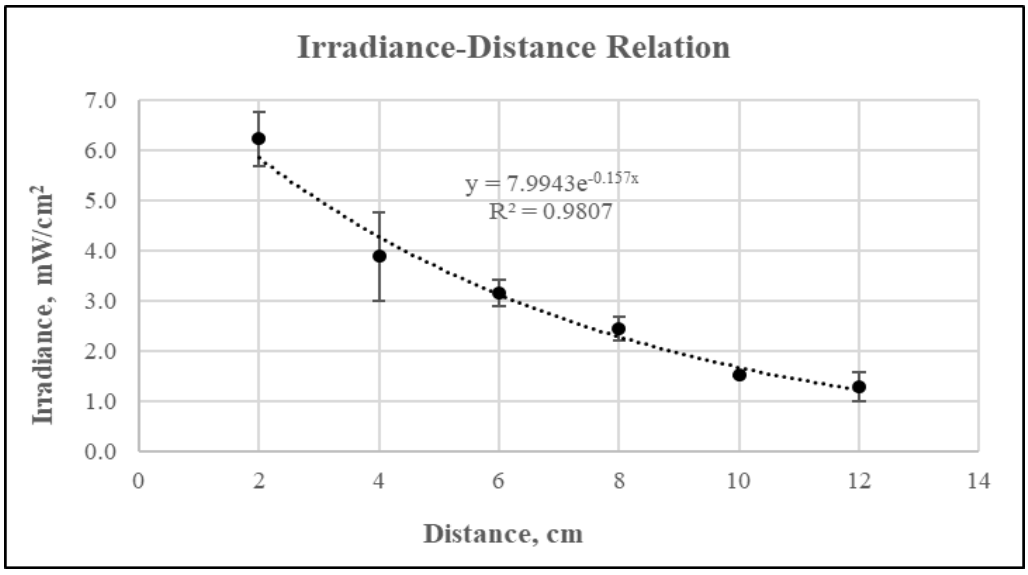

Figure 4. 5. Irradiance Change Depending on the Vertical Distance to the UVC Lamp

According to Beer-Lambert Law, the maximum irradiance value should be obtained at the 2 cm distance from the lamp and then decrease exponentially away from the lamp. Generally, the irradiance values obtained from the actinometry fitted to the law. Yet, the most significant deviation among the trials was observed at a 4 cm vertical distance. This might be due to pipetting errors when diluting the actinometer solution. When an inhomogeneous dilution was made, a denser or more dilute irradiated solution could be obtained. When the absorbance values of these solutions were read in the spectrophotometer, high or low values were obtained and caused the deviation to increase between different readings of the same sample.

The irradiance-time relations at different distances were also examined (Figures 4.6 and 4.7). It has been revealed that UV irradiance tended to decrease at 4 and 6 cm distances, but fluctuations occurred at other distances. These fluctuations were expected, and there might be several reasons for that. First, the UV light scatters from the lamp to the environment and spreads into the broader area (Koutchma, Forney, and Moraru 2009); therefore, transmitted UV light to the solution surface has decreased, and the measured irradiance might be lower than the actual one. Secondly, UV light collides with the particles in the air and causes a decrease in the transmitted UV light throughout the path (Qualls and Johnson 1983). Thirdly, the low-pressure mercury lamp transmits the light irregularly. Throughout the lamp, the maximum UV energy was obtained at the center point of lamp. The amount of UV energy decreased towards the endpoints of the lamp, in line with the findings of Jin et al. (2005). Hence, the applied UV energy throughout the lamp at the specified area was not the same, and the actinometer solution might be exposed to different amounts of UV light at each surface point. The fluctuations in UV irradiance measured at a distance of 2 cm could be explained by the inhomogeneous transmission of UV light through the lamp. The effect of this phenomenon was observed more at close distances to the lamp. However, the predominant effect of fluctuations in UV irradiance values measured at 8, 10, and 12 cm distances was light scattering with respect to distance, as evidenced by the standard deviations of the data at different exposure times.

The fluence values obtained from the potassium iodate actinometry were calculated by multiplying the UV irradiance with the exposure times. The change of UV fluence values depending on the exposure times and the distance from the lamp was given in Figure 4.8. This graph showed a variation similar to the predicted UV fluence variation

based on the radiometer values. The only difference among the graphs was surface behavior. While the radiometer fluence values decreased sharply with the distance from the lamp, a smooth decrease was observed in the actinometer fluence values.

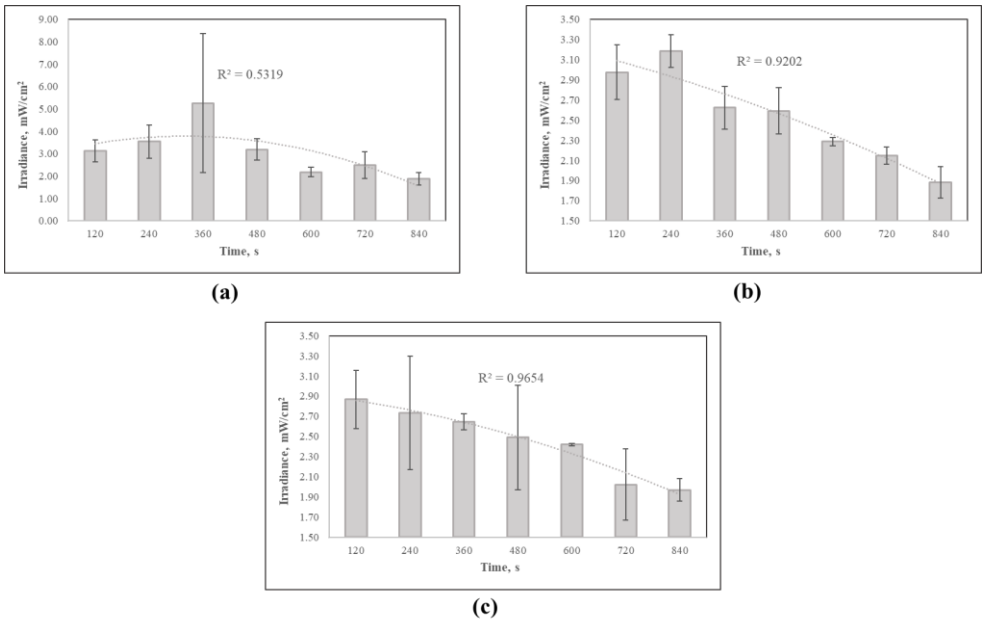

Figure 4. 6. Irradiance Change Depending on the Exposure Time at (a) 2 cm, (b) 4 cm, and (c) 6 cm Vertical Distance to the Lamp

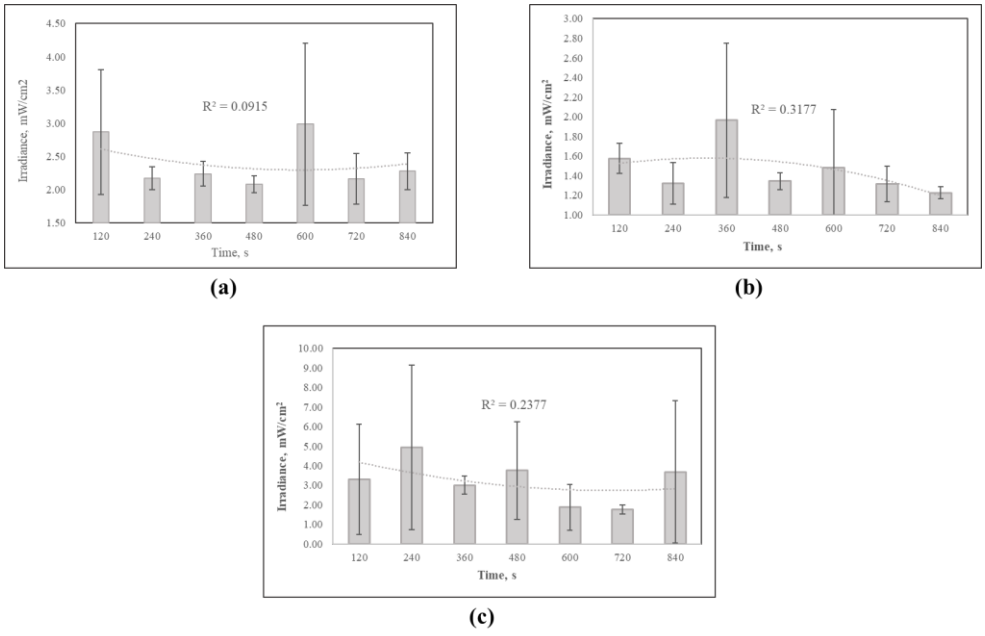

Figure 4. 7. Irradiance Change Depending on the Exposure Time at (a) 8 cm, (b) 10 cm, and (c) 12 cm Vertical Distance to the Lamp

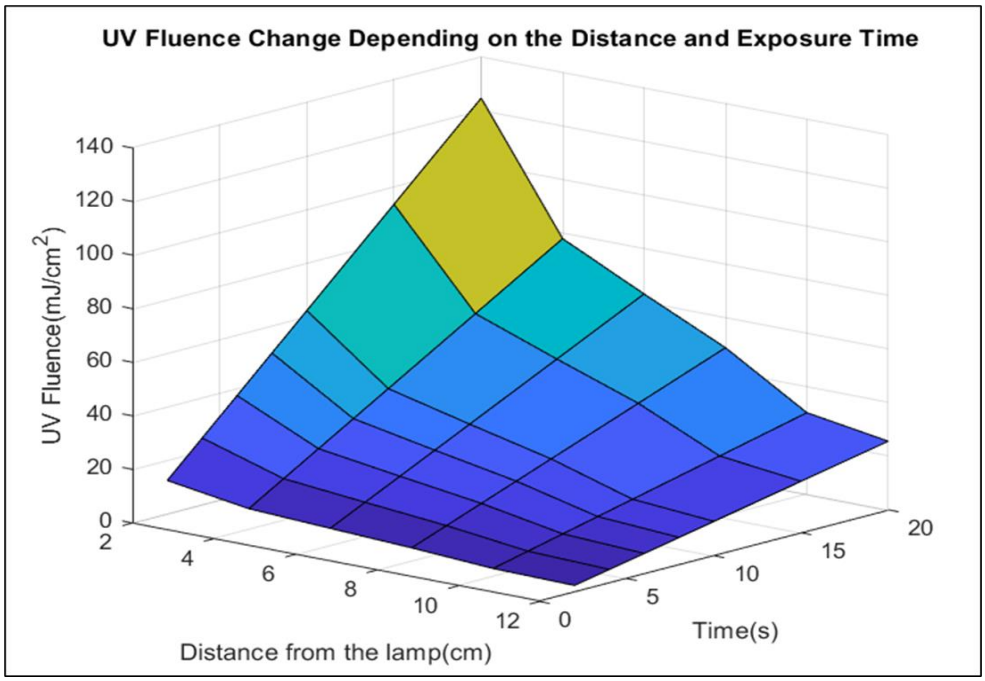

Figure 4. 8. UV Fluence Change Depending on the Exposure Time and Vertical Distance

Additionally, chemical actinometry method gave higher UV irradiance values than radiometer results. KI actinometry results were approximately 6-fold higher than radiometer readings. This situation has been encountered in various studies. For example, Rahn et al. (2003) indicated that radiometry readings were 20% smaller than those obtained using potassium iodide actinometry. Moreover, Jin, Mofidi, and Linden (2006) stated that KI/KIO_3 actinometry measured the incident, average, and germicidal UV intensities higher than the radiometer. The researchers also compared KI/KIO_3 and uridine actinometry for MPM lamps stating that the uridine actinometer was more effective than the KI actinometer for MPM lamps. Qiang et al. (2015) reported that the KI/KIO3 actinometer was used to calibrate three different radiometers, and the radiometers read 13%, 40%, and 50% smaller irradiance values than the actinometer results, respectively. The cause of this problem may be related to the measurement area. It is known that UV light scatters away from the lamp, not planarly dispersed. Therefore, the light is scattered in the medium at different angles. The measuring area (~1cm^2) of the radiometer sensor may not be able to capture the scattered light. In this case, integrating a sphere radiometer might be a good option. In this study, UV radiation values were taken from five different points using a radiometer. However, it is thought that these points may poorly represent the determined measurement area. On the other hand, the actinometry solution had a surface area of about 20 cm^2; therefore, the directly transmitted

and scattered UV light is considered to be completely absorbed by the solution. For this reason, it is decided that the actinometry method gives better results for determining the UV irradiance (intensity).

4.3. Determination of UV Fluence by Image Analysis

4.3.1. Selection of Appropriate Shooting Conditions

The trials for photograph shooting were done to obtain the same quality photos taken under constant conditions. Hence, the standard images were provided and prevented the problems caused by the photos, such as the resolution of the images, the light-dark degree of the photos, etc. A manual shooting mod was chosen to set the working condition. Diaphragm and instantaneous adjustments were examined, and potential diaphragm-instantaneous pairs were determined. The appliable diagram-instantaneous pairs obtaining the standard shooting setup are given in Appendix B. The most explicit images were obtained at f 4.8 and 1/1000. The other aperture priorities were set up according to these values. For f 4.8 and 1/1000 properties, clear photos were obtained at a 7 cm vertical distance from the camera lens. The closer or farther distance than 7 cm caused unclear images.

4.3.2. Exposure Time Interval for Color Development of RCFs

The importance of selecting the exposure time interval was given in Section 3.2.3. The color change of the films when exposed to UVC light was so rapid; thus, there is no significant difference between the RCFs color. Obtained L*, a*, and b* values from pretrial experiments were given in Table 4.1.

Table 4. 1. L*, a*, b*, C* and h^o values of RCFs for Pre-treatment Experiments

Time(s)	**L***	**a***	**b***	**C***	**h^o**	**ΔE**
0	83.9	0.62	-9.13	9.15	-0.068	**0.00**
10	46.69	26.27	-61.73	67.09	-0.402	**69.35**
20	43.87	35.82	-66.52	75.55	-0.494	**78.33**
30	37.38	47.7	-74.18	88.19	-0.571	**92.80**
40	35.32	51.58	-75.53	91.46	-0.599	**96.78**
50	36.21	51.98	-74.34	90.71	-0.610	**95.73**
60	34.92	54.04	-75.28	92.67	-0.623	**98.13**

According to the results, the more suitable time interval for analyzing the color development of RCFs was stated as 0-20 s since the net color changes were so close to each other after 20 s treatment time. It means that after 20 s treatment, nearly the same deep blue color was obtained, or CM failed to determine the color space values of RCFs irradiated more than 20 s. Hence, the net color transitions of films could be observed between 0-20 s exposure times (Figure 4.9).

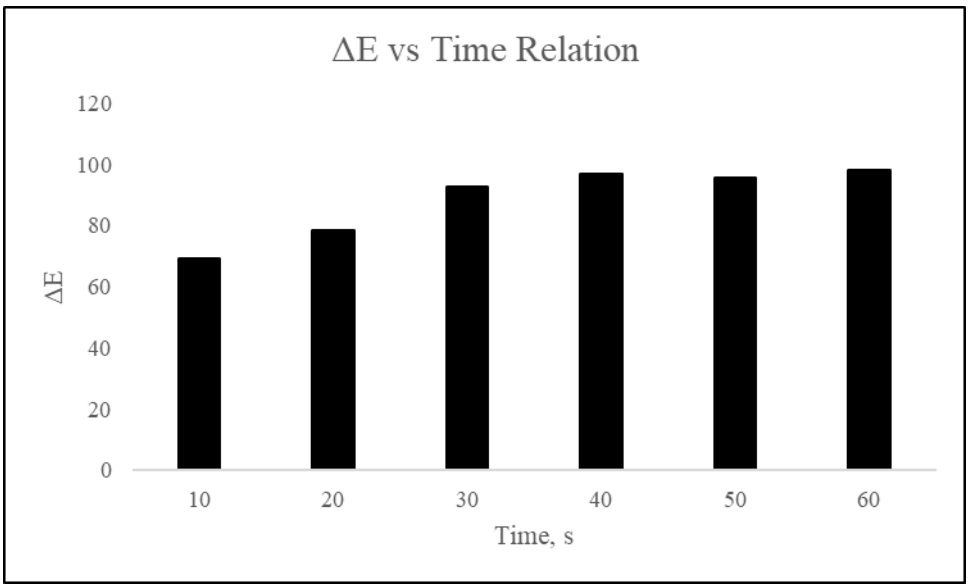

Figure 4. 9. Total Color Change for Different Exposure Times at Constant UVC Irradiance

4.3.3. Color Development of RCFs in Response to Different UV Fluence Values

Different UV fluence values were applied to the RCFs by changing UV irradiance and exposure times. The color L* a* b* values of the RCFs were determined using the MATLAB program and Konica Minolta Chromameter (CM). The color change of irradiated RCFs depending on the distance and exposure time was given in Appendix C. The color value of the unirradiated RCF by CM was determined as 80.65, 1.01, and -10.75 for L*, a*, and b* values, respectively. This result indicates that the unirradiated film includes some blue and red colors and has a brightness. However, the color value of the unirradiated RCF using MATLAB was determined as 79.8841, -6.0591, and 20.1567 for L*, a*, and b* values, respectively.

L* values were similar to each other for CM and MATLAB program. On the other hand, the a* and b* results obtained by MATLAB indicate that the unirradiated film includes yellow and green colors. The * and b* values of CM and the program are incompatible. The main reason behind this mismatch might be the working algorithm of CM and the program. Data processing of the CM was given in Appendix D. Color values of the films are determined by transmitting the light to the irradiated film with CM. In contrast, MATLAB analyzes the images of the irradiated films to determine L*, a*, and b* values.

Another reason for the difference between the two methods might be the background color used for the image shooting in CVS. The white paper was placed on the light source, and the backlighting technique was used due to the preventing reflections of the RCF surface (L* value of original films is approximately 80 out of 100) in the images. This situation caused the fiber colors in the whitepaper to be reflected in the background of the images when preventing the surface brightness of RCFs. The background L*, a*, and b* values obtained by the program were 83.8104, -3.2185, and 22.6448, respectively. These results indicate that the background has yellowness due to the positive b* value. The high-resolution camera might solve this problem, but it requires a big budget. Hence, the background correction should be made to prevent the yellowness of the background. Basically, background correction was made by subtracting the b* values of the background (white paper b* value) from the RCF b* values for both measurement techniques (CM and MATLAB). The graphs of the change in b* values

before and after the correction can be shown in Figure 4.10 for MATLAB. It can be said by examining the figure that MATLAB code perceives the unirradiated film as a yellow color. Therefore, it fails to distinguish the original film color from the background. It is expected since the original film has a brightness and very little transparent blueness.

Similarly, when moving away from the lamp, UV fluence to the films decreases and the color change of films occurs low. The color of RCFs resembles the color of the original RCF. Because of this, the color of irradiated films induced at low UV fluences has positive b* values, which means that irradiated films have a yellowness due to the inability to distinguish the irradiated film from the background. Therefore, adjustments of b* values are a necessary process to obtain meaningful results.

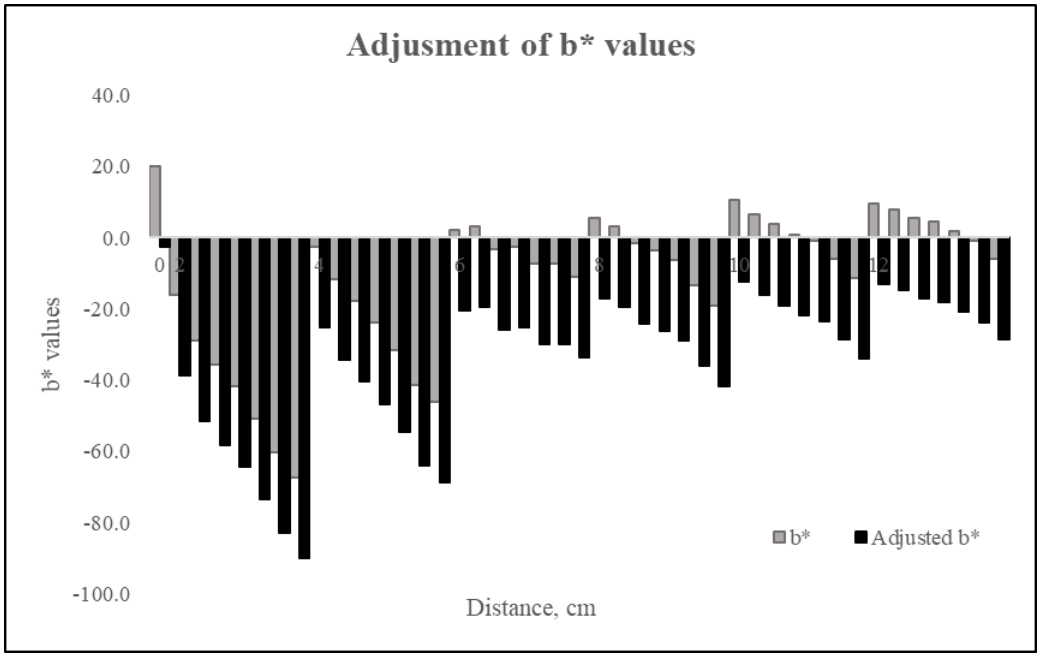

Figure 4. 10. Adjustments Graph of b*Values

The changes of L* and b* values in response to different UV fluence values were given in Figure 4.11 and Figure 4.12, respectively. The change of a* value was insignificant since it is representative of the greenness-redness value, but RCFs mainly turned transparent blue to deep blue color. Hence, L* and b* values were examined to evaluate the relationship between UV fluence and color change of RCFs. Generally, L* values reading from CM and obtained from the program showed a decreasing trend at increasing exposure times. At a specified exposure time such as t=2 s, L* values showed an increasing trend away from the lamp. While the lowest L* change was observed at a

12 cm distance from the lamp and 2 s exposure, the highest L* change was observed at a 2 cm distance and 20 s exposure treatment. In general, UV treatment causes a decreased brightness of films. Although both measurement techniques gave the same L* behavior depending on the irradiance and exposure time, the L* values reading from the CM were more extensive than the L* values calculated by the program. This difference might be based on the algorithm difference behind the measurement techniques.

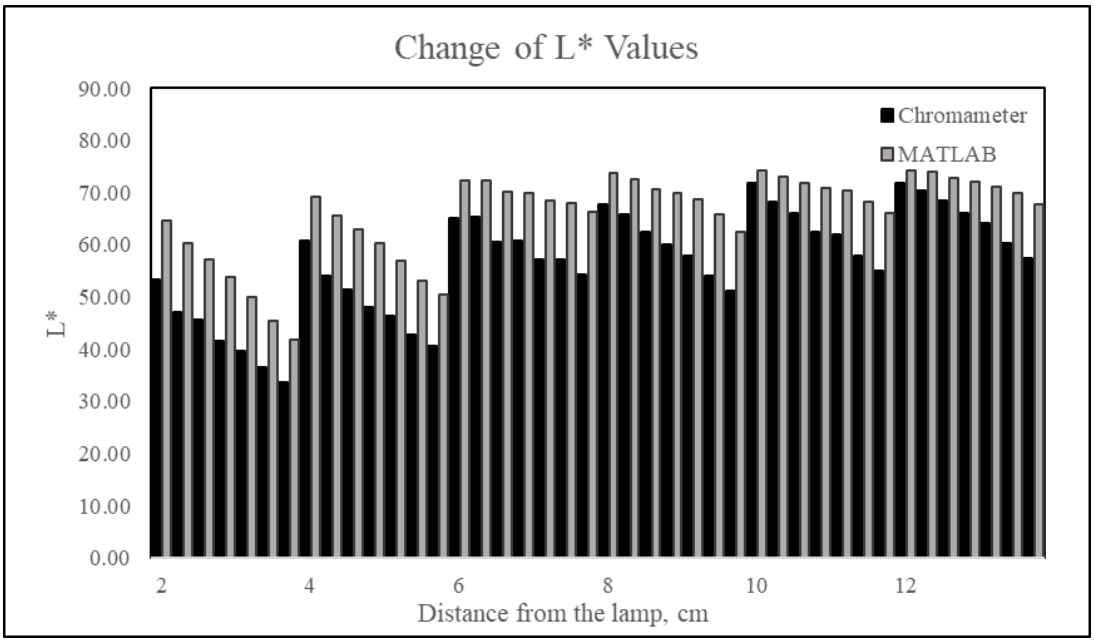

Figure 4. 11. Change of L* Values Depending on the Vertical Distance and Exposure Times for Chromameter and MATLAB

The b* value is the indicator of the bluish-yellowish (Pathare, Opara, and Al-Said 2013). It provides the main contribution to the color change of the irradiated film. Absolute b* values showed an increasing trend towards increasing exposure times at all distances. It means that the darkest blue colors can be observed at long exposure times for all distances. On the other hand, at a specified exposure time such as t=20 s for different vertical distances, the darkest blue color, which means the highest absolute b* value, was observed at a 2 cm vertical distance from the lamp due to the highest irradiance value at this distance. Furthermore, according to the change of the b* values, it can be inferred that the color change of films is related to the applied UV fluence. The maximum UV fluence transmitted to the films should be obtained at 2 cm distances from the lamp and 20 s exposure time by examining the b* values.

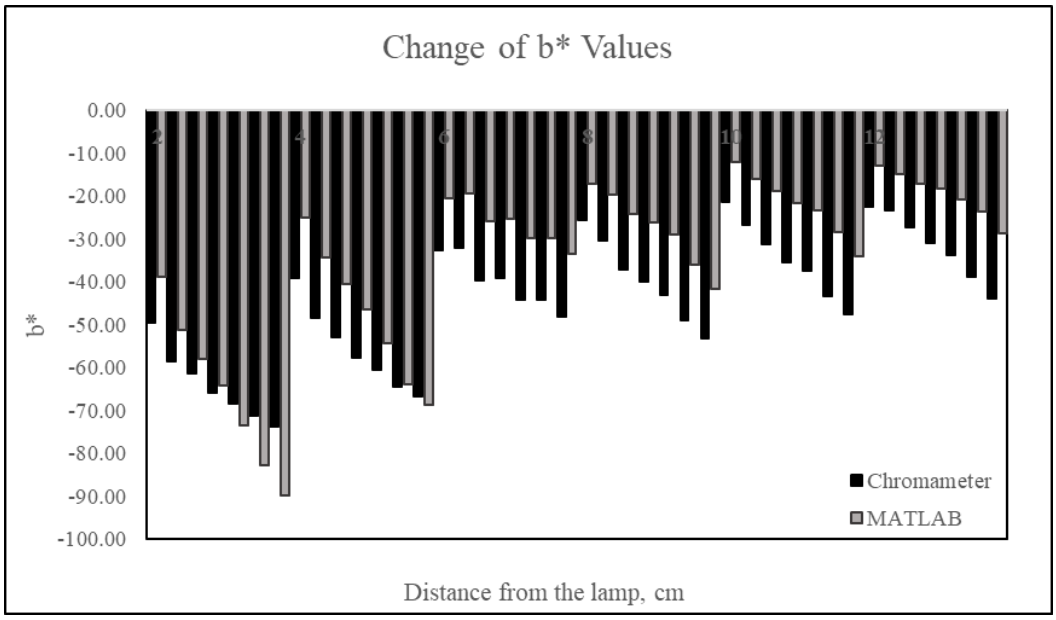

Figure 4. 12. Change of b* Values Depending on the Vertical Distance and Exposure Times for Chromameter and MATLAB

The meaningful and comparable results can be obtained by examining the total color change, ΔE value, rather than individually examining the L*, a*, and b* values since the ΔE value contains the contribution of L*, a*, and b* values of the color. According to Figure 4.13, the color change of films has shown an increasing trend towards the changing exposure time at all distances due to the growing UV fluence. The maximum color changes were observed at the nearest points to the lamp. When far away from the lamp, the total color change of films decreased. The color changes obtained from CM and the MATLAB were close to each other only at a 2 cm distance from the lamp and 15 and 20 s exposure time conditions. Except for these two conditions, CM gave enormous color change than the program. The closer values at these two conditions might be related to the longer exposure time. It is known from Section 4.3.2 that the determination of color change is a problematic issue at longer exposure time, and close ΔE values are obtained. Therefore, the color change determination might be challenging for CM and MATLAB code at longer exposure times.

Furthermore, Figure 4.14 shows the same surface properties as radiometric and actinometric fluence readings. This situation verifies the thesis objective that the color of the RCFs changes in parallel with the applied UV fluence; thus, there is a relation between UV fluence and the color change degree of films. The degree of the color change of film

when exposed to UVC light can be used to estimate the fluence values of films replaced on the surface of the food samples.

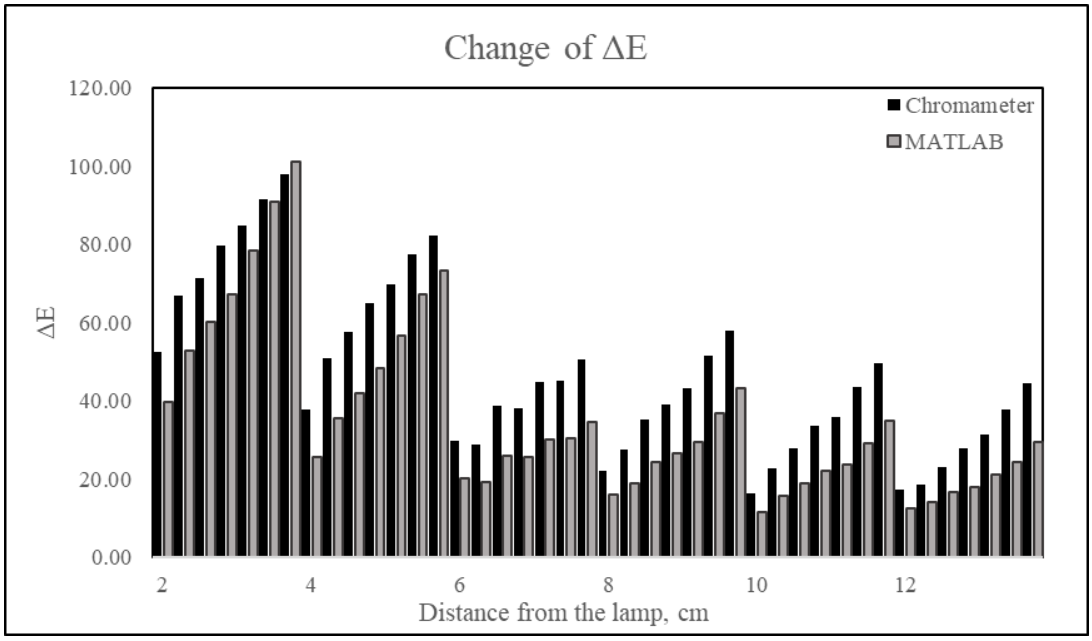

Figure 4. 13. Total color Change of RCFs with CM and MATLAB

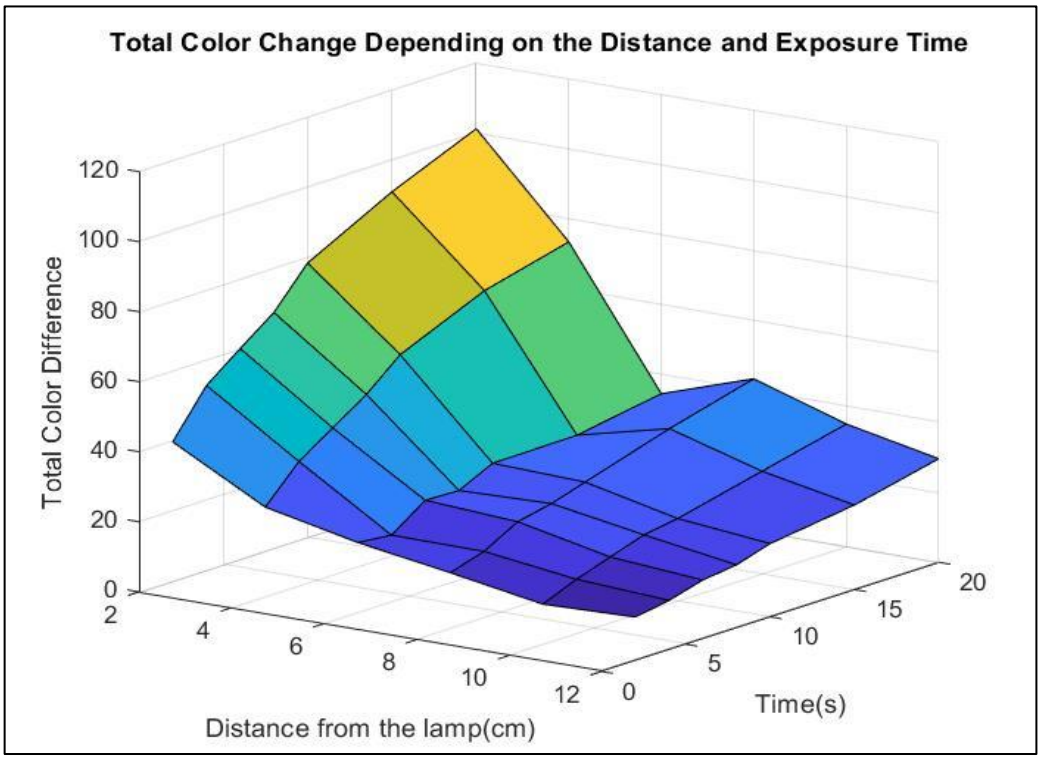

Figure 4. 14. UV Fluence Change Depending on the Exposure Time and Vertical Distance

4.3.4. Color Stability of RCFs

Irradiated RCFs at a 6 cm distance were stored at 4°C (refrigerator temperature) and 25°C (room temperature) for 15 days. The relative color changes of films were observed at 1., 7. and 15. days. Color measurements were taken with the MATLAB program. Figure 4.15 was given to summarize the color change of the films on different days at room and refrigerator temperatures, respectively.

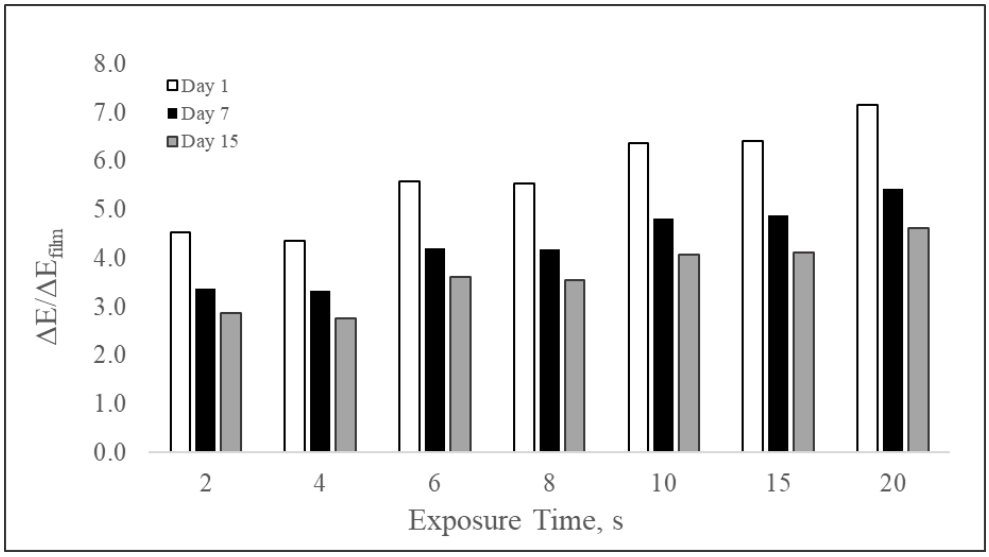

(a)

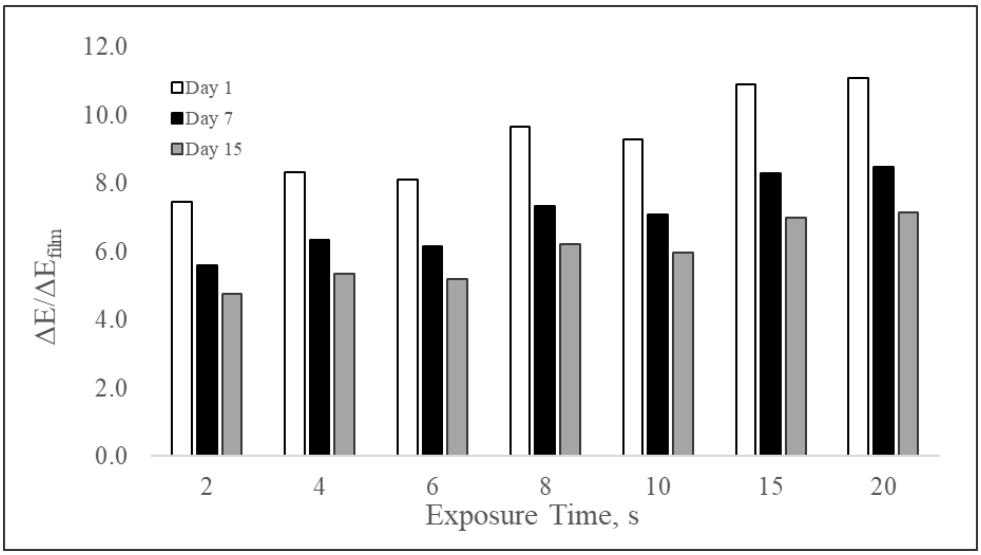

(b)

Figure 4. 15. Color Stability of RCFs for 15 Days at (a) Room Temperature and (b) Refrigerator Temperature

The relative color change of RCFs decreased for 15 days at 4°C and 25°C. Color change decrease was expected compared to day 1. The decrease between 1- and 7- days

were sharper than the decrease between 7- and 15-days. Therefore, the difference in RCF color depending on the storage time and the temperature has been revealed by ANOVA results in Table 4.2. It can be inferred that the color of RCFs statistically remained stable for 15 days of storage at both temperatures. However, storage temperature influences the color change of RCFs. The room temperature caused lower color change values than refrigerator temperature (e.g., ΔE_{room} ~5.0 whereas $\Delta E_{refrigerator}$ ~8.0 at 2 s exposure time for day 1) despite the similar relative color change patterns. It was stated by Yan et al. (2017) that the color of RCFs remained stable at 4°C and 21°C for 15 days. The researchers have given the results over the total color change, not the relative one. Therefore, the color of RCFs has remained stable for 15. days storage at different storage temperatures, but the degree of the color change of RCFs is the function of the storage temperature.

Table 4. 2. Mean Color Change of RCFs for 15 Days at 4°C and 25°C

Storage Temperature, °C	**Storage Time, day**	**Mean Color Change**
4	1	50.47[a]
	7	50.07 [a]
	15	50.06 [a]
25	1	31.07[b]
	7	30.65 [b]
	15	30.74 [b]

4.4. Calibration Curve of UV Fluence-ΔE

Obtained ΔE values from the different UV irradiance and exposure times were used to construct the calibration curve. It is vital to construct a calibration curve to consistently evaluate the usability of radiochromic films in determining the UV fluence distribution on the surface of food samples. After the calibration curve trials made according to Section 3.3, it was realized that the UV fluence and color change could be correlated using different equations. Then, different degrees of polynomial equations and linear equations were tested. The equations are summarized in Table 4.3. It was found that the best model that fits the experimental data was a linear relationship.

The accuracy of the linear model selection was also confirmed with low RMSE value and the convergence of R^2 and adjusted-R^2 values. According to Saeys, Mouazen,

and Ramon (2005), it was stated that the sufficiency of a model or equation could be measured with an R^2 value that is an indicator of the percentage of the variance in the dependent variable (Y) that is accounted for by the independent variable (X). Therefore, the R^2 value between 0.66 and 0.81 indicates approximate quantitative prediction, whereas the R^2 value between 0.82 and 0.90 means good model prediction. Besides these, the R^2 value above 0.91 is considered an excellent model prediction. Furthermore, the convergence of R^2 and adj-R^2 values indicates that the model prediction is reasonable.

Table 4. 3. Model Estimation Results for UV Fluence-Color Change Relationship

Model	Robust	Equation	R^2	Adj-R^2	RMSE	SSE
Linear	Off	$y=0.8687x$	0.7716	0.7716	12.45	6350
	LAR	$y=0.7795x$	0.9801	0.9801	3.673	553.2
	Bi-square	$y=0.7354x$	0.8698	0.8698	9.397	3620
2. degree polynomial	Off	$y=0.005712x^2+0.5109x$	0.83	0.8257	10.87	4727
	LAR	$y=0.00693x^2+0.3972x$	0.97	0.9692	4.569	835
	Bi-square	$y=0.005933x^2+0.4487x$	0.8771	0.874	9.243	3418
3. degree polynomial	Off	$y=0.0001181x^3-0.008837x^2+0.8796x$	0.844	0.836	10.54	4337
	LAR	$y=0.0001252x^3-0.007623x^2+0.716x$	0.957	0.9548	5.539	1196
	Bi-square	$y=0.0001167x^3-0.007342x^2+0.7552x$	0.8897	0,8841	8.866	3066

In the applied equations, linear relation without robust option gave weaker model estimation, but 3rd-degree polynomial was provided a good estimation. Yan et al. (2017) also declared that the relationship between UV fluence and ΔE could be expressed as 3rd-degree polynomial equation. In LAR robust option, the performance of the model prediction decreased by the increasing degree of the equations. On the other hand, the Bi-square robust option provided better model estimation by increasing the degree of the equations. For all models, LAR robust option gave the best value compared to others. In conclusion, the best fitting equation for representing the data was a linear polynomial equation with the LAR robust. The calibration curve constructed with UV fluence and ΔE values and residuals of the curve are given in Figure 4.16 and Figure 4.17.

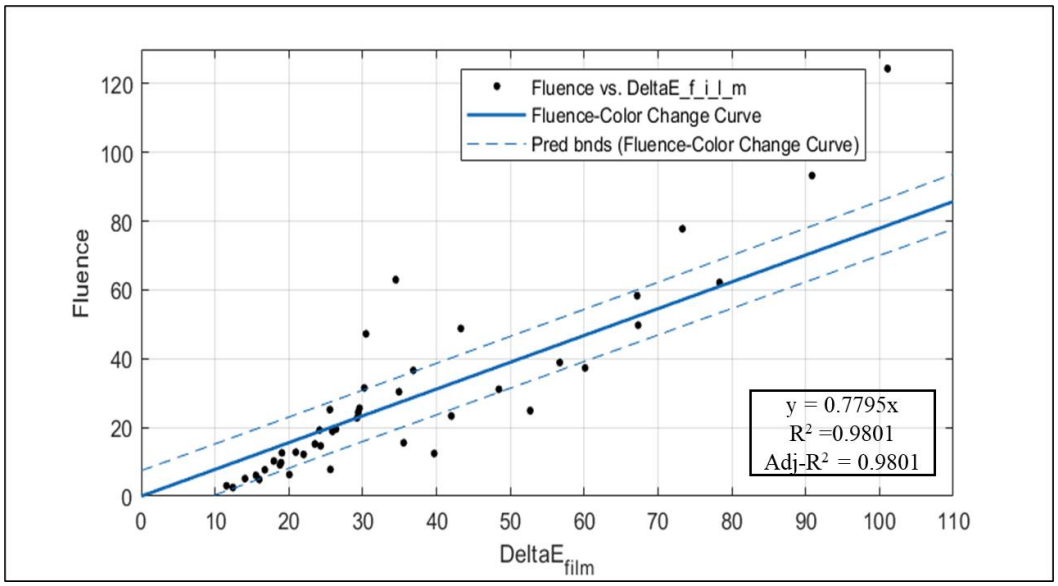

Figure 4. 16. Calibration Curve for Determination of UV Fluence

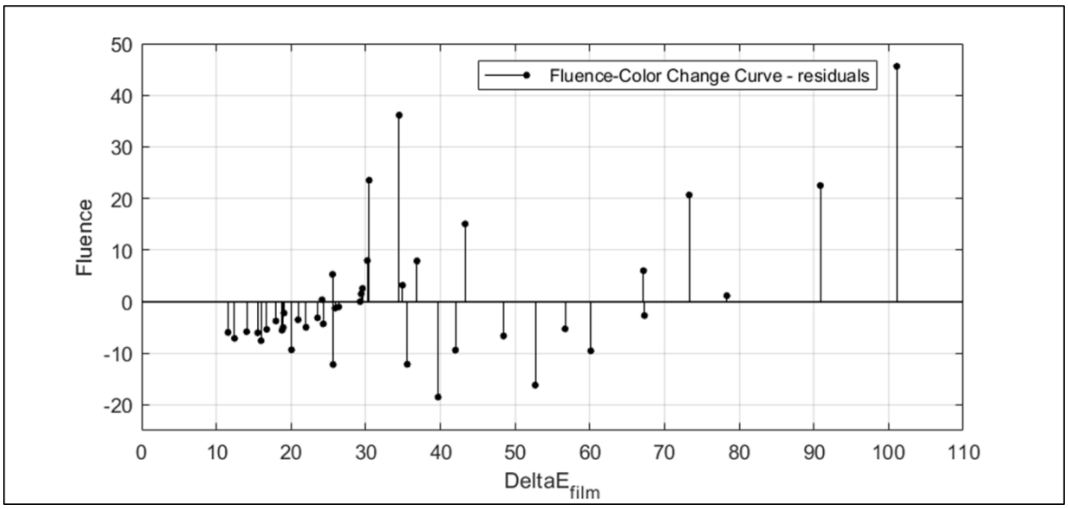

Figure 4. 17. Residuals of Calibration Curve

The accuracy of this constructed calibration curve was tested with validation experiments. For these experiments, a point was chosen each inner (t=7 s) and outer (t= 25 s) point in the previous time interval (0-20 s) for all distances. Then, UV fluence values of films estimated from the calibration curve were tested with those found using actinometric irradiance values belonging to these points. Validation experiment results are given in Table 4.4.

Table 4. 4. Validation Experiments Results for UV Fluence Determination

Distance, cm	**Time, s**	**ΔE**	**UV Fluence, mW/cm^2**	**Predicted UV Fluence, mW/cm^2**
2	7	46.8783	**43.5**	**36.5**
4		32.5065	**27.2**	**25.3**
6		29.6578	**22.1**	**23.1**
8		26.8645	**17.1**	**20.9**
10		22.5844	**10.6**	**17.6**
12		19.4703	**9.0**	**15.2**
2	25	85.2059	**155.5**	**66.4**
4		73.6646	**97.25**	**57.4**
6		66.4058	**78.75**	**51.8**
8		50.4430	**61**	**39.3**
10		48.4327	**38**	**37.8**
12		37.3181	**32**	**29.1**

The model showed a similar trend according to the results of color change and actual fluence values. The model successfully estimated UV fluence values at 7 s exposure time and all distances. However, considering the distances between 2 and 8 cm and the exposure time of 25 s, the UV fluence values were under-predicted by the model. In addition, the estimated UV fluence values for 10 and 12 cm distances were almost the same as those obtained at 2 and 4 cm vertical distances. The results suggested that there was a threshold for UV fluence that could be measured by RCFs. Therefore, the residuals were plotted, and it was revealed that the maximum UV fluence that could be estimated using RCF at 254 nm was approximately 60 mJ/cm^2 (Figure 4.18). Above this value, the color change in the films can not be determined. The difference between the actual and estimated UV fluence values increases, and therefore the error rate increases. In addition, the error of model prediction increased at far distances from the lamp for 7 s exposure time since UV fluence changed exponentially depending on the vertical distance, but the model assumed the linear relation between fluence and color change. However, the model can be accepted due to the statistically successful estimation compared to others. Nevertheless, 60 mJ/cm^2 is enough to inactivate microorganisms such as *E. coli, Giardia lamblia*, and *Cryptosporidium* species in water, according to EPA (Environmental Protection Agency) report (EPA 2022).

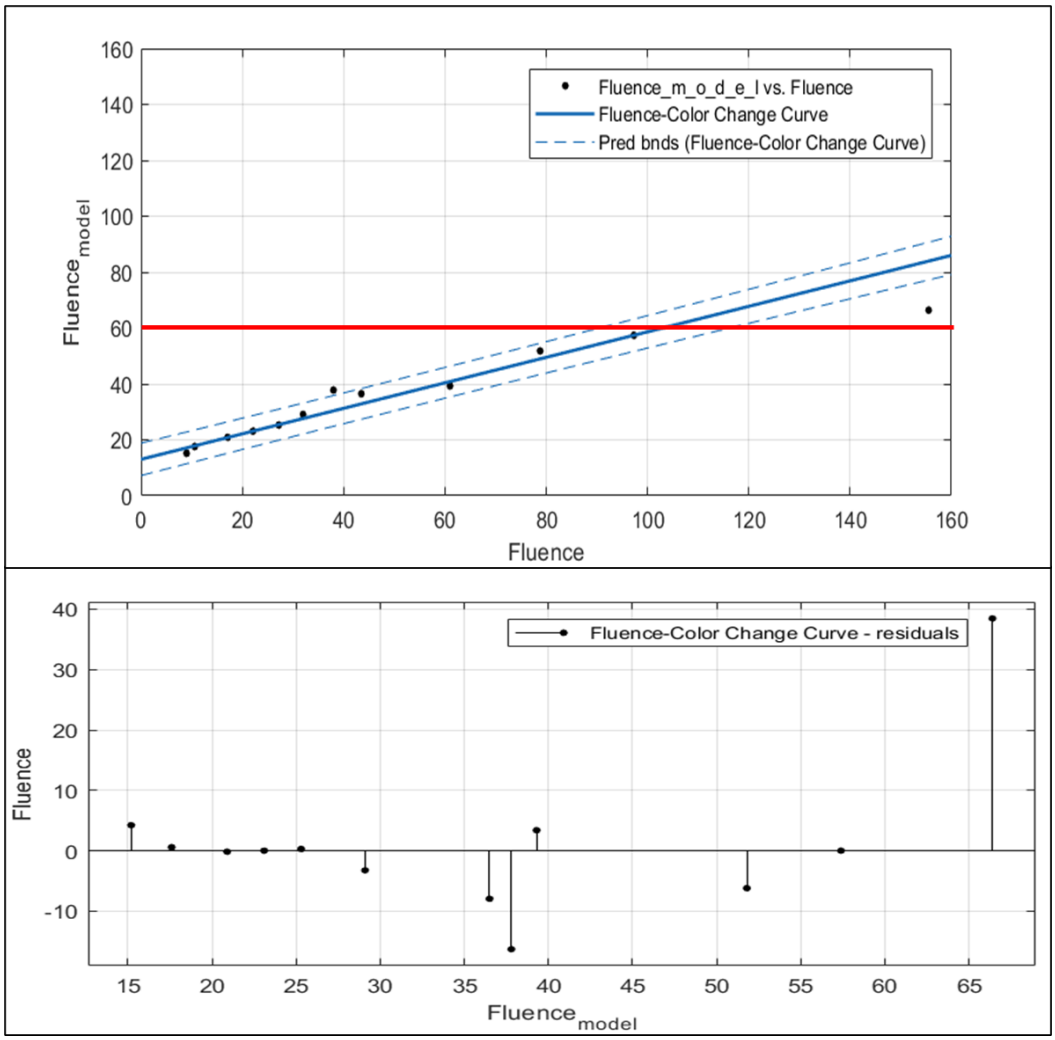

Figure 4. 18. Relationship Between Fluence and Model Fluence

4.5. UV Fluence on Sample Surfaces

4.5.1. Fluence Distribution on Surface of Spherical Apple Samples

The fluence distribution of UV light on the surface of non-uniform-spherical-shaped apple samples was determined using RCFs. For this purpose, RCFs were replaced with the six specified points on the surface of the seven apple samples with different diameters and heights. UVC treatment at a constant UV fluence (47.25 mJ/cm^2 was applied on the top point of samples), but the lateral area and the lowest point of samples were exposed to fewer UV fluences. UV fluence values corresponding to the lateral area and the lowest point of apples were approximately 36.6 and 13.3 mJ/cm^2, respectively. The color of the films on samples before and after the UVC treatment were given in Appendix E. Then, the total color change of RCFs was analyzed with MATLAB.

Absorbed UV fluence values of RCFs were determined from the curve. The total color change and absorbed UV fluence results were summarized in Table 4.5 and Table 4.6.

Table 4. 5. Total Color Change of RCFs at Different Locations on Apple Surface

	LOCATION OF THE FILMS					
SAMPLE NO	**1**	**2**	**3**	**4**	**5**	**6**
1	7.98	8.11	10.34	9.15	73.75	6.19
2	7.35	6.72	8.64	14.56	69.83	5.30
3	5.84	6.28	12.04	8.39	71.75	6.08
4	5.57	6.40	10.74	8.88	69.47	4.68
5	13.63	5.96	7.02	9.72	69.57	5.23
6	6.62	7.95	7.05	9.64	73.14	5.41
7	5.68	6.81	13.76	10.00	68.32	4.75
ΔE_{MEAN}	**7.53**	**6.89**	**9.94**	**10.05**	**70.83**	**5.38**
STD	**2.84**	**0.83**	**2.53**	**2.06**	**2.06**	**0.59**

Table 4. 6. Fluence Distribution on the Surface of Different Apple Samples

	LOCATION OF THE FILMS					
SAMPLE NO	**1**	**2**	**3**	**4**	**5**	**6**
1	6.22	6.32	8.06	7.13	57.48	4.82
2	5.73	5.23	6.73	11.35	54.43	4.13
3	4.55	4.89	9.39	6.54	55.93	4.74
4	4.34	4.99	8.37	6.92	54.16	3.64
5	10.63	4.64	5.47	7.57	54.23	4.08
6	5.16	6.20	5.49	7.51	57.01	4.22
7	4.43	5.31	10.72	7.79	53.26	3.70
UV $Fluence_{mean}$, mJ/cm^2	**5.87**	**5.37**	**7.75**	**7.83**	**55.21**	**4.19**
STD	**2.21**	**0.65**	**1.97**	**1.61**	**1.60**	**0.46**

All apple samples showed the same trend at the specified UV fluence value (47.25 mJ/cm^2). RCFs were exposed to different UV fluences depending on the location of the films. It is known that there is a relation between the total color change of RCFs and absorbed UV fluence. Therefore, it can be confirmed from the color change of the RCFs that the highest fluence induced to apples was observed at the top point of the samples. Locations 1, 2, 3, and 4 were exposed to UV light, but the amount of UV fluence applied to RCFs was much lower than the top point of the apple samples. The bottom points (Location 6) were hardly ever exposed to UVC light since these points remained dark.

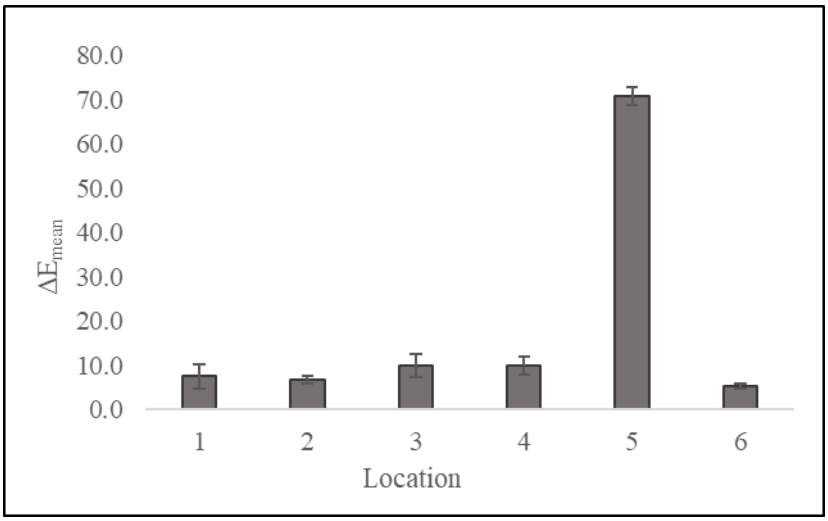

(a)

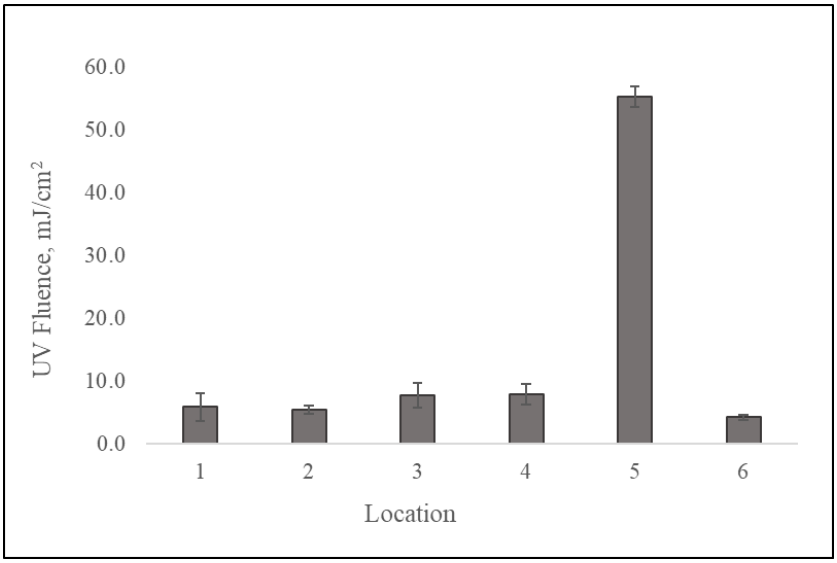

(b)

Figure 4. 19. (a) Color Change Depending on the Location of the Samples (b) Fluence Distribution Depending on the Location of the Samples

Moreover, the linear relation between total color change and absorbed UV fluence and UV fluence distribution on samples was examined in Figure 4.19. It could be concluded that UV distribution on samples had a linear relation with the total color change of films. The results were logical. The nearest point (Location 5) of apples to the lamp had the maximum absorbed UV fluence. In contrast, the bottom of the samples (Location 6) had the lowest UV fluence since RCFs at the top of the samples (stem of apples) was directly exposed to the UV light. Still, RCFs at the bottom of samples (blossom of apples) were rarely exposed to UV light. The total color change value of the original RCF compared to the white background was determined as 5.45. This value confirmed that Location 6 of all apples was never exposed to UV light.

According to Figure 4.19. (b)., lateral points absorbed about 6.7 mJ/cm^2 of UV light, but this fluence value was meager in response to the transmitted UV fluence (36.6 mJ/cm^2). Similarly, the bottom points of the samples had 4.19 mJ/cm^2 absorbed fluence. It was not the expected fluence value. It was concluded that absorption of UV light was ineffective at the lateral area and bottom area of apples. Thus, the shape of a sample is an important factor to be evaluated when applying the UV treatment.

The standard deviation of positions among apple samples was slight enough. However, fluence distribution on all surfaces of samples was unbalanced. Placing apples in the cabin might also cause an unbalanced fluence distribution. RCFs at Locations 1, 2, 3, and 4 were exposed to UVC light poorly, while RCFs at Position 5 absorbed more UVC light due to the vertical distance to the lamp and the shape of apples. Therefore, there is a need to evaluate fluence distribution on the surface of the samples with a different view. More clear results can be obtained by working on the hemispherical surface of different shaped apple samples. Hence, the effect of sample shape will also be revealed.

4.5.2. Fluence Distribution on Surface of Hemispherical Apple Samples

The RCFs were placed on the hemispherical surface of the numbered apple samples as 2, 4, and 7 in Section 4.5.1. These samples were chosen due to having different dimensions from each other. The diameters of the 2, 4, and 7 numbered samples were determined as 8.3, 7.9, and 8 cm, respectively. The height of these samples was measured as 8, 7.6, and 7.8 cm, respectively. Therefore, the effect of the shape of a food product on

UV fluence distribution would be revealed. The same UVC treatment conditions were applied to the hemispherical surfaces of the samples. Nine positions were determined on the hemispherical surface of the samples to evaluate the fluence distribution at almost every surface point. In this way, the color change values of these points represented the overall fluence distribution on the hemispherical surface of the samples. The color change values of RCFs and fluence distribution after UVC treatment at different positions were given in Tables 4.7 and 4.8, and the color change of the films on samples before and after UVC treatment was given in Appendix F. Locations 2, 3, 4, and 5 were determined as the furthest points of the hemispherical surfaces. Hence, these positions were exposed to less UVC light than inner surface points. Locations 6, 7, 8, and 9 were inner points of the hemispherical surface and exposed to more UVC light than outer points, but the maximum UV fluence belonged to the peak point (Location 1) of the surface. This point (Location 1) was the nearest place on the surface to the lamp compared to others and should be exposed to the highest UV fluence among the RCF positions.

Table 4. 7. Total Color Change of RCFs at Different Locations on Apple Hemispherical Surface

SAMPLE NO	**LOCATION OF THE FILMS**								
	1	**2**	**3**	**4**	**5**	**6**	**7**	**8**	**9**
2	64.48	43.39	32.09	8.56	7.77	65.14	54.44	44.86	23.10
4	67.13	38.35	27.32	15.57	9.42	61.84	55.13	47.47	46.04
7	66.72	30.02	18.10	11.85	23.37	52.89	47.51	51.55	43.41
ΔE_{MEAN}	66.11	37.25	25.84	11.99	13.52	59.96	52.36	47.96	37.52
STD	**1.43**	**6.75**	**7.11**	**3.51**	**8.57**	**6.34**	**4.21**	**3.37**	**12.55**

Table 4. 8. Fluence Distribution on the Surface of Different Apple Samples

SAMPLE NO	**LOCATION OF THE FILMS**								
	1	**2**	**3**	**4**	**5**	**6**	**7**	**8**	**9**
2	50.26	33.82	25.02	6.67	6.06	50.78	42.44	34.97	18.01
4	52.33	29.89	21.30	12.14	7.34	48.21	42.98	37.00	35.89
7	52.01	23.40	14.11	9.23	18.21	41.23	37.04	40.18	33.84
UV $Fluence_{mean}$ mJ/cm^2	**51.53**	**29.04**	**20.14**	**9.35**	**10.54**	**46.74**	**40.82**	**37.38**	**29.25**
STD	**1.11**	**5.26**	**5.55**	**2.74**	**6.68**	**4.94**	**3.28**	**2.63**	**9.79**

When the effect of the size of the samples on the UV fluence distribution was examined, it could be said that point 1 was not a good location for comparison since all

samples had the almost same absorbed fluence values at this point, according to Figure 4.20. On the other hand, locations 6, 7, 8, and 9 were the intersection points of Location 2 and 3, Location 2 and 4, Location 3 and 5, and Location 4 and 5, respectively. The UV fluence values at the intersection points could be more than those of outer points, even though they showed a parallel trend with outer points. For instance, the fluence value of Location 9 in Sample 2 was higher than the intersection points 4 and 5. Additionally, sample 2 had the highest color change values. It was due to the fact that sample 2 was larger and had the highest diameter. Thus, the apple was much closer to the lamp than the other samples.

In the light of this information, for Sample 4, the lowest color change and fluence value were expected. Locations 7, 8, and 9 of Sample 4 had a higher UV fluence value than Sample 2. This may be mainly due to the shape of the product. It is known that the UV irradiance decreases from midpoint to endpoint throughout the lamp. The midpoint of the lamp corresponds to the apex of the hemisphere, while the outer points correspond to the place away from the midpoint of the lamp. In this case, it was speculated that the points on the samples could be exposed to varying beam intensity throughout the lamp. Sample 2 had a flatter shape than Sample 4. Therefore, the outer points of Sample 2 may have been exposed to less UV light than the outer points of Sample 4.

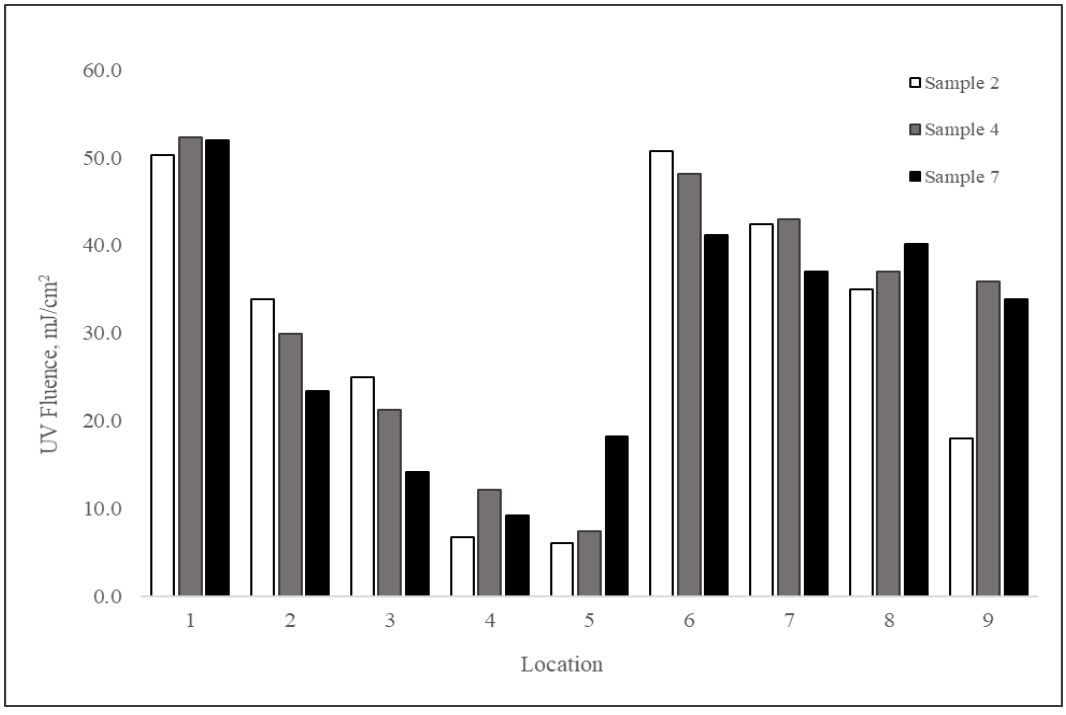

Figure 4. 20. Fluence Distribution on Different Locations of the Hemispherical Surface of the Apples

CHAPTER 5

CONCLUSION

UV-C light is widely used in different industries, including the food industry, for its germicidal effects. UV-C technology is a preferred application for disinfection contaminated smooth and flat surfaces. However, most solid food products have rough and non-uniform structures. Due to the surface morphology of food products, blind spots on the surface of the products pose a challenge to the effectiveness of the UVC disinfection process. Because it becomes difficult to provide a homogeneous UV fluence distribution on the surface. UV fluence is calculated by multiplying UV irradiance and exposure time. In food processing, applied UV irradiance can be measured using biodosimetry, chemical actinometry, and computational fluid dynamics (CFD). All methods have their own advantages but also have drawbacks. In this study, as an alternative technique to these methods, it is assumed that the UV fluence applied to the surfaces can be determined by considering the color change of radiochromic films exposed to UV rays. Radiochmic films are colorless, transparent films, and they turn to a colored form depending on the applied UV fluence. Thus, the aim of this thesis is to examine the color change of RCFs in response to UV intensity (irradiance), exposure time, temperature, and storage time by image analysis, to compare the accuracy of the UV intensity (irradiance) measurement with the radiometer and actinometer methods, and to determine the usability of RCFs for UV fluence measurement on surfaces of solid food products. For this purpose, different UV irradiance values were obtained at different distances from the UV lamps (e.g., 2, 4, 6, 8, 10, and 12 cm) and different exposure times (2, 4, 6, 8, 10, 15, and 20 s) were initially selected. Hence, several UV fluence values were obtained. It was found that a time interval of 0-20 s should be chosen since color changes of more than 20 s cannot be distinguished in RCFs.

UVC treatment was applied to the RCFs for specified UV irradiance and time values, and a color change matrix was formed for irradiated RCFs. The darker colors were obtained for higher UV fluences, while the less UV treated films remained the lighter colors. The color measurement of films was taken with both CM and MATLAB to compare the accuracy of the MATLAB code. The results showed that both methods determined the L*and b* values with a similar pattern, but L* and b* readings were

mismatched. The reason behind this problem was stated as working algorithms of methods. However, the total color change pattern was parallel to each other. The maximum color changes were obtained at the highest exposure time (t=20 s) for each distance. At a specified distance (e.g., 6 cm), the total color change of RCF increased at increasing exposure times.

On the other hand, for a specified exposure time (e.g., 10 s), the color change of RCF showed reverse behavior at increasing vertical distances to the lamp. Furthermore, the color stability of the RCFs was examined. The results indicate that RCFs remain stable at room and refrigerator temperature for 15-day storage. Finally, the relationship between the color change of RCF and applied UV fluence was investigated. For this purpose, the UV fluence values depending on the vertical distance and exposure time were determined with a radiometer and actinometer.

In radiometer experiments, measurements were taken for each selected vertical distance to the UV lamp. It can be stated that UV irradiance decreases exponentially when moving away from the UV lamp, and the curve pattern obeys the Beer-Lambert Law. The maximum UV irradiance value was measured as 1.88 mW/cm^2, decreasing to 0.16 mW/cm^2 at a 12 cm vertical distance. Similarly, the maximum UV fluence value was obtained as 37.6 mJ/cm^2 at a 2 cm vertical distance to the lamp and 20 s exposure time.

In actinometry studies, potassium iodide/iodate actinometer was used for UV fluence measurement. UV irradiance values were determined as a function of changing absorbance values of irradiated solutions at 352 nm wavelength. The UV fluence matrix was obtained as in radiometry. The results showed that the maximum UV irradiance was 6.22 mW/cm2, and the minimum was 1.28 mW/cm^2. UV irradiance behavior of the actinometer obeyed the Beer-Lambert Law. Also, the maximum and minimum UV fluence was determined as 124.4 and 2.56 mJ/cm^2, respectively.

Irradiance values of the radiometer and actinometer gave different results for a specified distance, but the pattern of them was similar. Both values fitted the Beer-Lambert Law. Actinometer measured the UV irradiance values approximately 6-fold bigger than the radiometer. For fluence values obtained from the radiometer and actinometer, it can be concluded that UV fluence changes exponentially with distance but there is a linear relation between UV fluence and exposure time. To associate the color change of RCF with UV fluence, the actinometric UV fluence values were chosen due to

the accuracy of them. Then, according to curve fitting trials, it can be confirmed that the relationship between UV fluence and the color change of the RCF can be expressed with linear equation. It was revealed that the maximum UV fluence that could be estimated using RCF at 254 nm was approximately 60 mJ/cm^2. Above this value, the color change in the films can not be determined. Therefore, RCFs can be used to determine the applied UV fluence on the food sample.

In the second part of the thesis, RCFs were replaced on the different positions of apple samples to test the hypothesis confirmed from the previous experiments. Apple samples were exposed to UV light via two different view replacements. For Case 1, apple samples were replaced under the UV lamp as the stem point facing up. The results of Case 1 showed that UV fluence distribution was inhomogeneous on the samples. Films at the top positions of samples absorbed the higher fluences, while other positions rarely absorbed the UV light. Therefore, other replacements should have been applied to the apples to determine the surface fluence distribution. Apple samples were replaced under the UV lamp as hemispherical surfaces facing up for Case 2. The outcome of this experiment can be summarized as that the outer points of samples are rarely exposed to UV light, but the color change of RCFs at inner points indicates the absorbed UV fluences. Furthermore, the shape of apples causes different UV fluence distribution profiles.

In overall conclusion, RCFs can be used for determination of UV fluence distribution on surface of solid food samples in the food industry. However, rotation is necessary to provide homogeneous fluence distribution on the surface of the products. The application of RCFs on food samples can be tested on a pilot production line. Furthermore, the problem encountered in image analysis can be prevented by changing this method with other modernist techniques, such as using artificial neural networks.

REFERENCES

Adhikari, C., T. Koutchma, and T. Beecham-Bowden. 2005. “Evaluation of HHEVC (4, 4′, 4″-Tris-Di-B-Hydroxyethyl Aminotriphenylacetonitrile) Dye as a Chemical Actinometer in Model Buffers for UV Treatment of Apple Juice and Cider.” *LWT - Food Science and Technology* 38 (7): 717–25. https://doi.org/10.1016/j.lwt.2004.09.009.

Antonio-Gutiérrez, Oscar, Andrea López-Díaz, Enrique Palou, Aurelio López-Malo, and Nelly Ramírez-Corona. 2019. “Characterization and Effectiveness of Short-Wave Ultraviolet Irradiation Reactors Operating in Continuous Recirculation Mode to Inactivate Saccharomyces Cerevisiae in Grape Juice.” *Journal of Food Engineering* 241: 88–96. https://doi.org/https://doi.org/10.1016/j.jfoodeng.2018.08.011.

Arshak, Khalil. 2006. *Advanced Materials and Techniques for Radiation Dosimetry*. Artech. http://ieeexplore.ieee.org/document/9100990.

Atılgan, M.R. 2013. “DESIGN OF A CONTINUOUS FLOW UV REACTOR FOR OPAQUE LIQUID FOODS BY USING COMPUTATIONAL FLUID DYNAMICS (CFD).” İzmir Institute of Technology.

Banerjee, S, E G Hoch, P D Kaplan, and E L P Dumont. 2017. “A Comparative Study of Wearable Ultraviolet Radiometers.” In *2017 IEEE Life Sciences Conference (LSC)*, 9–12. https://doi.org/10.1109/LSC.2017.8268131.

Barth, J. 1987. “[Johann Wilhelm Ritter (1776-1810) and the discovery of ultraviolet irradiation 185 years ago].” *Der Hautarzt; Zeitschrift fur Dermatologie, Venerologie, und verwandte Gebiete* 38 (5): 301–3.

Bartwal, Naman, and Pradeep Kumar. 2018. *CALCULATION OF NON-GRAY RADIATION ABSORPTIVITY AND ABSORPTION COEFFICIENT OF MIXTURE OF GASES FROM HITEMP-2010 DATABASE*. https://doi.org/10.1615/IHTC16.cms.023070.

Barut Gök, Sila, Volker Gräf, and Mario R. Stahl. 2020. “Engineering Aspects of UV-C Processing for Liquid Foods.” *Innovative Food Processing Technologies: A Comprehensive Review*, 171–81. https://doi.org/10.1016/b978-0-08-100596-5.23000-x.

Bintsis, Thomas, Evanthia Litopoulou-Tzanetaki, and Richard K Robinson. 2000. “Existing and Potential Applications of Ultraviolet Light in the Food Industry - a Critical Review.” *Journal of the Science of Food and Agriculture* 80 (6): 637–45. https://doi.org/10.1002/(SICI)1097-0010(20000501)80:6<637::AID-JSFA603>3.0.CO;2-1.

Bolton, Ian Mayor-Smith, and Karl G Linden. 2015. “Rethinking the Concepts of Fluence (UV Dose) and Fluence Rate: The Importance of Photon-Based Units - A Systemic Review.” *Photochemistry and Photobiology* 91 (6): 1252–62. https://doi.org/10.1111/php.12512.

Bolton, R.J., and K. Linden. 2003. “Standardization of Methods for Fluence (UV Dose) Determination in Bench-Scale UV Experiments.” *Journal of Environmental Engineering* 129 (3): 209–15. https://doi.org/10.1061/(ASCE)0733-9372(2003)129:3(209).

Bolton, Mihaela I Stefan, Ping-Shine Shaw, and Keith R Lykke. 2011. “Determination of the Quantum Yields of the Potassium Ferrioxalate and Potassium Iodide–Iodate Actinometers and a Method for the Calibration of Radiometer Detectors.” *Journal of Photochemistry and Photobiology A: Chemistry* 222 (1): 166–69. https://doi.org/https://doi.org/10.1016/j.jphotochem.2011.05.017.

Bouslimi, Lotfi, Mongi, Ezzedine Ben Braiek, Georges, and Jean Pascal Cambronne. 2012. “High Power Discharge Lamps and Their Photochemical Applications: An Evaluation of Pulsed Radiation.” *Molecular Photochemistry - Various Aspects*. https://doi.org/10.5772/37769.

Briones, Vilbett, and Josè M Aguilera. 2005. “Image Analysis of Changes in Surface Color of Chocolate.” *Food Research International* 38 (1): 87–94.

https://doi.org/https://doi.org/10.1016/j.foodres.2004.09.002.

Butot, Sophie, Frédérique Cantergiani, Mireille Moser, Julie Jean, Anthony Lima, Lise Michot, Thierry Putallaz, Thomas Stroheker, and Sophie Zuber. 2018. "UV-C Inactivation of Foodborne Bacterial and Viral Pathogens and Surrogates on Fresh and Frozen Berries." *International Journal of Food Microbiology* 275: 8–16. https://doi.org/https://doi.org/10.1016/j.ijfoodmicro.2018.03.016.

Butson, Martin J, Peter K N Yu, Tsang Cheung, and Peter Metcalfe. 2003. "Radiochromic Film for Medical Radiation Dosimetry." *Materials Science and Engineering: R: Reports* 41 (3): 61–120. https://doi.org/https://doi.org/10.1016/S0927-796X(03)00034-2.

Casolaro, Pierluigi, Luigi Campajola, Giovanni Breglio, Salvatore Buontempo, Marco Consales, Andrea Cusano, Antonello Cutolo, Francesco Di Capua, Francesco Fienga, and Patrizio Vaiano. 2019. "Real-Time Dosimetry with Radiochromic Films." *Scientific Reports* 9 (1): 5307. https://doi.org/10.1038/s41598-019-41705-0.

CFIA. n.d. "Canada Food Regulations." https://www.canada.ca/en/health-canada/services/food-nutrition/food-safety/food-irradiation/food-irradiation.html.

Cheung, Tsang, Martin J Butson, and Peter K N Yu. 2005. "Post-Irradiation Colouration of Gafchromic EBT Radiochromic Film." *Physics in Medicine and Biology* 50 (20): N281-5. https://doi.org/10.1088/0031-9155/50/20/N04.

Choudhary, Ruplal, and Srinivasarao Bandla. 2012. "Ultraviolet Pasteurization for Food Industry." *International Journal of Food Science and Nutrition Engineering* 2 (1): 12–15. https://doi.org/10.5923/j.food.20120201.03.

Devic, Slobodan, Nada Tomic, and David Lewis. 2016. "Reference Radiochromic Film Dosimetry: Review of Technical Aspects." *Physica Medica : PM : An International Journal Devoted to the Applications of Physics to Medicine and Biology : Official Journal of the Italian Association of Biomedical Physics (AIFB)* 32 (4): 541–56. https://doi.org/10.1016/j.ejmp.2016.02.008.

EFSA. 2016. “Safety of UV-treated Milk as a Novel Food Pursuant to Regulation (EC) No 258/97.” *EFSA Journal* 14 (1): 1–14. https://doi.org/10.2903/j.efsa.2016.4370.

EPA. 2022. “Ultraviolet (UV) Treatment Toolkit: Technical Resource for States Using EPA’s Ultraviolet Disinfection Guidance Manual to Evaluate UV Technology.” https://www.epa.gov/system/files/documents/2022-05/uv-toolkit-815-B-21-007_0.pdf.

Falguera, Víctor, Jordi Pagán, Salvador Garza, Alfonso Garvín, and Albert Ibarz. 2011. “Ultraviolet Processing of Liquid Food: A Review. Part 1: Fundamental Engineering Aspects.” *Food Research International* 44 (6): 1571–79. https://doi.org/https://doi.org/10.1016/j.foodres.2011.02.056.

Fan, Xuetong, Runze Huang, and Haiqiang Chen. 2017. “Application of Ultraviolet C Technology for Surface Decontamination of Fresh Produce.” *Trends in Food Science & Technology* 70: 9–19. https://doi.org/https://doi.org/10.1016/j.tifs.2017.10.004.

FAO. n.d. “Food Security.” https://www.fao.org/3/y4671e/y4671e06.htm#:~:text=Food security exists when all,an active and healthy life.

FDA. 2000. “FDA Food Regulations.” Title21-Chapter I- Subpart B -179.39. 2000. https://www.ecfr.gov/current/title-21/chapter-I/subchapter-B/part-179/subpart-B/section-179.39.

Feliciano, Rodney J, and Alonzo A Gabriel. 2019. “Juice Composition, Physicochemistry, and Efficacy of Ultraviolet Radiation against Cryptococcus Albidus.” *Journal of Food Composition and Analysis* 84: 103313. https://doi.org/https://doi.org/10.1016/j.jfca.2019.103313.

Fenoglio, Daniela, Mariana Ferrario, Marcela Schenk, and Sandra Guerrero. 2019. “UV-C Light Inactivation of Single and Composite Microbial Populations in Tangerine-Orange Juice Blend. Evaluation of Some Physicochemical Parameters.” *Food and Bioproducts Processing* 117: 149–59. https://doi.org/https://doi.org/10.1016/j.fbp.2019.07.005.

———. 2020. “Effect of Pilot-Scale UV-C Light Treatment Assisted by Mild Heat on E. Coli, L. Plantarum and S. Cerevisiae Inactivation in Clear and Turbid Fruit Juices. Storage Study of Surviving Populations.” *International Journal of Food Microbiology* 332: 108767. https://doi.org/https://doi.org/10.1016/j.ijfoodmicro.2020.108767.

Ferreira, Cristiano Dietrich, Gustavo Heinrich Lang, Igor da Silva Lindemann, Newiton da Silva Timm, Jessica Fernanda Hoffmann, Valmor Ziegler, and Maurício de Oliveira. 2021. “Postharvest UV-C Irradiation for Fungal Control and Reduction of Mycotoxins in Brown, Black, and Red Rice during Long-Term Storage.” *Food Chemistry* 339: 127810. https://doi.org/https://doi.org/10.1016/j.foodchem.2020.127810.

Florian, D., and G. Knapp. 2001. “High-Temperature, Microwave-Assisted UV Digestion: A Promising Sample Preparation Technique for Trace Element Analysis.” *Analytical Chemistry* 73 (7): 1515–20. https://doi.org/10.1021/ac001180y.

FWT. 2022. “FWT-60-00 Radichromic Film Properties.” 2022. https://www.fwt.com/racm/fwt60ds.htm.

Gabriel, Alonzo A, Ma. Luisa P Ballesteros, Leo Mendel D Rosario, Roy B Tumlos, and Henry J Ramos. 2018. “Elimination of Salmonella Enterica on Common Stainless Steel Food Contact Surfaces Using UV-C and Atmospheric Pressure Plasma Jet.” *Food Control* 86: 90–100. https://doi.org/https://doi.org/10.1016/j.foodcont.2017.11.011.

Gabriel, Alonzo A, Katrina Moira D Melo, and Juan Carlos D Michelena. 2020. “Determination of the Utility of Ultraviolet-C Irradiation for Dried Bay Leaves Microbial Decontamination through Safety and Quality Evaluations.” *LWT* 117: 108634. https://doi.org/https://doi.org/10.1016/j.lwt.2019.108634.

Gabriel, Alonzo A, Desiree D Vera, Olga Monina Y Lazo, Vallerie B Azarcon, Cleomelle G De Ocampo, Jovelyn C Marasigan, and Gloria T Sandel. 2017.

"Ultraviolet-C Inactivation of Escherichia Coli O157:H7, Listeria Monocytogenes, Pseudomonas Aeruginosa, and Salmonella Enterica in Liquid Egg White." *Food Control* 73: 1303–9. https://doi.org/https://doi.org/10.1016/j.foodcont.2016.10.060.

Gafchromic. 2022. "Radiochromic Film Properties." 2022. http://www.gafchromic.com/gafchromic-film/index.asp.

García Carrillo, Mercedes, Mariana Ferrario, and Sandra Guerrero. 2017. "Study of the Inactivation of Some Microorganisms in Turbid Carrot-Orange Juice Blend Processed by Ultraviolet Light Assisted by Mild Heat Treatment." *Journal of Food Engineering* 212: 213–25. https://doi.org/https://doi.org/10.1016/j.jfoodeng.2017.06.005.

Gayán, Elisa, Santiago Condón, and Ignacio Álvarez. 2014. "Continuous-Flow UV Liquid Food Pasteurization: Engineering Aspects." *Food and Bioprocess Technology* 7 (10): 2813–27. https://doi.org/10.1007/s11947-014-1267-0.

GEX. 2022. "GEX B3 Radiochromic Film Properties." 2022. https://www.gexcorp.com/b3-dosimeters.html.

Gidari, Anna, Samuele Sabbatini, Sabrina Bastianelli, Sara Pierucci, Chiara Busti, Desirée Bartolini, Anna Maria Stabile, et al. 2021. "SARS-CoV-2 Survival on Surfaces and the Effect of UV-C Light." *Viruses* 13 (3). https://doi.org/10.3390/v13030408.

Gogo, E O, A M Opiyo, K Hassenberg, Ch. Ulrichs, and S Huyskens-Keil. 2017. "Postharvest UV-C Treatment for Extending Shelf Life and Improving Nutritional Quality of African Indigenous Leafy Vegetables." *Postharvest Biology and Technology* 129: 107–17. https://doi.org/https://doi.org/10.1016/j.postharvbio.2017.03.019.

Golombek, Patricia, Michael Wacker, Nina Buck, and Dominik Durner. 2021. "Impact of UV-C Treatment and Thermal Pasteurization of Grape Must on Sensory Characteristics and Volatiles of Must and Resulting Wines." *Food Chemistry* 338: 128003. https://doi.org/https://doi.org/10.1016/j.foodchem.2020.128003.

Guerrero-Beltrán, J A, and G V Barbosa-Cánovas. 2004. “Advantages and Limitations on Processing Foods by UV Light.” *Food Science and Technology International* 10 (3): 137–47. https://doi.org/10.1177/1082013204044359.

Gündüz, Gülten Tiryaki, and Ayça Korkmaz. 2019. “UV-C Treatment for the Inhibition of Molds Isolated from Dried Persimmons (Diospyros Kaki L.) and Modelling of UV-C Inactivation Kinetics.” *LWT* 115: 108451. https://doi.org/https://doi.org/10.1016/j.lwt.2019.108451.

Ha, Jae-Won, Jae-Ik Lee, and Dong-Hyun Kang. 2017. “Application of a 222-Nm Krypton-Chlorine Excilamp to Control Foodborne Pathogens on Sliced Cheese Surfaces and Characterization of the Bactericidal Mechanisms.” *International Journal of Food Microbiology* 243: 96–102. https://doi.org/https://doi.org/10.1016/j.ijfoodmicro.2016.12.005.

Hakguder Taze, Bengi, and Sevcan Unluturk. 2018. “Effect of Postharvest UV-C Treatment on the Microbial Quality of ‘Şalak’ Apricot.” *Scientia Horticulturae* 233: 370–77. https://doi.org/https://doi.org/10.1016/j.scienta.2018.02.012.

Holck, Askild, Kristian Hovde Liland, Mats Carlehög, and Even Heir. 2018. “Reductions of Listeria Monocytogenes on Cold-Smoked and Raw Salmon Fillets by UV-C and Pulsed UV Light.” *Innovative Food Science & Emerging Technologies* 50: 1–10. https://doi.org/https://doi.org/10.1016/j.ifset.2018.10.007.

Hutchings, J., R. Luo, and W. Ji. 2000. “Calibrated Colour Imaging Analysis of Food.” In *Color in Food Improving Quality*, edited by D.B. MacDougall, 1st ed. Baco Raton: CRC Press LLC.

Izmirlioglu, Gulten, Beining Ouyang, and Ali Demirci. 2020. “Utilization of Pulsed UV Light for Inactivation of Salmonella Enteritidis on Shelled Walnuts.” *LWT* 134: 110023. https://doi.org/https://doi.org/10.1016/j.lwt.2020.110023.

Jeon, Min-Jin, and Jae-Won Ha. 2018. “Efficacy of UV-A, UV-B, and UV-C Irradiation on Inactivation of Foodborne Pathogens in Different Neutralizing Buffer Solutions.” *LWT* 98: 591–97.

https://doi.org/https://doi.org/10.1016/j.lwt.2018.09.030.

Jin, Shanshan, Karl G Linden, Joel Ducoste, and Dong Liu. 2005. “Impact of Lamp Shadowing and Reflection on the Fluence Rate Distribution in a Multiple Low-Pressure UV Lamp Array.” *Water Research* 39 (12): 2711–21. https://doi.org/https://doi.org/10.1016/j.watres.2005.04.071.

Jin, Shanshan, Alex Mofidi, and Karl Linden. 2006. “Polychromatic UV Fluence Measurement Using Chemical Actinometry, Biodosimetry, and Mathematical Techniques.” *Journal of Environmental Engineering-Asce - J ENVIRON ENG-ASCE* 132 (August). https://doi.org/10.1061/(ASCE)0733-9372(2006)132:8(831).

Karma, I Gede Made. 2020. “Determination and Measurement of Color Dissimilarity.” *International Journal of Engineering and Emerging Technology* 5 (July): 67. https://doi.org/10.24843/IJEET.2020.v05.i01.p13.

Kaya, Zehra, Semanur Yıldız, and Sevcan Ünlütürk. 2015. “Effect of UV-C Irradiation and Heat Treatment on the Shelf Life Stability of a Lemon–Melon Juice Blend: Multivariate Statistical Approach.” *Innovative Food Science & Emerging Technologies* 29: 230–39. https://doi.org/https://doi.org/10.1016/j.ifset.2015.03.005.

Kebbi, Yasmine, Aliyu Idris Muhammad, Anderson S. Sant’Ana, Leonardo do Prado-Silva, Donghong Liu, and Tian Ding. 2020. “Recent Advances on the Application of UV-LED Technology for Microbial Inactivation: Progress and Mechanism.” *Comprehensive Reviews in Food Science and Food Safety* 19 (6): 3501–27. https://doi.org/10.1111/1541-4337.12645.

Keklik, N. M., and Ali Demirci. 2009. “Food Safety Series--Pulsed UV-Light: Advantages for Food Decontamination.” *Resource Magazine* 16 (5): 18–19. https://elibrary.asabe.org/abstract.asp?aid=29318&t=11.

Koutchma. 2018. “Status of International Regulations for Ultraviolet Treatment of Foods.” *IUVA News* 20 (2): 13–16. http://www.efsa.europa.eu/en/efsajournal/.

———. 2021. “Fluence Concept, Theoretical Evaluation and Practical Validation in UVC Preservation of Opaque Food Liquids and Beverages.” In *Innovative Food Processing Technologies*, 136–45. https://doi.org/10.1016/B978-0-08-100596-5.22961-2.

Koutchma, Larry J. Forney, and Carmen I. Moraru. 2009. *Ultraviolet Light in Food Technology Principles and Applications*. Edited by Da-wen Sun. 1. Boca Raton: CRC Press Taylor&Francis Group.

Koutchma, Marta Orlowska, and Yan Zhu. 2012. “Fruits and Fruit.” In *Fruit Preservation*, edited by Amauri Rosires Rosenthal, Jorge Welti-Chanes Deliza, and Gustavo V. Barbosa-Cánovas, 457–504.

Koutchma, Tatiana, Vladimir Popović, and Andrew Green. 2019. “Overview of Ultraviolet (UV) LEDs Technology for Applications in Food Production.” *Ultraviolet LED Technology for Food Applications: From Farms to Kitchens*, 1–23. https://doi.org/10.1016/B978-0-12-817794-5.00001-7.

Kowalski, Wladyslaw. 2009. *Ultraviolet Germicidal Irradiation Handbook: UVGI for Air and Surface Disinfection*. *Ultraviolet Germicidal Irradiation Handbook: UVGI for Air and Surface Disinfection*. https://doi.org/10.1007/978-3-642-01999-9.

Kuhn, H, Silvia Braslavsky, and R Schmidt. 1989. “Chemical Actinometry.” *Pure and Applied Chemistry, v.76, 2105-2146 (2004)* 61 (February). https://doi.org/10.1351/pac198961020187.

Kumar, Amit, Rojalin Nayak, Soumya Ranjan Purohit, and Pavuluri Srinivasa Rao. 2021. “Impact of UV-C Irradiation on Solubility of Osborne Protein Fractions in Wheat Flour.” *Food Hydrocolloids* 110: 105845. https://doi.org/https://doi.org/10.1016/j.foodhyd.2020.105845.

Lehóczki, Tímea, Éva Józsa, and Katalin Ősz. 2013. “Ferrioxalate Actinometry with Online Spectrophotometric Detection.” *Journal of Photochemistry and Photobiology A: Chemistry* 251: 63–68. https://doi.org/https://doi.org/10.1016/j.jphotochem.2012.10.005.

LightTech. 2013. “Germicidal Lamp Basics.”

Lukinac, Jasmina, Kristina Habschied, Krešimir Mastanjević, Gjore Nakov, and Marko Jukić. 2019. “Computer Vision Method in Beer Quality Evaluation—A Review.” *Beverages* 5 (June): 38. https://doi.org/10.3390/beverages5020038.

Ly, Bao Chau K, Ethan B Dyer, Jessica L Feig, Anna L Chien, and Sandra Del Bino. 2020. “Research Techniques Made Simple: Cutaneous Colorimetry: A Reliable Technique for Objective Skin Color Measurement.” *Journal of Investigative Dermatology* 140 (1): 3-12.e1. https://doi.org/https://doi.org/10.1016/j.jid.2019.11.003.

Martínez-Sánchez, Ascensión, Pedro Lozano-Pastor, Francisco Artés-Hernández, Francisco Artés, and Encarna Aguayo. 2019. “Preharvest UV-C Treatment Improves the Quality of Spinach Primary Production and Postharvest Storage.” *Postharvest Biology and Technology* 155: 130–39. https://doi.org/https://doi.org/10.1016/j.postharvbio.2019.05.021.

Martínez-Zamora, Lorena, Noelia Castillejo, and Francisco Artés-Hernández. 2021. “Postharvest UV-B and UV-C Radiation Enhanced the Biosynthesis of Glucosinolates and Isothiocyanates in Brassicaceae Sprouts.” *Postharvest Biology and Technology* 181: 111650. https://doi.org/https://doi.org/10.1016/j.postharvbio.2021.111650.

Mathworks. 2022a. “General Information about MATLAB.” 2022. https://www.mathworks.com/products/matlab.html.

———. 2022b. “MATLAB Program Curve Fitting.” 2022. https://www.mathworks.com/matlabcentral/answers/183690-what-is-the-difference-between-lar-and-the-bisquare-remain-robust-in-regression-curve-fitting-tool.

Mayerhöfer, Thomas G, Susanne Pahlow, and Jürgen Popp. 2020. “The Bouguer-Beer-Lambert Law: Shining Light on the Obscure.” *Chemphyschem : A European Journal of Chemical Physics and Physical Chemistry* 21 (18): 2029–46.

https://doi.org/10.1002/cphc.202000464.

Miller, A, W Batsberg, and W Karman. 1988. “A New Radiochromic Thin-Film Dosimeter System.” *International Journal of Radiation Applications and Instrumentation. Part C. Radiation Physics and Chemistry* 31 (4): 491–96. https://doi.org/https://doi.org/10.1016/1359-0197(88)90216-0.

Murov, Carmichael, Hug Ian., Gordon L., Gordon L., and Steven L. 1993. *Handbook of Photochemistry*. New York: Marcel Dekker.

Nicolau-Lapeña, Iolanda, Pilar Colás-Medà, Inmaculada Viñas, and Isabel Alegre. 2022. “Inactivation of Escherichia Coli, Salmonella Enterica and Listeria Monocytogenes on Apple Peel and Apple Juice by Ultraviolet C Light Treatments with Two Irradiation Devices.” *International Journal of Food Microbiology* 364: 109535. https://doi.org/https://doi.org/10.1016/j.ijfoodmicro.2022.109535.

Niroomand-Rad, A, C R Blackwell, B M Coursey, K P Gall, J M Galvin, W L McLaughlin, A S Meigooni, R Nath, J E Rodgers, and C G Soares. 1998. “Radiochromic Film Dosimetry: Recommendations of AAPM Radiation Therapy Committee Task Group 55. American Association of Physicists in Medicine.” *Medical Physics* 25 (11): 2093–2115. https://doi.org/10.1118/1.598407.

Noori, Ansara, Parvez Mahbub, Miloš Dvořák, Arko Lucieer, and Mirek Macka. 2018. “Radiometric Analysis of UV to near Infrared LEDs for Optical Sensing and Radiometric Measurements in Photochemical Systems.” *Sensors and Actuators B: Chemical* 262: 171–79. https://doi.org/https://doi.org/10.1016/j.snb.2018.01.179.

Pagal, Gladess A, and Alonzo A Gabriel. 2020. “Individual and Combined Mild Heat and UV-C Processes for Orange Juice against Escherichia Coli O157:H7.” *LWT* 126: 109295. https://doi.org/https://doi.org/10.1016/j.lwt.2020.109295.

Palmieri, L., and D. Cacae. 2005. “High Intensity Pulsed Light Technology.” In *Emerging Technologies for Food Processing*, edited by Da-Wen Sun, 1st ed., 279–307. San Diego: Elsevier Ltd.

Pathare, Pankaj B, Umezuruike Linus Opara, and Fahad Al-Julanda Al-Said. 2013. "Colour Measurement and Analysis in Fresh and Processed Foods: A Review." *Food and Bioprocess Technology* 6 (1): 36–60. https://doi.org/10.1007/s11947-012-0867-9.

Patras, Ankit, Manreet Bhullar, Brahmaiah Pendyala, and Ferdinando Crapulli. 2020. "Ultraviolet Treatment of Opaque Liquid Foods: From Theory to Practice." In . https://doi.org/10.1016/B978-0-08-100596-5.22941-7.

Pedrós-Garrido, S, S Condón-Abanto, I Clemente, J A Beltrán, J G Lyng, D Bolton, N Brunton, and P Whyte. 2018. "Efficacy of Ultraviolet Light (UV-C) and Pulsed Light (PL) for the Microbiological Decontamination of Raw Salmon (Salmo Salar) and Food Contact Surface Materials." *Innovative Food Science & Emerging Technologies* 50: 124–31. https://doi.org/https://doi.org/10.1016/j.ifset.2018.10.001.

Possas, Arícia, Antonio Valero, Rosa María García-Gimeno, Fernando Pérez-Rodríguez, and Poliana Mendes de Souza. 2018. "Influence of Temperature on the Inactivation Kinetics of Salmonella Enteritidis by the Application of UV-C Technology in Soymilk." *Food Control* 94: 132–39. https://doi.org/https://doi.org/10.1016/j.foodcont.2018.06.033.

Qiang, Zhimin, Wentao Li, Mengkai Li, James R Bolton, and Jiuhui Qu. 2015. "Inspection of Feasible Calibration Conditions for UV Radiometer Detectors with the KI/KIO3 Actinometer." *Photochemistry and Photobiology* 91 (1): 68–73. https://doi.org/10.1111/php.12356.

Qualls, R G, and J D Johnson. 1983. "Bioassay and Dose Measurement in UV Disinfection." *Applied and Environmental Microbiology* 45 (3): 872–77. https://doi.org/10.1128/aem.45.3.872-877.1983.

Rabani, Joseph, Hadas Mamane, Dana Pousty, and James R Bolton. 2021. "Practical Chemical Actinometry—A Review." *Photochemistry and Photobiology* 97 (5): 873–902. https://doi.org/https://doi.org/10.1111/php.13429.

Rahn. 1997. “Potassium Iodide as a Chemical Actinometer for 254 Nm Radiation: Use of Lodate as an Electron Scavenger.” *Photochemistry and Photobiology* 66 (4): 450–55. https://doi.org/https://doi.org/10.1111/j.1751-1097.1997.tb03172.x.

Rahn, R O, P Xu, and S L Miller. 1999. “Dosimetry of Room-Air Germicidal (254 Nm) Radiation Using Spherical Actinometry.” *Photochemistry and Photobiology* 70 (3): 314–18.

Rahn, Mihaela I Stefan, James R Bolton, Evan Goren, Ping-Shine Shaw, and Keith R Lykke. 2003. “Quantum Yield of the Iodide-Iodate Chemical Actinometer: Dependence on Wavelength and Concentrations.” *Photochemistry and Photobiology* 78 (2): 146–52. https://doi.org/10.1562/0031-8655(2003)078<0146:qyotic>2.0.co;2.

Reed, Nicholas G. 2010. “The History of Ultraviolet Germicidal Irradiation for Air Disinfection.” *Public Health Reports* 125 (1): 15–27. https://doi.org/10.1177/003335491012500105.

Riganakos, Kyriakos A, Ioannis K Karabagias, Ioanna Gertzou, and Mario Stahl. 2017. “Comparison of UV-C and Thermal Treatments for the Preservation of Carrot Juice.” *Innovative Food Science & Emerging Technologies* 42: 165–72. https://doi.org/https://doi.org/10.1016/j.ifset.2017.06.015.

Rios de Souza, Vanessa, Vladimir Popović, Keith Warriner, and Tatiana Koutchma. 2020. “A Comparative Study on the Inactivation of Penicillium Expansum Spores on Apple Using Light Emitting Diodes at 277 Nm and a Low-Pressure Mercury Lamp at 253.7 Nm.” *Food Control* 110: 107039. https://doi.org/https://doi.org/10.1016/j.foodcont.2019.107039.

Saeys, W, A M Mouazen, and H Ramon. 2005. “Potential for Onsite and Online Analysis of Pig Manure Using Visible and Near Infrared Reflectance Spectroscopy.” *Biosystems Engineering* 91 (4): 393–402. https://doi.org/https://doi.org/10.1016/j.biosystemseng.2005.05.001.

Sauceda-Gálvez, J N, M Tió-Coma, M Martinez-Garcia, M M Hernández-Herrero, R

Gervilla, and A X Roig-Sagués. 2020. “Effect of Single and Combined UV-C and Ultra-High Pressure Homogenisation Treatments on Inactivation of Alicyclobacillus Acidoterrestris Spores in Apple Juice.” *Innovative Food Science & Emerging Technologies* 60: 102299. https://doi.org/https://doi.org/10.1016/j.ifset.2020.102299.

Shen, Ming-Hsun, and Rakesh K Singh. 2022. “Effective UV Wavelength Range for Increasing Aflatoxins Reduction and Decreasing Oil Deterioration in Contaminated Peanuts.” *Food Research International* 154: 111016. https://doi.org/https://doi.org/10.1016/j.foodres.2022.111016.

Skåra, Torstein, and Jan T Rosnes. 2016. “6 - Emerging Methods and Principles in Food Contact Surface Decontamination/Prevention.” In *Woodhead Publishing Series in Food Science, Technology and Nutrition*, edited by C E B T - Innovation and Future Trends in Food Manufacturing and Supply Chain Technologies Leadley, 151–72. Woodhead Publishing. https://doi.org/https://doi.org/10.1016/B978-1-78242-447-5.00006-X.

Soares, Christopher G. 2006. “Radiochromic Film Dosimetry.” *Radiation Measurements* 41: S100–116. https://doi.org/https://doi.org/10.1016/j.radmeas.2007.01.007.

Song, Kai, Madjid Mohseni, and Fariborz Taghipour. 2016. “Application of Ultraviolet Light-Emitting Diodes (UV-LEDs) for Water Disinfection: A Review.” *Water Research* 94: 341–49. https://doi.org/10.1016/j.watres.2016.03.003.

Soro, Arturo B, Paul Whyte, Declan J Bolton, and Brijesh K Tiwari. 2021. “Application of a LED-UV Based Light Technology for Decontamination of Chicken Breast Fillets: Impact on Microbiota and Quality Attributes.” *LWT* 145: 111297. https://doi.org/https://doi.org/10.1016/j.lwt.2021.111297.

Templeton, Michael. n.d. “Basic Principles of UV Disinfection.”

Udomkun, Patchimaporn, Bhundit Innawong, and Kitiya Jeepetch. 2019. “Computer Vision System (CVS) for Color and Surface Oil Measurements of Durian Chips

during Post-Frying." *Journal of Food Measurement and Characterization* 13 (3): 2075–81. https://doi.org/10.1007/s11694-019-00128-1.

Udovicki, Bozidar, Slavica Stankovic, Nikola Tomic, Ilija Djekic, Nada Smigic, Bojana Spirovic Trifunovic, Dragan Milicevic, and Andreja Rajkovic. 2022. "Evaluation of Ultraviolet Irradiation Effects on Aspergillus Flavus and Aflatoxin B1 in Maize and Peanut Using Innovative Vibrating Decontamination Equipment." *Food Control* 134: 108691. https://doi.org/https://doi.org/10.1016/j.foodcont.2021.108691.

URL1. 2016. "CCOHS." Ultraviolet Radiation. 2016. https://www.ccohs.ca/oshanswers/phys_agents/ultravioletradiation.html.

URL2. 2017. "Just Paint." Munsell Notations for Goldenand Williamsburg Paints. 2017. https://justpaint.org/munsell-notations-for-golden-and-williamsburg-paints/.

Völz, H. G. 2002. "How Colors Depend on Spectra(Colorimetry)." In *Industrial Color Testing*, 2nd ed., 15–66. Weinheim: Wiley-VCH GmbH.

Wang, Bei, Wenli Wei, Jiazila Aputexiakere, Yunliang Li, and Haile Ma. 2021. "Surface Decontamination of Whole Eggs Using Pulsed Light Technology and Shelf Life Study of Combined Pulsed Light and Vaseline Coating during Room Temperature Storage." *Food Control*, 108411. https://doi.org/https://doi.org/10.1016/j.foodcont.2021.108411.

Wang, Dan, Likun Chen, Yue Ma, Min Zhang, Yuwei Zhao, and Xiaoyan Zhao. 2019. "Effect of UV-C Treatment on the Quality of Fresh-Cut Lotus (Nelumbo Nucifera Gaertn.) Root." *Food Chemistry* 278: 659–64. https://doi.org/https://doi.org/10.1016/j.foodchem.2018.11.102.

Wang, Qiong, Lijun Chu, and Liping Kou. 2017. "UV-C Treatment Maintains Quality and Delays Senescence of Oyster Mushroom (Pleurotus Ostreatus)." *Scientia Horticulturae* 225: 380–85. https://doi.org/https://doi.org/10.1016/j.scienta.2017.07.019.

WHO. 2022. “Food Safety.” 2022. https://www.who.int/health-topics/food-safety.

Yan, Ruixiang, Juan Yun, Joshua Gurtler, and Xuetong Fan. 2017. “Radiochromic Film Dosimetry for UV-C Treatments of Apple Fruit.” *Postharvest Biology and Technology* 127: 14–20. https://doi.org/https://doi.org/10.1016/j.postharvbio.2017.01.003.

Yao, Shiyun, and Haiqiang Chen. 2021. “Development and Evaluation of a Point-of-Use UV Appliance for Fresh Produce Decontamination.” *International Journal of Food Microbiology* 339: 109024. https://doi.org/https://doi.org/10.1016/j.ijfoodmicro.2020.109024.

APPENDIX A

TRIIODIDE FORMATION CURVES AT DIFFERENT DISTANCES FROM THE UV LAMP VERTICALLY

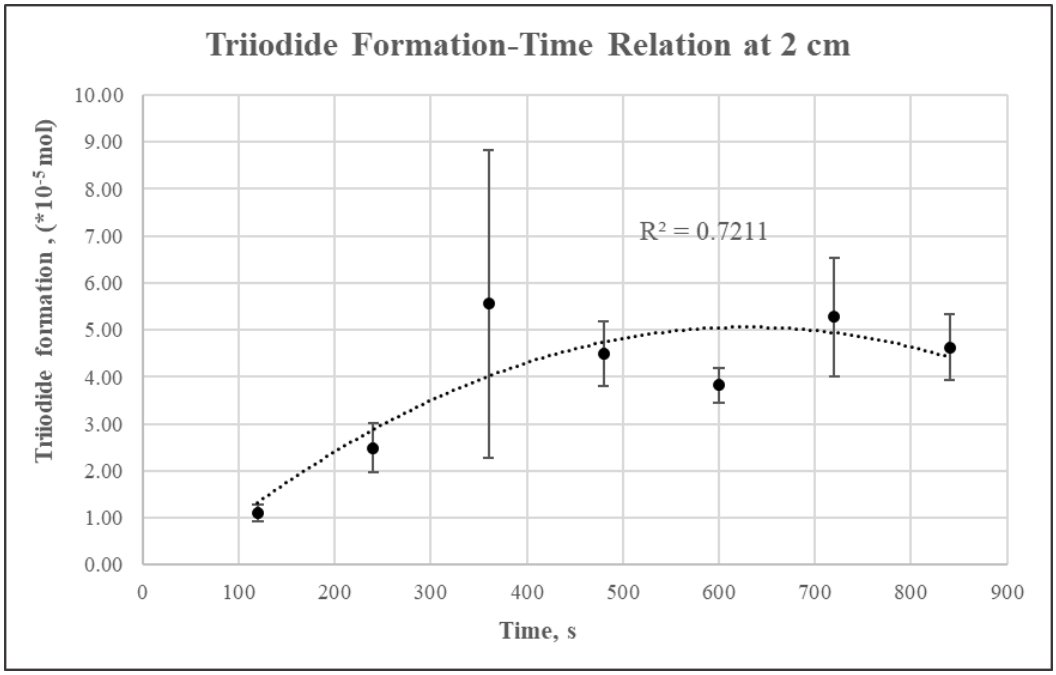

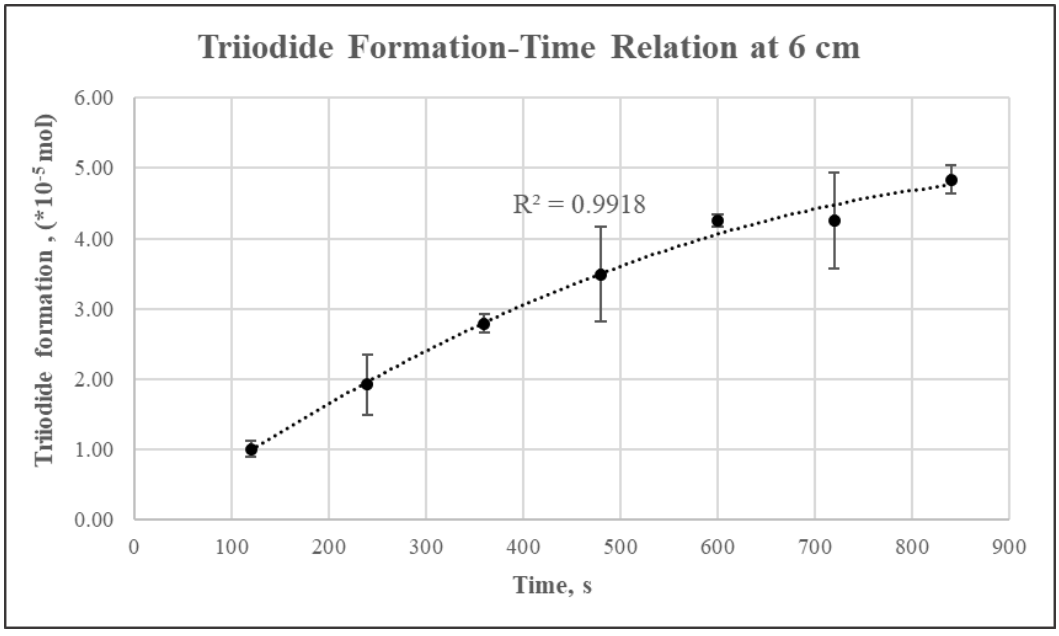

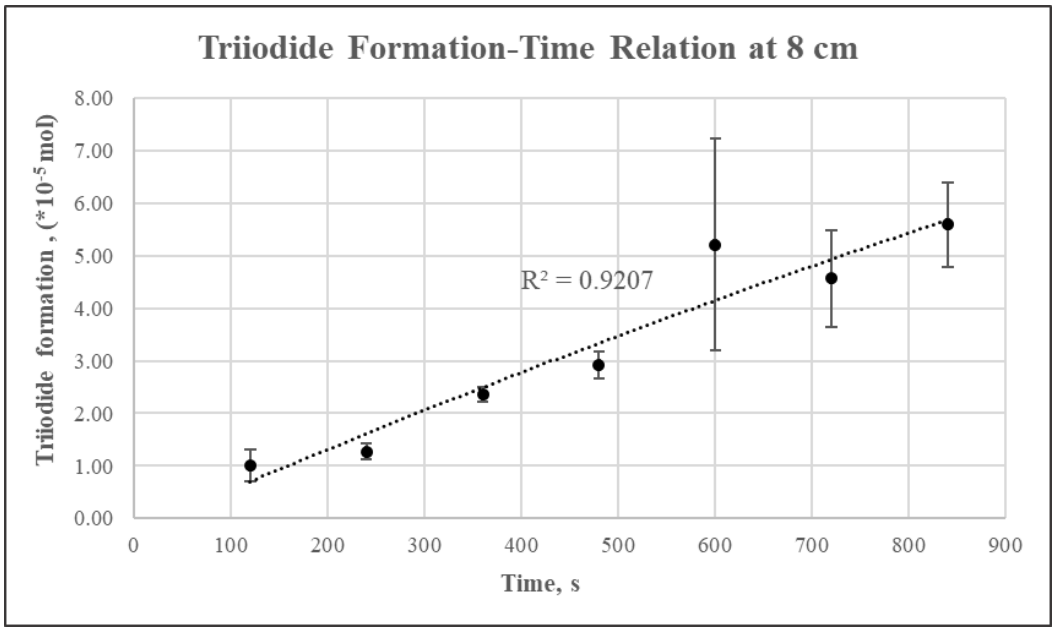
Triiodide Formation-Time Relation at 8 cm
Triiodide formation , (*10-5 mol)
8.00
7.00
6.00
5.00
4.00
3.00
2.00
1.00
0.00
R² = 0.9207
0
100
200
300
400
500
600
700
800
900
Time, s

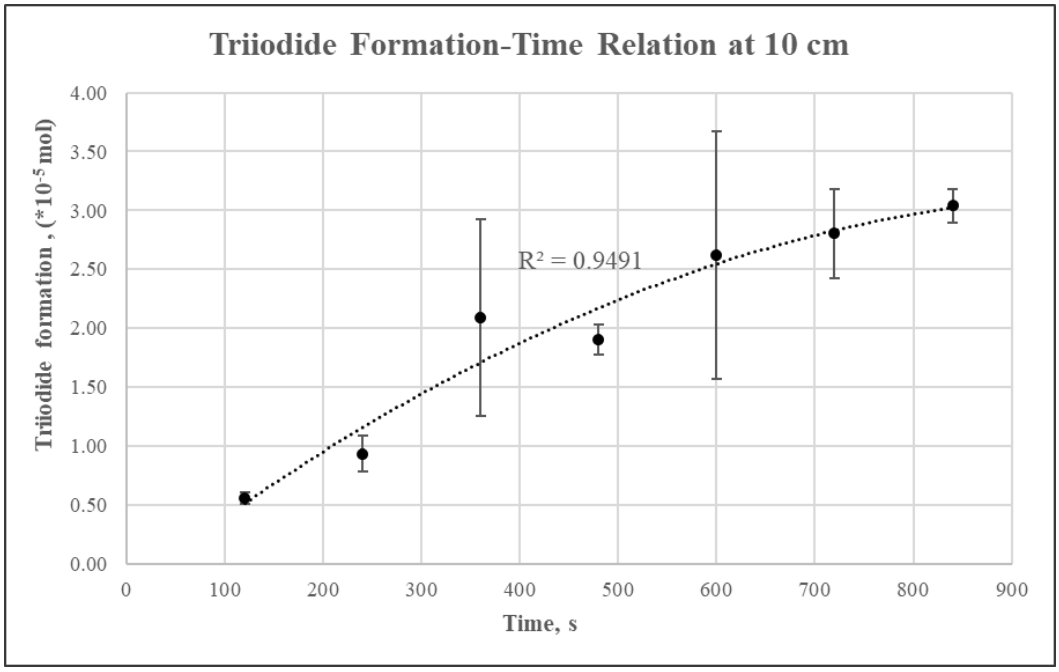
Triiodide Formation-Time Relation at 10 cm
Triiodide formation , (*10-5 mol)
4.00
3.50
3.00
2.50
2.00
1.50
1.00
0.50
0.00
R² = 0.9491
0
100
200
300
400
500
600
700
800
900
Time, s

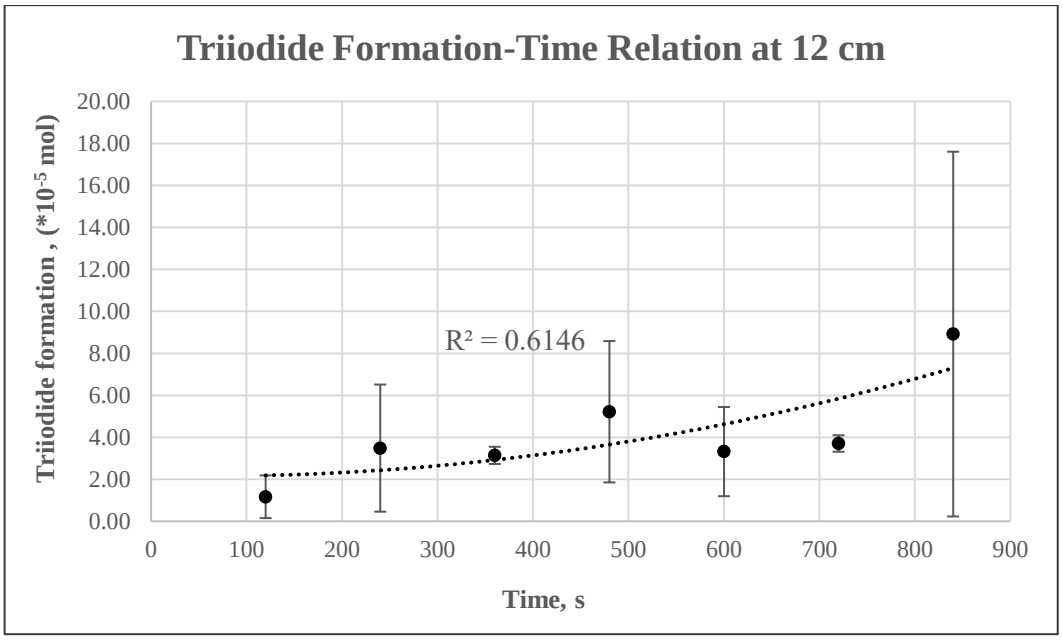
Triiodide Formation-Time Relation at 12 cm
Triiodide formation , (*10-5 mol)
20.00
18.00
16.00
14.00
12.00
10.00
8.00
6.00
4.00
2.00
0.00
R² = 0.6146
0
100
200
300
400
500
600
700
800
900
Time, s

APPENDIX B

SPECIFIED DIAPHRAGM-INSTANTANEOUS PAIRS

ID \ I	60	80	100	125	160	200	250	320	500	640	800	1000	1250	1600	2000	2500	3200	4000
f4.8												√				√	√	
f5											√					√	√	
f5.6											√					√		
f6.3									√	√				√	√	?		
f7.1									√					√				
f8													√					
f9						√	√				√							
f10					√	√			√		√	√						
f11					√													
f13				√					√									
f14			√	√			√											
f16		√	√			√	√											
f18	√	√				√	√	√										
f20	√					√												
f22	√	√	√	√	√													

APPENDIX C

THE COLOR CHANGE OF RCFS

Appendix C. Color Change of RCFs in Response to Varying Exposure Times and UV Irradiance Values

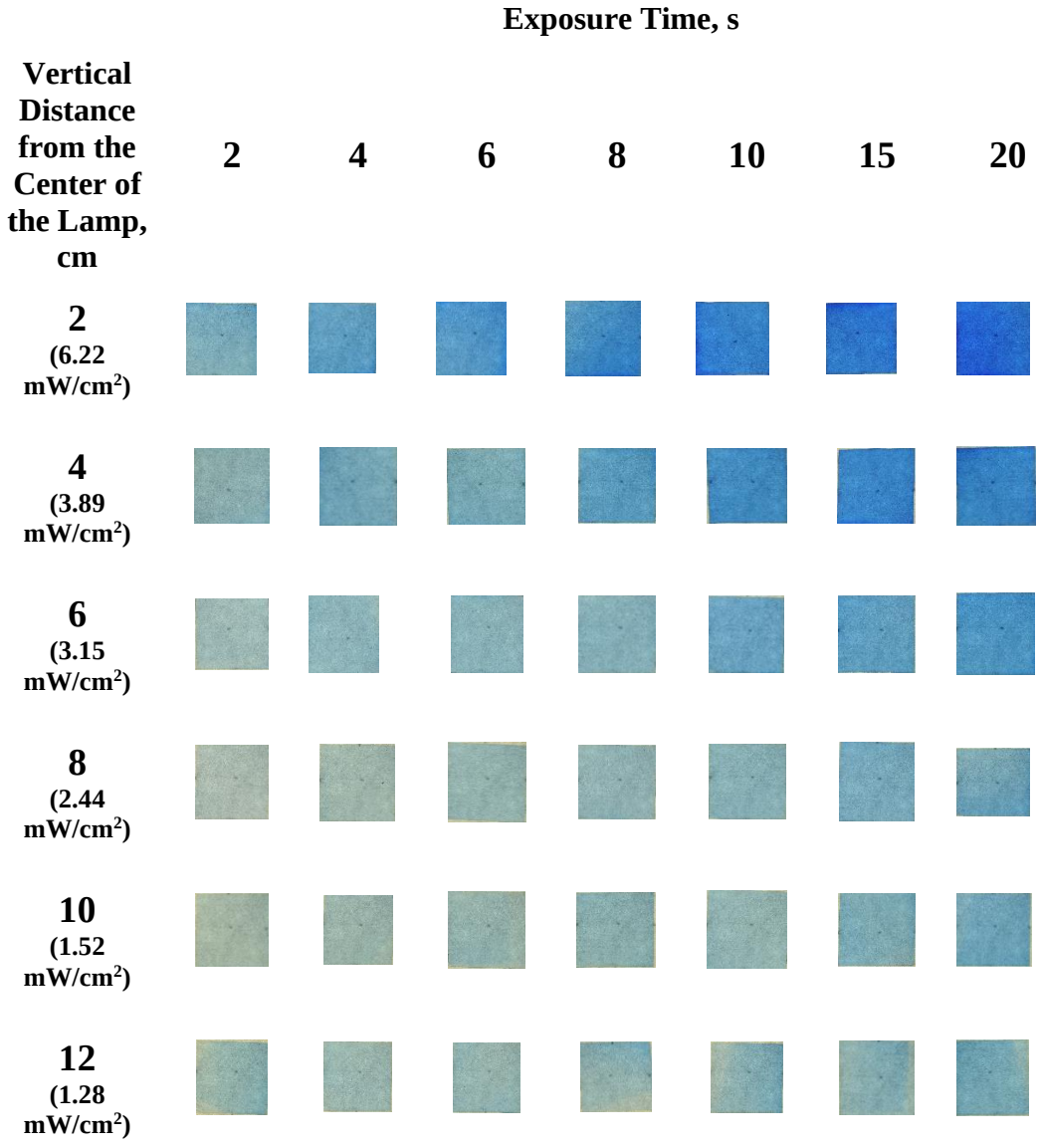

APPENDIX D

CALCULATION ALGORITHM OF COLOR SPACE IN THE KONICA MINOLTA CR-400 CHROMAMETER

X_{2s}', Y_s', Z_s' ; the specimen measuring point, measurement data

X_{2r}', Y_r', Z_r' ; the monitoring illumination part, measurement data gotten when illuminating

X_{2r}", Y_r", Z_r" ; the monitoring illumination part, measurement data gotten when not illuminating

$X_{2s} = X_{2s}' - X_{2s}''$ $X_{2r} = X_{2r}' - X_{2r}''$

$Y_s = Y_s' - Y_s''$ $Y_r = Y_r' - Y_r''$

$Z_s = Z_s' - Z_s''$ and $Z_r = Z_r' - Z_r$

To eliminate the influence of subtle changes in the illuminant

$$X_{2m} = \frac{X_{2s}}{X_{2r}} \qquad Y_m = \frac{Y_s}{Y_r} \qquad Z_m = \frac{Z_s}{Z_r}$$

$\bar{X}_{1\lambda}$ data is calculated by Z_m

$X_{1m} = 0.1672 \times Z_m$

$\therefore X_m = X_{1m} + X_{2m}$

The tristimulus value X, Y, Z

$X = \alpha X_m$

$Y = \beta Y_m$

$Z = \gamma Z_m$

where α, β, and γ are calibration constants.

The value functions X*, Y*, and Z*

$$X^* = \sqrt[3]{\frac{X}{X_n}} \qquad Y^* = \sqrt[3]{\frac{Y}{Y_n}} \qquad Z^* = \sqrt[3]{\frac{Z}{Z_n}}$$

where X_n, Y_n, and Z_n are CIE tristimulus values for the illuminant used with Yn= 100 for all standard illuminants.

However, for X/ X_n, $Y/100$, and $Z/ Z_n \leq 0.008856$

$$X^* = 7.787 \frac{X}{X_n} + 0.138$$

$$Y^* = 7.787 \frac{Y}{Y_n} + 0.138$$

$$Z^* = 7.787 \frac{Z}{Z_n} + 0.138$$

Then, L*, a*, and b* values are calculated as

$$L^* = 116Y^* - 16$$

$$a^* = 500(X^* - Y^*)$$

$$b^* = 200(Y^* - Z^*)$$

In polar coordinates,

$C^*_{ab} = \sqrt{a^{*2} + b^{*2}}$ (Chroma, as radius vector)

$h_{ab} = Arctan \frac{b^*}{a^*}$ (Hue angle, as polar angle)

APPENDIX E

THE COLOR CHANGE OF RCFS ON SPHERICAL APPLE SAMPLES

(a)

(b)

Appendix E. Color Change of RCFs on Different Location of Apple Samples (a) Before and (b) After UVC Treatment

APPENDIX F

THE COLOR CHANGE OF RCFS ON HEMISPHERICAL APPLE SAMPLES

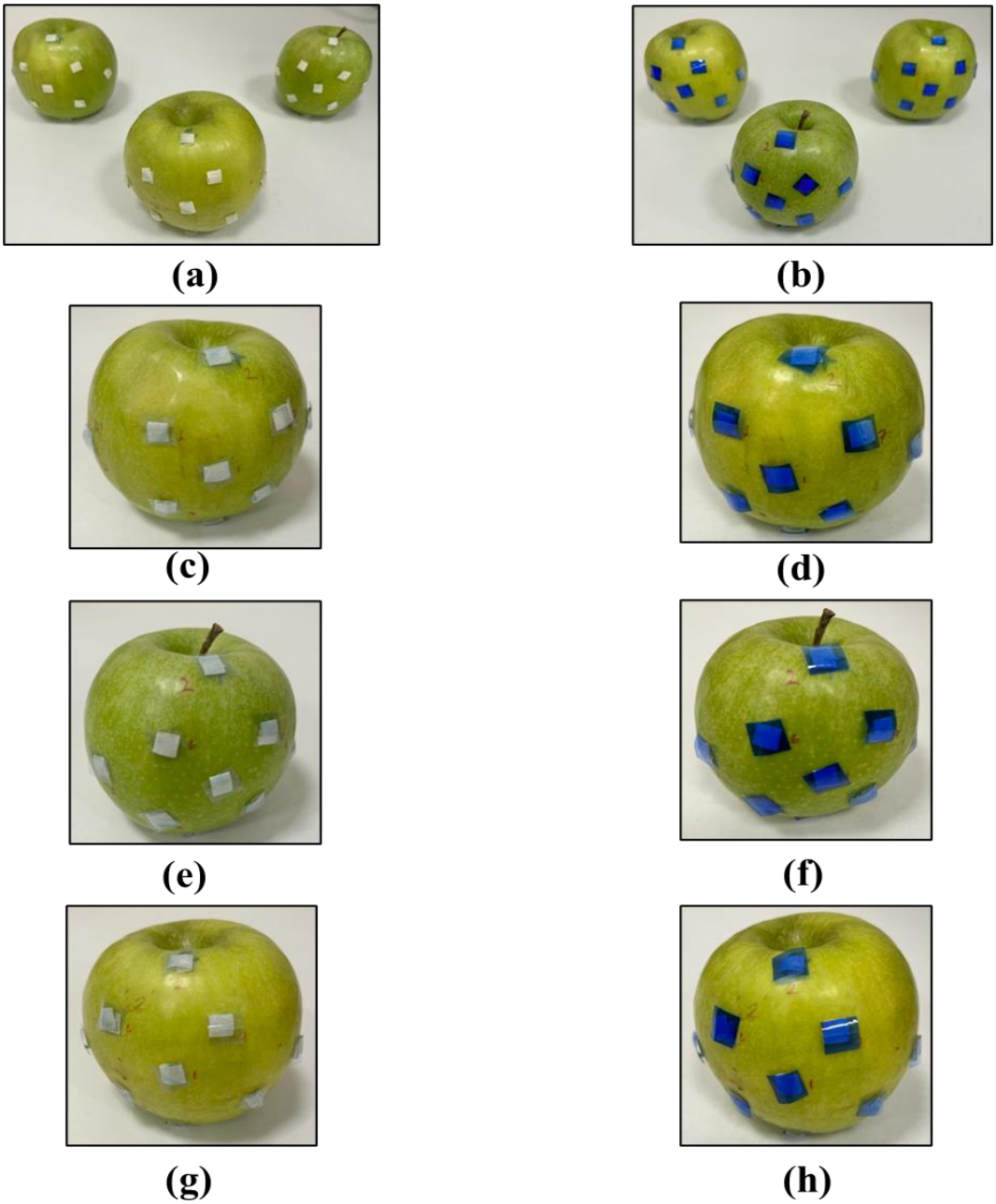

Appendix F. Color Change of RCFs on the Surface of Samples before (a) all Samples (c) Sample 2 (e) Sample 4 (f) Sample 7 and After (b) all Samples (d) Sample 2 (f) Sample 4 (h) Sample 7 UVC treatment